Journal of Animal Diversity

Online ISSN 2676-685X

Volume 4, Issue 2 (2022)

Research Article

http://dx.doi.org/10.52547/JAD.2022.4.2.1
http://zoobank.org/urn:lsid:zoobank.org:pub:53147CC3-4CF4-411A-9859-C169F230A1F3

Two new *Bryodelphax* Thulin, 1928 species (Heterotardigrada: Echiniscidae) from the Republic of Ireland with comments on the '*weglarskae* group' and other heterotardigrade taxa, including the controversial genus *Bryochoerus* Marcus, 1936

Erica DeMilio[1*], Denis V. Tumanov[2], Colin Lawton[1], Reinhardt Møbjerg Kristensen[3] and Jesper Guldberg Hansen[3]

[1]*Zoology, School of Natural Sciences, Ryan Institute, National University of Ireland Galway, Galway, Ireland*
[2]*Independent researcher*
[3]*Natural History Museum of Denmark, University of Copenhagen, Copenhagen, Denmark*
[*]*Corresponding author*✉: *erica.demilio@gmail.com*

Citation: DeMilio, E., Tumanov, D. V., Lawton, C., Kristensen, R. M. and Hansen, J. G. (2022). Two new *Bryodelphax* Thulin, 1928 species (Heterotardigrada: Echiniscidae) from the Republic of Ireland with comments on the '*weglarskae* group' and other heterotardigrade taxa, including the controversial genus *Bryochoerus* Marcus, 1936. *Journal of Animal Diversity*, 4 (2): 1–52. http://dx.doi.org/10.52547/JAD.2022.4.2.1

Received: 24 March 2022
Accepted: 5 June 2022
Published online: 30 June 2022

Abstract

Two new heterotardigrade (Tardigrada) species, *Bryodelphax pucapetricolus* sp. nov. and *Bryodelphax wallacearthuri* sp. nov., are described from moss associated with limestone pavement in the Republic of Ireland. The species description process for these two taxa initiated a more detailed exploration of several morphological characters of importance in *Bryodelphax* Thulin including cuticular sculpture elements and ventral plate morphology. Division of the third dorsal median plate in the context of the genera *Bryochoerus* Marcus and *Bryodelphax* is further discussed. We recommend minor emendations to the generic diagnoses of *Bryochoerus* and *Bryodelphax*. Also, we emend the species diagnoses of *Bryodelphax aaseae* Kristensen, Michalczyk and Kaczmarek and *Bryodelphax parvuspolaris* Kaczmarek, Zawierucha, Smykla and Michalczyk, record the genus *Parechiniscus* Cuénot from the Republic of Ireland for the first time, and make suggestions relevant to the taxonomy of limnoterrestrial heterotardigrades.

Key words: Biodiversity, the Burren, scanning electron microscopy, Heterotardigrada, Echiniscidae, new species

Introduction

Tardigrades (Phylum Tardigrada Doyère, 1840) are obligate aquatic, microscopic animals that occur in marine, freshwater, and diverse limnoterrestrial situations. The All-Ireland Tardigrade Survey (AITS) is an on-going research project with an aim to investigate the biodiversity and ecology of Tardigrada within multiple habitat types in all 32 counties of the Republic of Ireland and Northern Ireland (subsequently referred to together as 'Ireland'). Limestone pavement, a habitat of particular focus of the AITS project, occurs over a larger area in Ireland than elsewhere in the European Union (Wilson and Fernández, 2013). The majority of this habitat type is concentrated in Burren region in the west of Ireland.

The Burren is renowned for its characteristic and expansive limestone karst topography and further recognized as a complex mosaic of biological and habitat diversity of international conservation importance (Parr et al., 2009). Yet, only two previous records of tardigrades existed from the region prior to the present investigation: *Isohypsibius panovi* Tumanov, 2005 described from lichen on sandy soil (Tumanov, 2005) and *Echiniscus quadrispinosus quadrispinosus* Richters, 1902 recorded in Ireland for the first time from moss on a tree trunk (DeMilio et

al., 2016). Neither of these previous samples was taken from limestone pavement substrate.

We found two undescribed species of *Bryodelphax* Thulin, 1928 in new AITS moss samples from limestone pavement in the Burren region. The heterotardigrade genus *Bryodelphax* contains 27 previously described species that have been considered to be divided into two taxonomically operational groups (Kristensen et al., 2010) that are characterized by the presence of ventral plates of sclerotized cuticle in the '*weglarskae* group' (14 species), or the absence of such plates in the '*parvulus* group' (13 species).

The genus *Bryochoerus* Marcus, 1936 was essentially separated from *Bryodelphax* by the division of all three median plates of the dorsal cuticle on the former, compared to only the two anteriormost median plates divided in the later. There are taxonomic issues surrounding *Bryochoerus* that originate in part from the outdated practice of erecting, moving, or otherwise emending taxa from another geographic area (sometimes very distant) on the basis of observations made on local material that the author believed to represent the original description without having observed the type (which was often loosely described by modern standards).

Murray (1910) described '*Echiniscus intermedius intermedius*' and its Hawaiian variety (both from Oceania) and Canadian variety (Pacific North America). All three taxa were indicated to have divided median plates. However, the third median plate seems to have been considered by Murray (1910) to be structured slightly different between the type and Hawaiian variety compared to the Canadian variety, although this was ambiguously stated. Thulin (1911) collected Swedish heterotardigrade specimens that he determined to be the '*Echiniscus intermedius'* Canadian variety with the identification confirmed by Murray. Thulin (1928) considered this Swedish material (treated as equivalent to the '*Echiniscus intermedius*' Canadian variety), the Australian type, and Hawaiian variety described by Murray (1910) to comprise the new genus *Bryodelphax*. The original diagnosis for that genus included 5–6 "Schaltplatten" (*i.e.* median plates) because Thulin (1928) stated that he interpreted Murray's description of these taxa to mean that the third median plate could be composed of two parts (in the type and Hawaiian variety, *i.e.* 6 median plate parts in total) or to have only one part as a result of the second part being completely fused with the caudal plate (the Canadian variety, *i.e.* 5 median plate parts in total). Thulin (1928) named the Canadian variety *Bryodelphax parvulus* Thulin 1928 and designated it as the genus type as he considered the other associated *intermedius* taxa as only temporarily placed in *Bryodelphax*.

Marcus (1936) later concluded that Murray's '*Echiniscus intermedius intermedius*', the Hawaiian variety, and a new German form, '*laevis*', should be placed into the new *Bryochoerus* based upon the shared character of a division in third median plate. Marcus (1936), in disagreement with Thulin (1928), considered both *Bryodelphax* and *Bryochoerus* as subgenera, not genera. Contrarily, Kristensen (1987) found evidence in Thulin's collection to indicate that Thulin regarded *Bryodelphax* and *Bryochoerus* as synonyms. Confusion over the status of *Bryochoerus* was perhaps further compounded by variation in how the "divisions" of the median plates have been precisely interpreted by the original and later authors, several of whom have also discussed the validity of the genus (Ramazzotti and Maucci, 1983; Kristensen, 1987; Kristensen et al., 2010; Lisi et al., 2017; Xue et al., 2017).

At the outset of our analyses of the two undescribed *Bryodelphax* and accompanying taxa collected from the Burren, we encountered two main obstacles that prevented straightforward descriptions of the two new species. First, our initial analysis showed conflicting evidence for the generic placement of one of the undescribed species as it exhibited characters of both the *Bryodelphax* '*weglarskae* group' and *Bryochoerus*. Second, our detailed analyses of both undescribed species and *Bryodelphax* comparative material as part of the species description process found variation in several morphological characters that had not been previously well accounted for in relation to *Bryodelphax*. Both of these issues required us to expand our work on these taxa to include a broader, more in-depth presentation of our observations of the morphological characters of these heterotardigrade taxa.

Material and Methods

Isolation of specimens

Moss samples were collected from limestone pavement surfaces with permission from the Irish National Parks and Wildlife Service (permit number: 2013-1234). Samples were immediately dried and subsequently stored in paper envelopes. Dried moss was rehydrated in distilled water for 24 hours prior to vigorous agitation in a glass jar, after which the contents were passed through 1.2 mm and 36 μm sieves. Material retained on the finer sieve was examined under a stereomicroscope at a minimum of 40x magnification in order to manually sort tardigrades from the host material.

Microscopy and imaging

Collected specimens were mounted either on permanent slides in Heinz's Polyvinyl Alcohol (PVA) or Hoyer's medium or on temporary slides in water to be identified prior to molecular analyses. Other individuals were prepared for scanning electron microscopy (SEM). Permanent slides for light microscopy (LM) were examined on an Olympus BX51 or Leica DM2500 microscope using differential interference contrast (DIC) and phase contrast (PhC) techniques and/or an AMScope T720

with PhC kit. Specimens on permanent and temporary slides were measured and photographed up to the maximum magnification (100x oil objective (and 2x magnification changer)) with digital camera and AMScope capture software (Version 3.7). Drawings for figures were made using a drawing tube. Specimens were prepared for and examined with SEM as per the protocol described by Pérez-Pech et al. (2020). All figures were assembled with Corel Draw Graphics Suite X6.

Morphometrics, terminology, and identification

Morphometric data are given in micrometers (µm). Measured traits were checked for the influence of allometric growth following Bartels et al. (2011) in order to validate the use of morphometric ratios and to eliminate body size effects in intra- and interspecific comparisons. For each measured trait (except scapular plate length) a *psc* value, *i.e.* the per cent ratio between the length of a structure and the scapular plate length (Dastych, 1999; Fontoura and Morais, 2011; Kaczmarek et al., 2021) was calculated. An additional morphometric index, *pbl*, which we define as the per cent ratio of a length of the structure and the body length, was calculated for the measured distance between the gonopore and anus (see below). Body length (bl) was measured from the cephalic to caudal extremities excluding legs IV. Cirri were measured including the cirrophore. Secondary clavae were measured in two dimensions with length (l) measured as the distance from the base at the point of attachment to the head to the distal apex, and width (w) at the widest point across the circumference. If claws were oriented in a position for reliable measurement, claw length, claw height, spur length, and spur insertion point were obtained as shown in Fig. 1A, B. Female gonopore diameter (⌀) was measured at the widest transverse distance including the surrounding rosette of myoepithelial cells (Fig. 1C). Male gonopore diameter (⌀) was measured at the widest transverse distance across the external circumference (Fig. 1D). Gonopore to anus distance was measured from the center of the gonopore aperture to the center of the anal aperture (Fig. 1C, D). Statistical analyses were performed with JASP (Version 12.2).

Species identifications and determinations of new species were performed by comparisons with the original descriptions, any subsequent related literature, and type or museum specimens of previously described species. We followed the most recent checklist of tardigrades species (2009–2021, 40th Edition: 19-07-2021) by Degma et al. (2021a) (Guidetti and Bertolani, 2005; Degma and Guidetti, 2007). We used the general terminology of Kristensen (1987) and Tumanov (2020a) for *Pseudechiniscus* with modification, and our own terms. Regarding features of the cuticle, we employ the traditional usage of the term 'sculpture' to include both the outermost structures and those visible within more internal layers (*i.e.* pillars). Terminology of the anal system was adapted from Møbjerg et al. (2019). We used the abbreviations for the genera *Bryochoerus* Marcus, 1936 (*Brc.*), *Bryodelphax* Thulin, 1928 (*Bry.*), *Parechiniscus* Cuénot, 1926 (*Par.*), and *Pseudechiniscus* Thulin, 1911 (*Pse.*) recommended by Perry et al. (2019).

Additional material studied

We examined the following museum material (slides) for comparative purposes: *Bryochoerus intermedius intermedius* (Murray, 1910) (one specimen (Australia), Natural History Museum of Denmark (NHMD), slide NHMD-111560); *Bryochoerus intermedius laevis* (Marcus, 1936) (eight specimens (Greenland), slides NHMD-111559, NHMD-111605, NHMD-866887); *Bryodelphax aaseae* Kristensen, Michalczyk and Kaczmarek, 2010 (holotype and 41 paratypes, slides NHMD-111877–111879, NHMD-111882, NHMD-111891–111892, NHMD-111894–111896); *Bryodelphax arenosus* Gąsiorek, 2018 (one paratype, slide NHMD-304931); *Bryodelphax australasiaticus* Gąsiorek, Vončina, Degma and Michalczyk, 2020a (four paratypes, slides NHMD-304919–304921); *Bryodelphax decoratus* Gąsiorek, Vončina, Degma and Michalczyk, 2020a (three paratypes, slide NHMD-915770); *Bryodelphax instabilis* Gąsiorek and Degma, 2018 (two paratypes, slides NHMD-304929–304930); *Bryodelphax iohannis* Bertolani, Guidi and Rebecchi, 1996 (holotype and 27 paratypes, Bertolani Collection, University of Modena and Reggio Emilia); *Bryodelphax maculatus* Gąsiorek, Stec, Morek, Marnissi and Michalczyk, 2017 (2 paratypes, slide NHMD-304922); *Bryodelphax mareki* Kayastha, Roszkowska, Mioduchowska, Gawlak and Kaczmarek, 2021 (two paratypes, slides NHMD-916144–916145); *Bryodelphax nigripunctatus* Gąsiorek, Vončina, Degma and Michalczyk, 2020a (seven paratypes, slides NHMD-304923–304928); *Bryodelphax olszanowskii* Kaczmarek, Parnikoza, Gawlak, Esefeld, Peter, Kozeretska and Roszkowska, 2018 (6 paratypes, slide NHMD-645471); and *Bryodelphax weglarskae* (Pilato, 1972) (holotype, Binda and Pilato Collection, University of Catania and one paratype, Bertolani Collection).

For our analyses of morphological characters (in addition to the comparative material above and the newly collected specimens) we studied all published LM and/or SEM micrographs of previously described *Bryodelphax* or *Bryochoerus* species in: Węglarska, 1959; Maucci, 1986; Bertolani et al., 1996; Kaczmarek and Michalczyk, 2004; Kaczmarek et al., 2005; Fontoura et al., 2008; Kristensen et al., 2010; Pilato et al., 2010; Kaczmarek et al., 2012; Lisi et al., 2017; Gąsiorek et al., 2017; Xue et al., 2017; Gąsiorek, 2018; Gąsiorek and Degma, 2018; Kaczmarek et al., 2018; Gąsiorek et al., 2020a; and Kayastha et al., 2021. We also examined unpublished micrographs of the holotype of *Bryodelphax parvuspolaris* (courtesy of Ł. Kaczmarek).

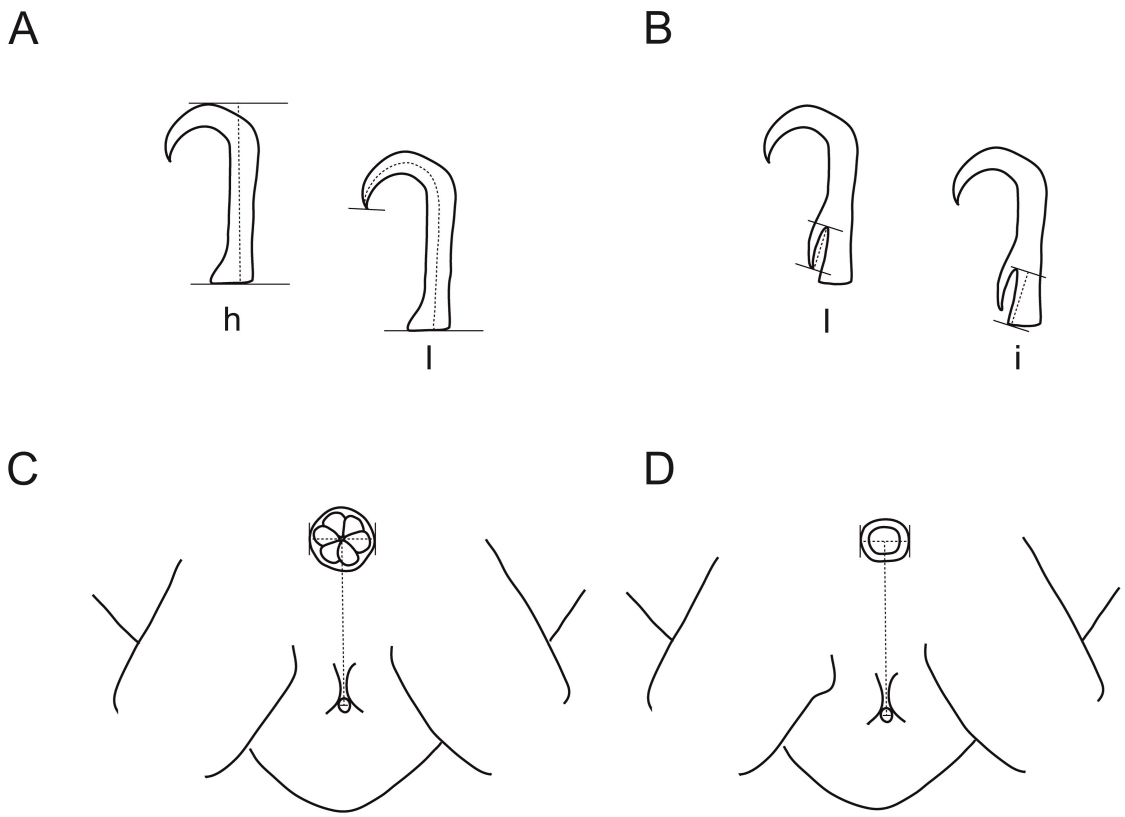

Figure 1: Diagrams demonstrating performance of measurements. **A** claw measurements, h= claw height, l= claw length; **B** spur measurements, l= spur length, i= spur insertion point; **C** measurements of the female gonopore diameter and distance between female gonopore and anus; **D** measurements of the male gonopore diameter and distance between male gonopore and anus.

Genotyping

Molecular analyses were executed for 10 specimens fixed in RNA*later*® (Qiagen, Hilden, Germany) solution. DNA was extracted using QuickExtract™ DNA Extraction Solution (Lucigen Corporation, USA) (complete protocol description in Tumanov, 2020b). Four genetic regions were sequenced: small ribosome subunit (18S rRNA), large ribosome subunit (28S rRNA), internal transcribed spacer (ITS-1), and cytochrome oxidase subunit I (COI). PCR reactions included 5 µl template DNA, 1 µl of each primer, 1 µl dNTP, 5 µl Taq Buffer (10X) (−Mg), 4 µl 25 mM $MgCl_2$ and 0.2 µl Taq DNA Polymerase (Thermo Scientific™) in a final volume of 50 µl. The primers and PCR programs used are provided in Supplementary File 1. PCR products were visualized in 1.5% agarose gel stained with ethidium bromide. All amplicons were sequenced directly using the ABI PRISM Big Dye Terminator Cycle Sequencing Kit (Applied Biosystems, Foster City, CA, USA) with the help of an ABI Prism 310 Genetic Analyzer. Sequences were edited and assembled using ChromasPro software (Technelysium, USA). COI sequences were translated to amino acids using the invertebrate mitochondrial code, implemented in AliView version 1.27 (Larsson, 2014), in order to check for the presence of stop codons and therefore of pseudogenes.

Phylogenetic analysis

All sequences of 18S and 28S genes available in GenBank for *Bryodelphax* at the time of analysis were downloaded. Sequences of appropriate length that were homologous to the sequences obtained and that originated from publications with a reliable attribution of the investigated taxa were selected (Supplementary File 2). Both 18S rRNA and 28S rRNA are nuclear markers used in phylogenetic analyses to investigate high taxonomic levels (Jørgensen et al., 2010, 2011; Bertolani et al., 2014; Gąsiorek, 2018; Guil et al., 2019). COI and ITS-1 were not included in the analysis because too few sequences were available for these markers. Two sequences of *Echiniscus* Schultze, 1840 (*E. testudo* (Doyère, 1840) and *E. masculinus* Gąsiorek, Vončina and Michalczyk, 2020) were used as an outgroup. Sequences were automatically aligned using the MAFFT algorithm (Katoh et al., 2002) using AliView version 1.27 (Larsson, 2014); the alignments were cropped to a length of 968 bp for 18S and 748 bp for 28S. Sequences of both genes were concatenated using SeaView 4.0 (Gouy et al., 2010) (final alignment presented in Supplementary File 3). The best substitution model and partitioning scheme for posterior phylogenetic analysis was chosen under the Akaike Information Criterion (AICc), using IQ-TREE multicore version 1.6.12

(Kalyaanamoorthy et al., 2017; Minh et al., 2020). IQ-TREE suggested to retain two predefined partitions separately, and GTR+G4+F model was recognized as the most suitable for both datasets.

Maximum-likelihood (ML) topologies were constructed using IQ-TREE software (Minh et al., 2020) with GTR+G4+F model. Bayesian analysis of the same datasets was performed using MrBayes ver. 3.2.6, GTR model with gamma correction for intersite rate variation (8 categories) and the covariation model (Ronquist and Huelsenbeck, 2003). Analyses were run as two separate chains (default heating parameters) for 20 million generations, by which time they had ceased converging (final average standard deviation of the split frequencies was less than 0.01). The quality of chains was estimated using built-in MrBayes tools. MrBayes program was run at the CIPRES ver. 3.3 website (Miller et al., 2010). Bayesian analysis quality was verified using the program Tracer v1.7.1 (Rambaut et al., 2018). Uncorrected pairwise distances were calculated for sequences automatically aligned with the help of the MUSCLE algorithm as implemented in SeaView 4.0 using MEGA7 (Kumar et al., 2016) with gaps/missing data treatment set to "complete deletion".

Abbreviations for morphological terms

alr anterior latitudinal ridge
bl body length
cap caudal plate
cep cephalic plate
clr central latitudinal ridge
cxp coxal plate
dfr distal femoral ridge
EE epicuticular element
fp femoral plate
l length
lcp lateral cephalic plate
lip lateral intersegmental plate
m1 median plate 1
m1a median plate 1 anterior part
m1p median plate 1 posterior part
m2 median plate 2
m2a median plate 2 anterior part
m2p median plate 2 posterior part
m3 median plate 3
m3a median plate 3 anterior part
m3p median plate 3 posterior part
np neck plate
p1 sense organ of leg I
p3 sense organ of leg III
p4 sense organ of leg IV
pfr proximal femoral ridge
plr posterior latitudinal ridge
pp1 paired plate 1
pp2 paired plate 2
scp scapular plate
svp subcephalic ventral plate
w width

Results

Collected taxa

Two samples of moss were collected from limestone pavement, one from the Burren National Park (BNP) (53° 0' 57" N, 8° 58' 58" W) and the other from Glensleade (53° 4' 12" N, 9° 9' 36" W), both in County Clare, Ireland. Each sample contained over 100 adult tardigrades. We identified three taxa from the BNP: an undescribed *Bryodelphax* species of the '*weglarskae* group' (*i.e. Bry. pucapetricolus* sp. nov., 91 specimens), *Pseudechiniscus* sp. (1 specimen), and *Hypsibius* cf. *convergens* (Urbanowicz, 1925) (3 specimens). We identified five taxa from Glensleade: a second undescribed species of the *Bryodelphax* '*weglarskae* group' (*i.e. Bry. wallacearthuri* sp. nov., 16 specimens), *Bryodelphax* cf. *parvulus* Thulin, 1928 (6 specimens), *Parechiniscus* cf. *chitonides* Cuénot, 1926 (23 specimens), *Pseudechiniscus* sp. (22 specimens), and *Paramacrobiotus* sp. of the '*richtersi* group' (31 specimens). In addition to the two new *Bryodelphax* species, *Par*. cf. *chitonides* is a new record for Ireland.

Observations of '*weglarskae* group' species morphology

Our morphological analyses of the collected specimens, comparative type material (Figs. 2–16, 18–27), and published micrographs identified a need for the appraisal of several characters relevant to taxonomic descriptions of *Bryodelphax* '*weglarskae* group' species (and perhaps other limnoterrestrial heterotardigrade genera). These characters were:

Cuticular sculpture and relief

We observed three main types of sculpture elements associated with the cuticular plates of all '*weglarskae* group' species that we examined (although not all three types were necessarily present on all plated areas). These were intracuticular pillars, cuticular pores, and epicuticular elements (EEs) (Fig. 2). EEs are elevations of the cuticle with varying morphologies. EEs are clearly observable in SEM (Fig. 2D), but are also inferable in LM with PhC as darkened areas on the cuticle (Fig. 2E, F) and more subtly with DIC when present in larger sizes as thickenings on the cuticle surface (Fig. 2B). Our SEM studies showed that the degree of development, shape, size, and distribution of EEs all exhibited interspecific variation (Fig. 3). EEs were observed as rounded or more subcircular elevations (*Bry. aaseae*, *Bry. australasiaticus*, *Bry. maculatus*, *Bry. mareki*, *Bry. pucapetricolus* sp. nov.) or as irregular, polygonal elevations (*Bry. instabilis*, *Bry. nigripunctatus, Bry. olszanowskii*, *Bry. wallacearthuri* sp. nov.). Individual EEs occurred in close proximity to one another forming a mosaic-like network (*e.g. Bry. instabilis*), more spaced apart so that individual elements were easily recognizable (*e.g. Bry. mareki*), or in combination of both situations depending on the area of the plate (*e.g. Bry. australasiaticus*). EEs also

varied in size on the same individual (*Bry. pucapetricolus* sp. nov.). On some areas of the dorsal plates EEs were merged resulting in a ridge-like appearance (*e.g.* along plate margins) (Fig. 4A). In addition to the three main types of sculpture elements, fine cuticular pillars were visible in LM on unplated areas of the cuticle, including areas immediately adjacent to or diffusing along plate margins (Fig. 2A).

The surfaces of most plated areas of the '*weglarskae* group' species that we observed all shared an unlevel, knobby relief. The dorsal plate relief viewed with PhC, gave a dappled appearance that consisted of circular (or subcircular) light and dark areas with a gradation of shades of greys to black (Fig. 4). The relief was also observable with DIC in which the dorsal plate surfaces appeared undulating (Fig. 2A, B). A similar relief to that of the dorsal plate surfaces was visible on lateral cephalic and ventral plate surfaces (Figs. 6A-D, 19B, D, 22B). The unlevel relief was not clearly observable in LM on the interior regions of the median plates and paired plates or on lateral intersegmental plates (lips), where intracuticular pillars tended to be the dominant sculpture element type.

While all of ten '*weglarskae* group' species that we observed in our microscopy studies displayed the knobby relief to some extent, the degree of development of the relief varied between species. The variation in the development of the relief was visualized with PhC as differences in the relative amount of contrast between light and dark areas, the size of the circular areas, and the relative abundances of light and dark areas (Fig. 4). Some species exhibited high relief with high contrast between light and dark areas, larger circular areas, and an abundance of very dark grey and black areas (*Bry. maculatus*, *Bry. nigripunctatus*, *Bry. wallacearthuri* sp. nov.) (Fig. 4A). Other species (*Bry. aaseae*, *Bry. australasiaticus*, *Bry. decoratus*, *Bry. pucapetricolus* sp. nov.) displayed the relief in a clear but less conspicuous manner than the high relief species, where there was moderate contrast between light and dark areas and less abundant but still clearly visible black areas (Fig. 4B). The remaining '*weglarskae* group' species that we examined *(Bry. instabilis*, *Bry. iohannis*, *Bry. mareki*, *Bry. olszanowskii*, *Bry. weglarskae*) showed low relief, which was observed with PhC as faintly dappled plated areas with low contrast between light and dark areas, smaller circular areas and with black areas still always present, but only scarcely (Fig. 4C).

The four '*weglarskae* group' species that we did not observe directly in our LM studies were *Bry. amphoterus* (Durante Pasa and Maucci, 1975), *Bry. kristenseni* Lisi, Daza, Londoño and Quiroga, 2017, *Bry. parvuspolaris,* and *Bry. sinensis* (Pilato, 1974). Our review of the primary literature found that the descriptions of *Bry. kristenseni* and *Bry. parvuspolaris* included PhC micrographs (Figure 1A-D in Lisi et al., 2017; Figures 2, 3 in Kaczmarek et al., 2012) which showed indications of weakly developed EEs (*i.e.* sparse black areas visible on the dorsal plates). The descriptions of *Bry. amphoterus* and *Bry. sinensis* included drawings but not micrographs, as was at the time common practice, thus we were not able to informally check these species for indications of EEs.

In SEM the three main types of sculpture elements we observed in the '*weglarskae* group' species, particularly pores and EEs, but also surface indications of intracuticular pillars (Fig. 2C), were found to be interrelated to, and contribute to the general relief of the plated areas of the cuticle. The depth of pores and the degree of development of the EEs observed in SEM corresponded to the appearance of the cuticle relief in LM. Species with shallow pores and small, weakly developed EEs in SEM images, showed only low relief in LM (*e.g. Bry. mareki*). Species with deep pores and large, strongly developed EEs showed high relief in LM (*e.g. Bry. wallacearthuri* sp. nov.). The relief type and corresponding sculpture elements were therefore determined not to be present/absent characters in the '*weglarskae* group', but ones occurring on spectra of conspicuousness.

Additionally, we examined two '*parvulus* group' taxa as part of our comparative material, *Bry. arenosus* (one paratype) and *Bry*. cf. *parvulus* (six Irish specimens), both of which exhibited very weakly developed EEs that appeared as scarce black areas on the dorsal plates when viewed with PhC (Fig. 5A). Our literature search found published micrographs of type material of 7/13 (total of 13 is including the probably wrongly placed *Bry. lijiangensis* Yang, 2002) described '*parvulus* group' species (*Bry. arenosus*, *Bry. asiaticus* Kaczmarek and Michalczyk, 2004, *Bry. atlantis* Fontoura, Pilato and Lisi, 2008, *Bry. brevidentatus* Kaczmarek, Michalczyk and Degma, 2005, *Bry. mateusi* (Fontoura, 1982), *Bry. meronensis* Pilato, Lisi and Binda, 2010, and *Bry. tatrensis* (Węglarska, 1959)). The published LM micrographs that we studied did indicate that weakly developed EEs were present in all seven species, except for those of *Bry. arenosus.* However, we did observe the indications of weakly developed EEs in our own DIC and PhC studies of *Bry. arenosus*. We did not find published SEM micrographs of any of these seven species. However, a SEM micrograph of a specimen identified as '*Bry. parvulus*' (Figure 91 in Maucci, 1986) from Italy showed the anterior dorsal plates with EEs present upon them.

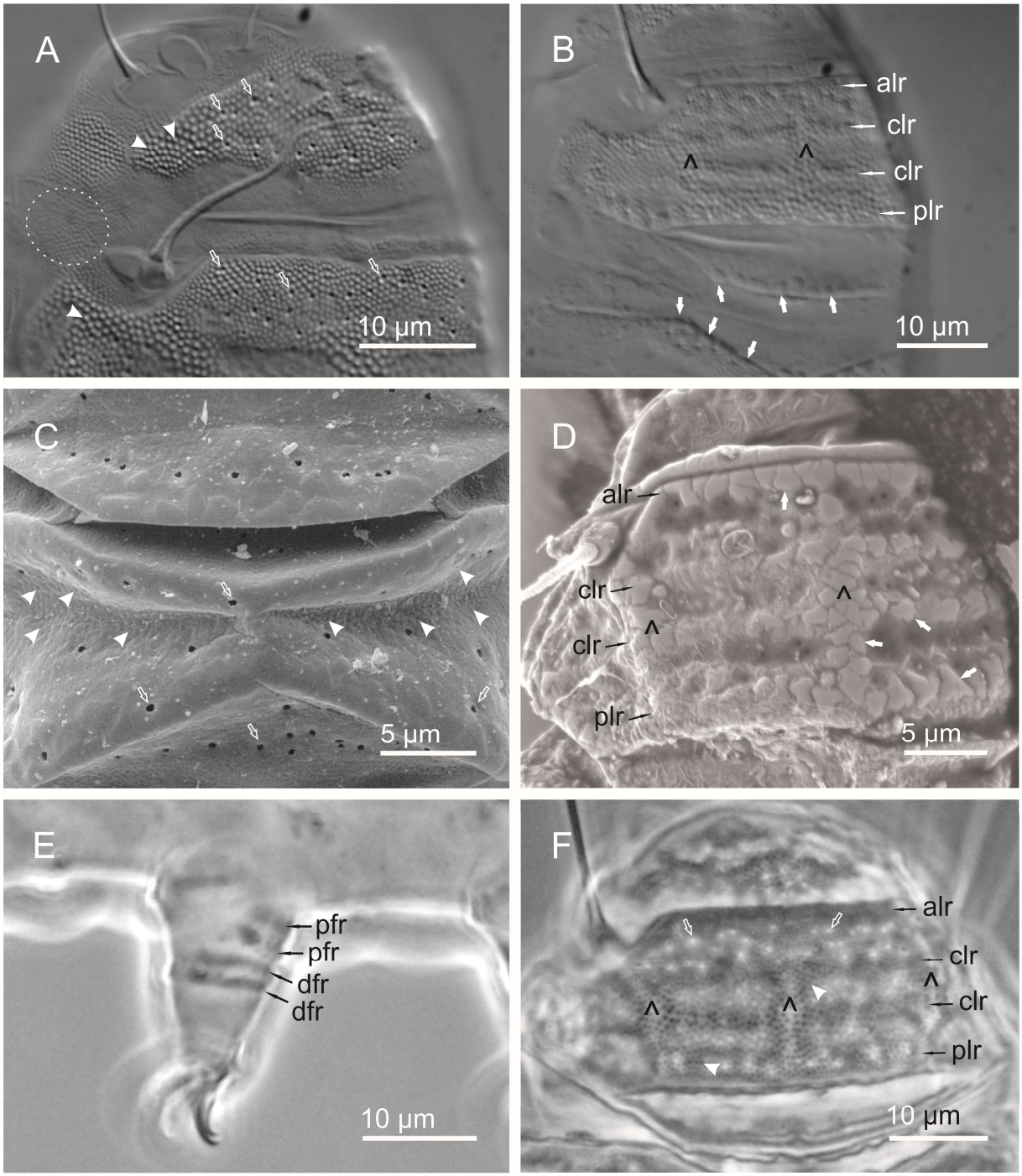

Figure 2: Cuticular structures present among *Bryodelphax* spp. **A** types of cuticular sculpture element (DIC); **B** scapular plate ridges and epicuticular elements (DIC); **C** types of cuticular sculpture element (SEM); **D** scapular plate ridges and epicuticular elements (SEM); **E** femoral plate ridges (PhC) including a pair of proximal femoral ridges (pfr) and a pair of distal femoral ridges (dfr); **F** scapular plate ridges and epicuticular elements (PhC). Filled white arrowheads= intracuticular pillars, hollow white arrows= pores, dashed circle= zone of fine pillars, filled white arrows= epicuticular elements, scapular plate ridges: ^= longitudinal ridge, alr= anterior latitudinal ridge, clr= central latitudinal ridge, plr= posterior latitudinal ridge.

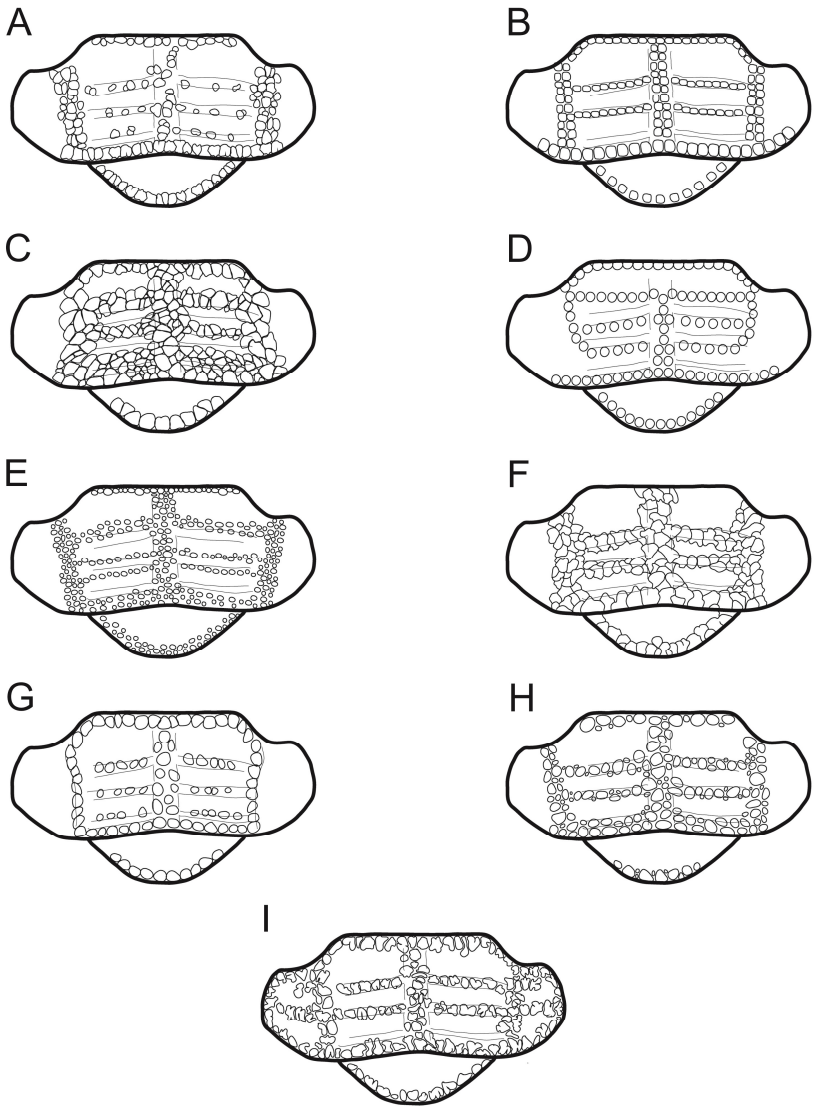

Figure 3: Schematic representations of epicuticular elements on scapular and m1a plates of *Bryodelphax* species. **A** *Bry. aaseae*; **B** *Bry. australasiaticus*; **C** *Bry. instabilis*; **D** *Bry. maculatus*; **E** *Bry. mareki*; **F** *Bry. nigripunctatus*; **G** *Bry. olszanowskii*; **H** *Bry. pucapetricolus* sp. nov.; **I** *Bry. wallacearthuri* sp. nov.

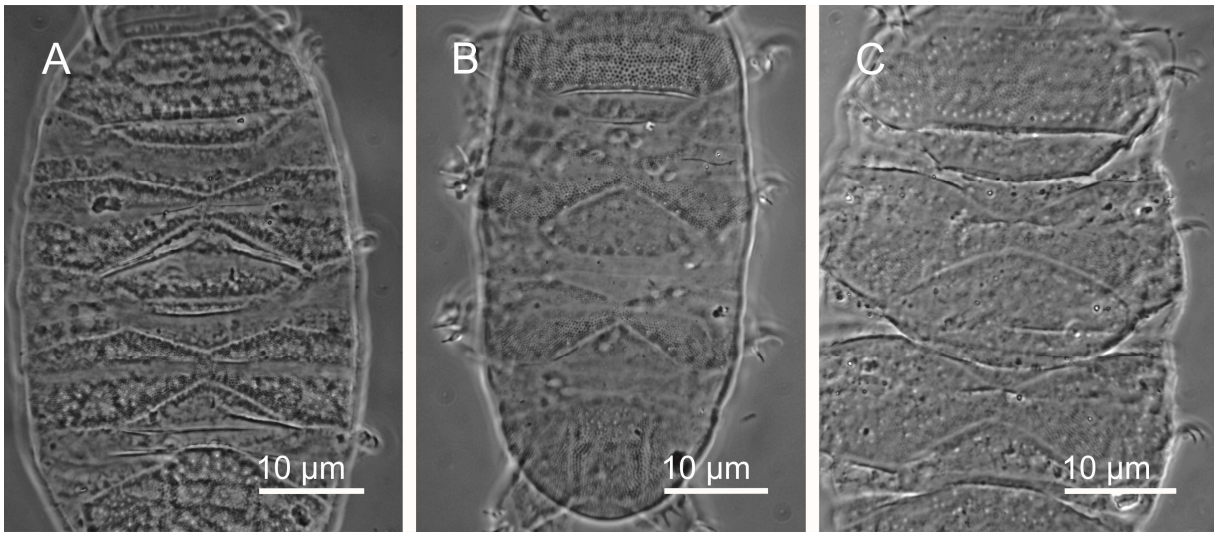

Figure 4: Degrees of relief of the dorsal cuticle in PhC. **A** high relief and contrast (*Bry. wallacearthuri* sp. nov.); **B** standard relief and contrast (*Bry. pucapetricolus* sp. nov.); **C** low relief and contrast (*Bry. iohannis* paratype).

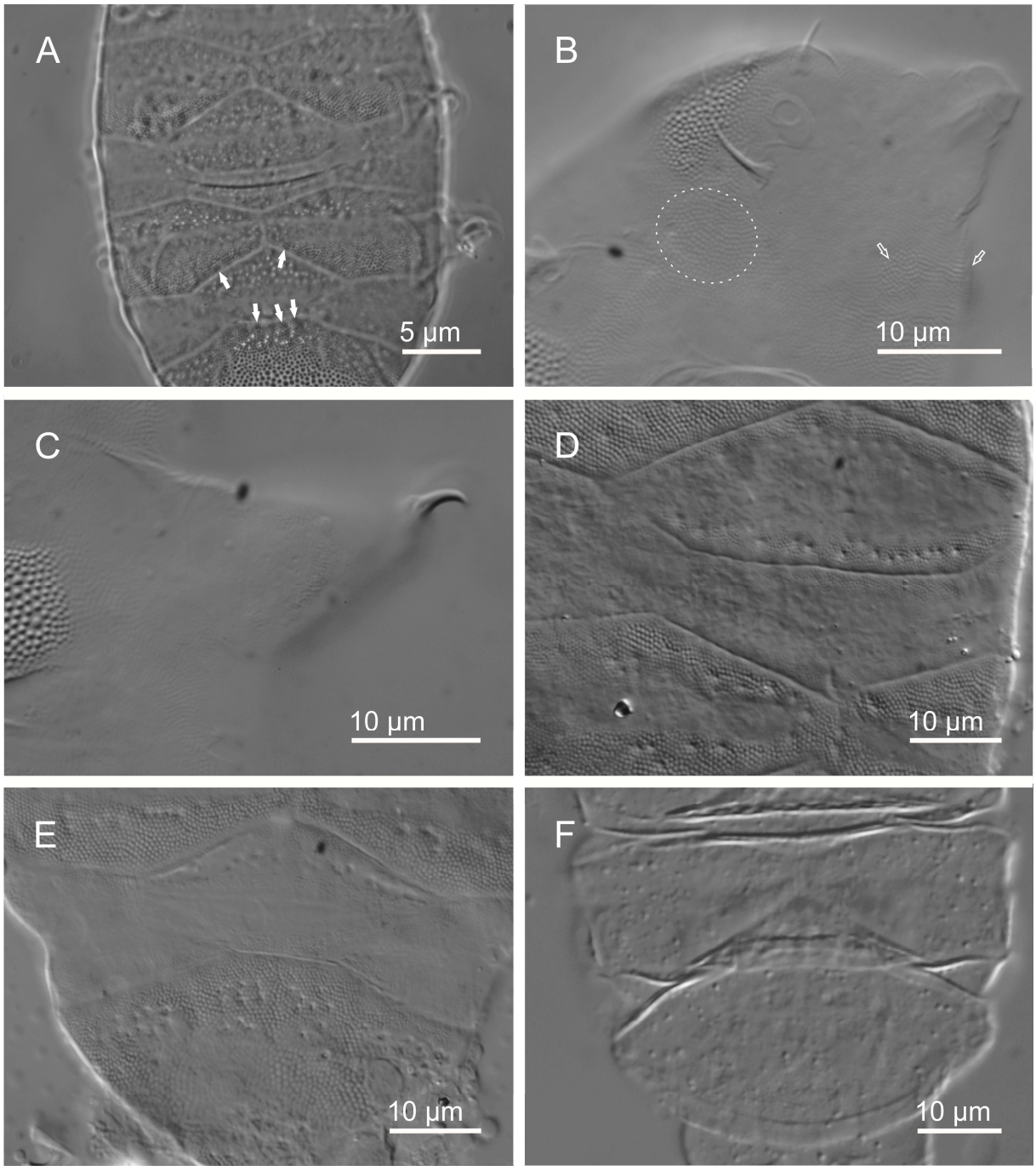

Figure 5: A–C *Bry.* cf. *parvulus* (Ireland). **A** dorsal cuticle with weakly developed epicuticular elements (= filled white arrows) (PhC); **B** patch of pillars at position of lateral cephalic plate (dashed circle) and weakly developed subcephalic ventral plates (= white hollow arrows) (DIC); **C** femoral region of legs I (DIC); **D, E** '*Brc. intermedius laevis*' (Greenland) (DIC), **D** smooth median plate 2 posterior part (m2p), **E** median plate 3 (m3); **F** *Brc. intermedius intermedius* (Australia), specimen with subducted median plate 3 (DIC).

Structure of median plates

The structure of the three dorsal cuticular median plates were observed with special attention to median plate 3 (m3). All observed *Bryodelphax* and *Bryochoerus* specimens shared a similar structure of median plates 1 and 2 (m1 and m2). M1 and m2 show a primary division formed by a transversal crest into an anterior part (m1a/m2a) and a posterior part (m1p/m2p). Each of these parts has a secondary division formed by a median transverse furrow further subdividing the part into an anterior portion and a posterior portion (Fig. 21A). Almost all species of *Bryodelphax* that we studied, as per the genus definition, displayed an m3 structure which lacked a primary division formed by a transversal crest (*i.e.*

m3 not divided into an anterior part (m3a) and posterior part (m3p)). Although typically among *Bryodelphax*, m3 did have a median transverse furrow (*i.e.* the source of the secondary division that subdivides anterior and posterior portions within m1a, m1p, m2a, and m2p) (Fig. 12A). A median longitudinal ridge occurs on all median plates at the body dorsomidline in some species (Fig. 15) but could be difficult to observe in LM.

Our LM observations found apparent difference between the m3 structure of *Bry. pucapetricolus* sp. nov. and the other studied *Bryodelphax* species in that both a primary and secondary division appeared to be present on the m3 of *Bry. pucapetricolus* sp. nov. (Figs. 4B, 10A, C, 12B, C, 13A, 14A). This condition appeared as an m3 divided into distinct m3a and m3p parts (as occurs in m1 and m2) resulting in an overlap of this character with the diagnosis of *Bryochoerus*. The published micrographs of *Brc. liupanensis* Xue, Li, Wang, Xian and Chen, 2017 that we studied (only LM available, Figures 1a, 2b, c in Xue et al., 2017) appeared to show similar divisions of the m3 to *Bry. pucapetricolus* sp. nov.

However, the results of our SEM analysis of the *Bry. pucapetricolus* sp. nov. m3 differed from our LM observations. SEM showed that rather than having both a primary division into m3a and m3p formed by a transversal crest and a secondary division formed by a transverse furrow, the *Bry. pucapetricolus* sp. nov. m3 has only a median transverse furrow (*i.e.* it lacks a primary division similar to that which occurs on m1 and m2). (Fig. 15A, C). The portion of the *Bry. pucapetricolus* sp. nov. m3 that is anterior to the median transverse furrow has an unusual distribution of sculpture elements where a heavily sculptured zone towards the m3 frontal margin is followed caudally by a distinct smooth band immediately preceding the median transverse furrow. In other *Bryodelphax* species sculpture elements appeared to be more uniformly distributed on the entire portion of m3 anterior up to the median transverse furrow (our own LM observations and published SEM micrographs: Figure 13 in Kristensen et al., 2010; Figures 2, 6, 8 in Gąsiorek et al., 2017; Figures 4B, 8A in Gąsiorek et al., 2020a). The distinct border between the sculptured and unsculptured areas of the *Bry. pucapetricolus* m3 anterior to the median transverse furrow (as seen in SEM) appeared to cause the appearance in LM of an m3 divided in a similar way to m1 and m2. We refer to this point on m3 between the very different sculpture element conditions as a tertiary division (Fig. 15C). It is known only from our studies in *Bry. pucapetricolus*. No published SEM images of *Bryochoerus* taxa were found for further comparison.

Lateral cephalic plates

A lateral cephalic plate (lcp) positioned at each lateral side of the head adjacent to the cephalic plate was observed on all of the studied '*weglarskae* group' species (Figs. 2A, 7A, 11A-C, 13B, 16B, 19A-D, 26B, 27). These plates exhibited morphological variation. Lcps were observed to occur to different degrees of sclerotization with some species having weakly defined, sometimes difficult to observe, lcps (*Bry. australasiaticus, Bry. decoratus*, *Bry. instabilis*, *Bry. maculatus*, *Bry. mareki*, *Bry. parvuspolaris*, *Bry. weglarskae*), while others showed evident, strongly developed lcps (*Bry. aaseae*, *Bry. iohannis*, *Bry. nigripunctatus*, *Bry. olszanowskii*, *Bry. pucapetricolus* sp. nov., *Bry. wallacearthuri* sp. nov.). The occurrence and development of the three main types of sculpture elements upon lcps also varied between species. Additionally, the lcp position was seen in some species to be in contact with the cephalic plate posterior corners (*e.g. Bry. aaseae*, *Bry. wallacearthuri* sp. nov. (Fig. 19A-D)) or set apart by a small distance (*e.g. Bry. iohannis*, *Bry. pucapetricolus* sp. nov. (Fig. 11A, B)).

We were not able to determine the status of lcps in *Bry. amphoterus*, *Bry. kristenseni*, or *Bry. sinensis* because we did not observe the type material of these species and we could not make determinations on the basis of the published drawings or micrographs. We were only able to evaluate the lcp area of one representative taxon of the '*parvulus* group', *Bry.* cf. *parvulus*, because the *Bry. arenosus* paratype we viewed was not suitably oriented to observe this feature. An lcp was not formed on the *Bry.* cf. *parvulus* specimens that we examined. Rather, a dense concentration of fine pillars was visible on the cuticle in the area corresponding to the lcp position on the examined '*weglarskae* group' species (Fig. 5B).

Subcephalic ventral plates

The paired subcephalic ventral plates (svps) were evaluated among '*weglarskae* group' species. We found these plates present in all examined taxa, but similarly to lcps, they occurred with different morphologies and degrees of development in different species (Figs. 7A, 11C, 13B, 16B, 19C-F, 27). We observed svps that appeared as ovoid or roundish defined elevations with clear sclerotization (*Bry. aaseae*, *Bry. iohannis, Bry. maculatus*, *Bry. olszanowskii*, *Bry. weglarskae*), rounded, weakly demarcated areas (*Bry decoratus*, *Bry. instabilis*, *Bry. mareki*, *Bry. parvuspolaris*, *Bry. nigripunctatus*, *Bry. pucapetricolus* sp. nov.), or more elongate, slightly triangulate areas (*Bry. australasiaticus*). All specimens of *Bry. wallacearthuri* sp. nov. showed an atypical svp form with a pair of well-developed plates merged together into a solid ridge-like structure (Figs. 19C-F).

We were not able to find any published micrographs of *Bry. amphoterus* or *Bry. sinensis*, but the PhC figures that accompany the description of *Bry. kristenseni* showed that the paired svps of that species are evident and strongly sculptured (Figure 1C in Lisi et al., 2017). We noticed the presence of weakly developed svps, sculptured only with intracuticular pillars, on all specimens of *Bry.* cf. *parvulus* from the Burren (Fig. 5B). The cephalic region of the paratype of *Bry. arenosus* that we viewed was not in a suitable condition to view this character. We found no published images of the ventral surfaces of other '*parvulus* group' species that could be used to study this character.

Ventral plate shape and size

We observed that '*weglarskae* group' species that share the same number of rows of ventral plates and the same numbers of plates within each row could exhibit interspecific variation in the ventral plate morphology. This variation was seen in the shape, size, development, and types of sculpture of the ventral plates. *Bry. aaseae* and *Bry. kristenseni* both have ten rows of ventral plates with each row containing the same number of plates (*N.B.* the presence of the unpaired plate at the level of legs I of *Bry. kristenseni* could not be definitely confirmed by the describing authors (Lisi et al., 2017)). The ventral plates of *Bry. aaseae* were observed to be well-developed and evident, while those of *Bry. kristenseni* were described as poorly developed and difficult to discern (Lisi et al., 2017). *Bry. wallacearthuri* sp. nov. (Fig. 27B) and *Bry. weglarskae* both have nine rows of ventral plates with the same number of plates per row. Our examination of the plates of these species found the ventral plates at corresponding positions to be of different shapes and sizes, and with different sculpturing upon them (compare Figs. 6A vs. 6B and 6C vs. 6D). Similarly, our comparisons of the ventral plates of paratypes of *Bry. maculatus* vs. *Bry. nigripunctatus* females (both share three rows of plates with the same configuration) and *Bry. pucapetricolus* sp. nov. (Fig. 27A) vs. *Bry. nigripunctatus* males (both have only a pair of subcephalic plates and a pair of lateral gonoplates (*i.e.* plates lateral to the gonopore)) showed morphological differences despite the overlaps in plate number per row (compare Fig. 6E vs 6F).

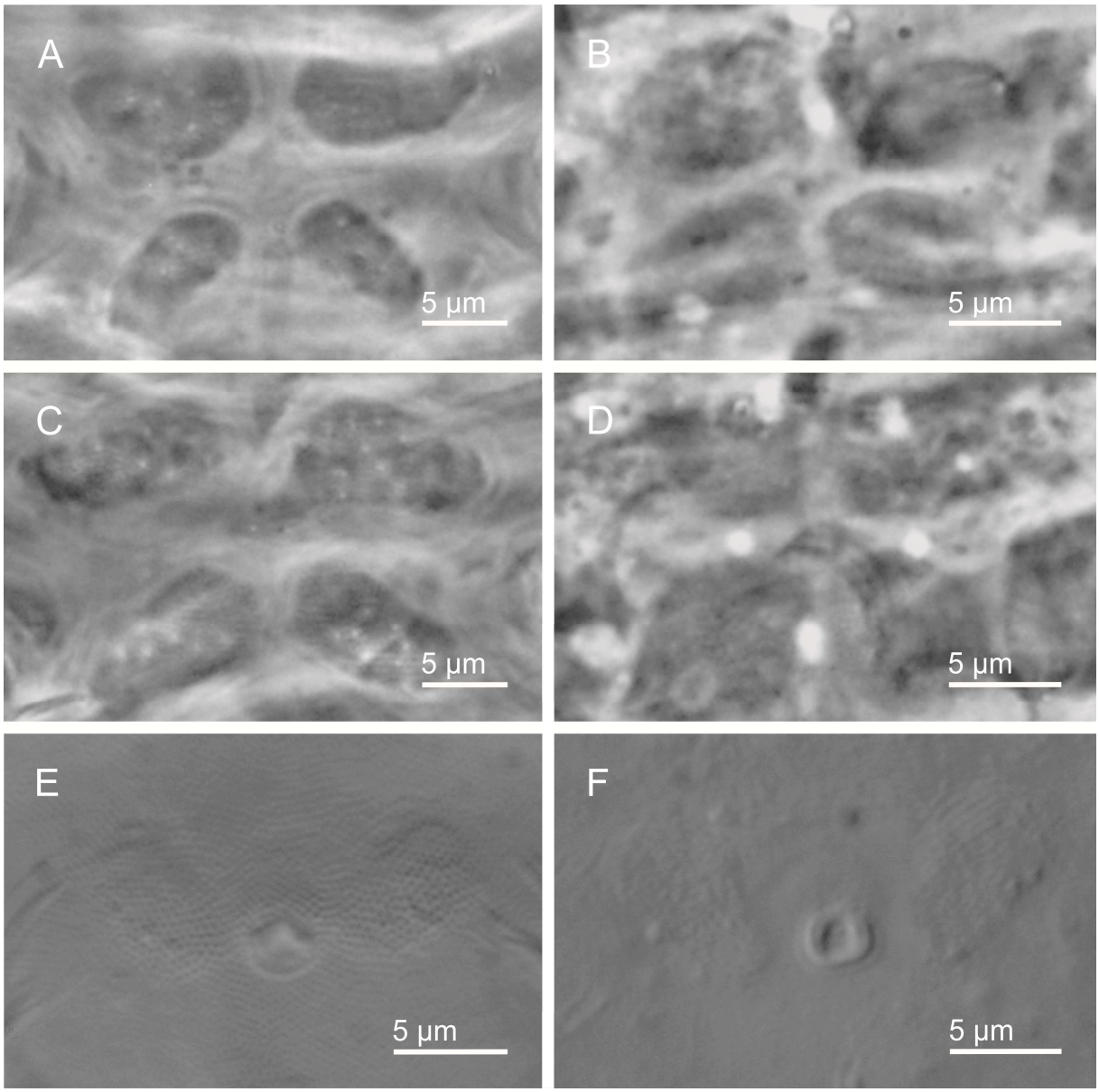

Figure 6: Comparisons of ventral plate shape in size in species that share the same plate configuration. **A, B** Rows four and five (PhC), **A** *Bry. wallacearthuri* sp. nov. vs. **B** *Bry. weglarskae* paratype; **C, D** Rows six and seven (PhC), **C** *Bry. wallacearthuri* sp. nov, vs. **D** *Bry. weglarskae* paratype; **E, F** lateral gonoplates, male (DIC), **E** *Bry. pucapetricolus* sp. nov. vs. **F** *Bry. nigripunctatus* paratype.

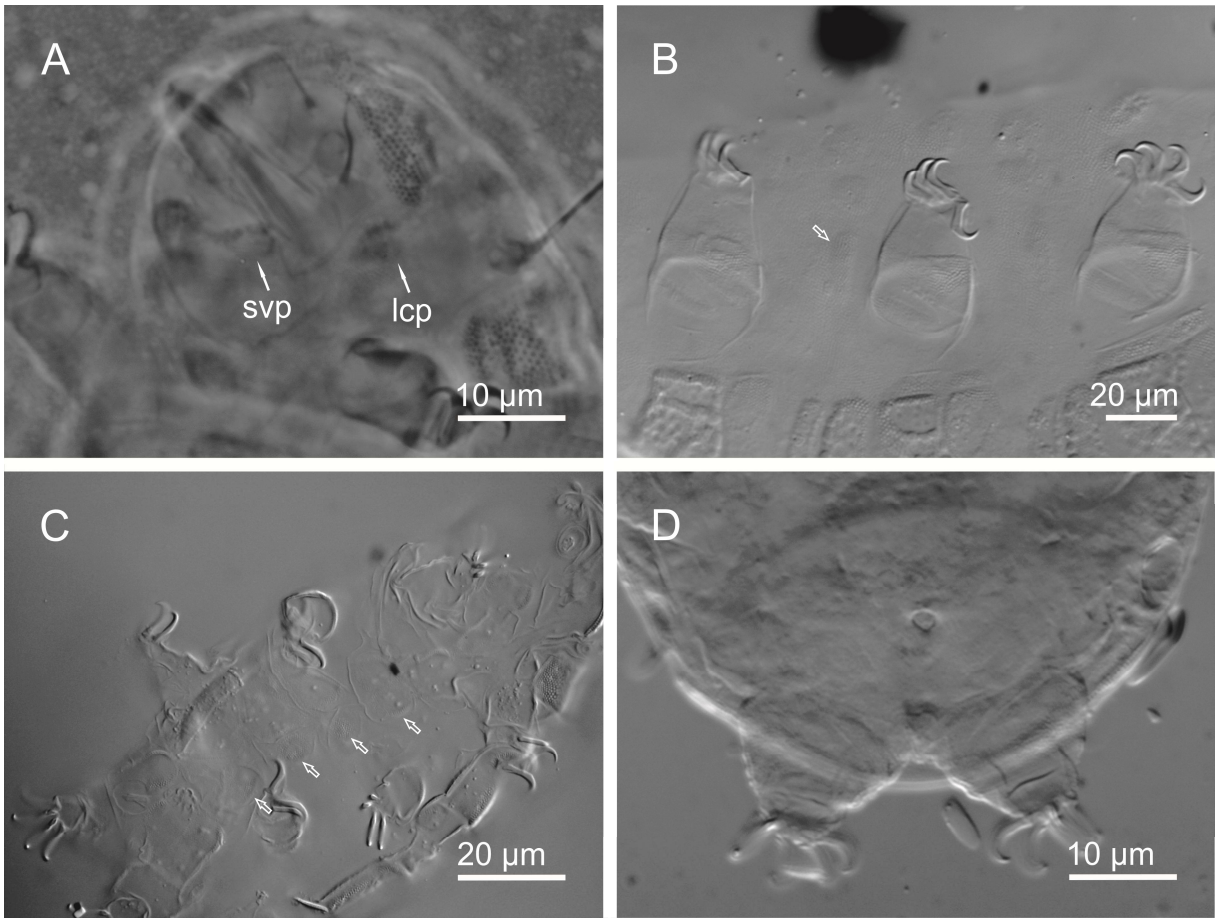

Figure 7: Observations on various type material. **A** *Bry. parvuspolaris* holotype (PhC image courtesy of Ł. Kaczmarek), undescribed lateral cephalic plates (lcp) and subcephalic ventral plates (svp) present; **B** *Bry. decoratus* paratype (DIC), undescribed lateral plates present in ventral row immediately anterior to legs II (Row two); **C** *Bry. mareki* paratype (DIC), additional rows of undescribed ventral plates present; **D** *Bry. aaseae* paratype (DIC), males not previously recognised. White hollow arrows= undescribed ventral plates.

During our examinations of *Bry. decoratus* and *Bry. mareki*, we unexpectedly encountered additional ventral plates than what were originally described for each species. The species diagnosis of *Bry. decoratus* includes seven rows of plates with two plates present in the row in line with legs II (Row II). We observed an additional pair of plates in that row that are positioned laterally to the described plates so that the row total includes four plates (Fig. 7B). The species diagnosis of *Bry. mareki* includes three rows of plates. We observed at least seven rows of plates on the examined paratypes (Fig. 7C). Indications of the additional plates were also observed on published SEM micrographs (Figures 1C and 3D in Kayastha et al., 2021).

Leg plates

Our examinations of the '*weglarskae* group' species revealed a range of conditions of the plated areas of the legs. Coxal and femoral leg plates were present on all 12 '*weglarskae* group' species that we directly viewed in our microscopy studies. These plates varied interspecifically in their degree of development and their sculpturing (types of elements present and morphology). The coxal plates of *Bry. aaseae*, *Bry. mareki*, and *Bry. pucapetricolus* sp. nov. appeared in LM and SEM to be sculptured only with intracuticular pillars and pores with EEs absent or not visible (Figure 14 in Kristensen et al., 2010;1A, 4B in Kayastha et al., 2021; Figs. 13, 14B, C). The coxal plates of *Bry. australasiaticus*, *Bry. decoratus,* and *Bry. olszanowskii* appeared in LM to be sculptured similarly to the former species, but we were not able to definitely confirm the sculpture morphology for these species because no published SEM images were available for *Bry. decoratus* and the published SEM images of *Bry. australasiaticus* and *Bry. olszanowskii* did not focus precisely on the coxal plates. A published SEM image of *Bry. instabilis* appeared to show coxal plates with intracuticular pillars and small, weakly developed EEs on the entire plate surfaces (Figure 7 in Gąsiorek and Degma, 2018). The coxal plates of *Bry. iohannis*, *Bry. maculatus, Bry. nigripunctatus*, and *Bry. wallacearthuri* sp. nov. all appeared in our LM studies to be sculptured with intracuticular pillars and a single row of well-developed EEs and with pores absent or not visible (Figs. 2E, 21A, 22A, 23A-C). With the exception of *Bry. iohannis* for which no

SEM images were available, the EEs that appeared to form a line on the coxal plates of these species were shown by SEM to be of differing morphologies. SEM images demonstrate that the coxal plate surfaces of all three species are not smooth, but only in *Bry. maculatus* do large, well-developed, rounded EEs form a line on the coxal plate as it appears in LM (Figure 18 in Gąsiorek et al., 2017). In *Bry. wallacearthuri* sp. nov. and *Bry. nigripunctatus* EEs actually cover the entire coxal plate surfaces with those along a more elevated ridge forming the illusion in LM of only a single line of EEs being present. EEs are well developed and clearly polygonal on the coxal plates of *Bry. wallacearthur*i sp. nov. (Fig. 23E, F) and irregularly shaped and less apparent on those of *Bry. nigripunctatus* (Figure 8B in Gąsiorek et al., 2020a). We were only able to study the coxal plates on legs IV of *Bry. weglarskae* due to specimen position. We were not able to clearly view the types of sculpturing present or degree of development of the coxal plates of that species. We were not able to determine more detailed information about the coxal plates of *Bry. parvuspolaris* from the published micrographs other than that coxal plates are present on that species.

The femoral plates of all observed '*weglarskae* group' species have epicuticular ridges which could appear differently in LM and SEM. All '*weglarskae* group' species have a pair of horizontally orientated distal femoral plate ridges and most species were observed to have an additional pair of shorter proximal plate ridges (Fig. 2E). The presence and morphology of sculpture elements on the femoral plates and on the associated ridges and the development of the ridges was not homogenous among the observed species. In our LM observations of *Bry. olszanowskii*, *Bry. pucapetricolus* sp. nov., and *Bry. weglarskae* only the distal pair of femoral plate ridges were visible. These appeared poorly defined, as did the femoral plates themselves, which sometimes were not discernible at all in LM. When the femoral plates of these species were observable in LM, the sculpture elements were poorly represented. Intracuticular pillars were present but individual EEs were either not visible or not well-defined and poorly visible, and pores could rarely be seen on the femoral plates (Figs. 13, 14A).

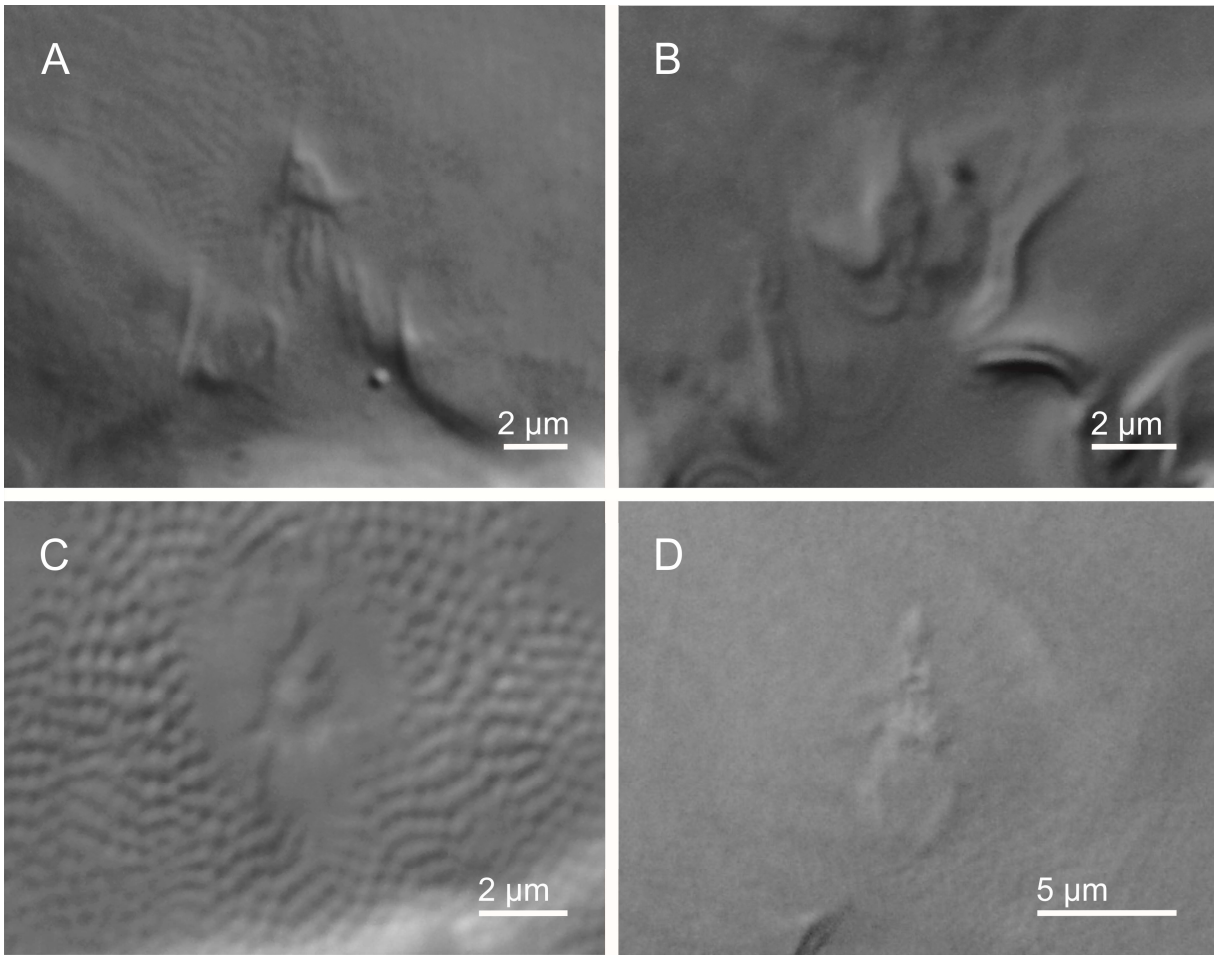

Figure 8: Morphology of the anal system in various limnoterrestrial heterotardigrade taxa (DIC). **A** *Bry. pucapetricolus* sp. nov.; **B** *Bry. wallacearthuri* sp. nov.; **C** *Par.* cf. *chitonides* (Ireland); **D** *Pseudechiniscus* sp. (Ireland).

A SEM image of the femoral plate of legs IV of *Bry. olszanowskii* showed that weakly developed EEs are present on a distal ridge (Figure 6b in Kaczmarek et al., 2018). The presence of the proximal pair of ridges on the femoral plates of *Bry. olszanowskii* was not able to be confirmed from the published SEM micrographs. The distal femoral ridges of *Bry. pucapetricolus* sp. nov. ridges were confirmed to have EEs present, though they also were only clearly distinguishable with SEM (Fig. 14B). We were not able to confirm the presence of proximal ridge pair on *Bry. pucapetricolus* sp. nov. femoral plates, but at least one weakly developed proximal ridge was observed with SEM (Fig. 14B). No published SEM micrographs of *Bry. weglarskae* were found, so the details of the femoral plate ridge morphology could not be confirmed for that species.

Bry. aaseae, *Bry. australasiaticus*, *Bry. instabilis*, *Bry. maculatus*, and *Bry. mareki* all show the full complement of ridges with both a distal and proximal pair present on the femoral plates. LM and SEM observations showed that the femoral plates of these species were sculptured with intracuticular pillars and with EEs distinctly formed along the plate ridges (visible with PhC as dark dots in rows), but not on the rough plate surface between ridges. EEs on the ridges of these species could be more weakly developed (*e.g. Bry. mareki*) or strongly developed and clearly visible as individual entities (*e.g. Bry. maculatus*). The femoral plates of *Bry. wallacearthuri* sp. nov. were sculptured with intracuticular pillars, and large, well-developed EEs along the femoral plates ridges that were clearly visible in LM (Figs. 21, 22, 23A-D). The EEs could be seen (only with SEM) to also occur on the entire femoral plates surface between ridges on *Bry. wallacearthuri* sp. nov. (Fig. 23E-G). *Bry. decoratus*, *Bry. iohannis*, and *Bry. nigripunctatus* all had both the distal and proximal pair of femoral plate ridges sufficiently well developed to be observed in LM. Although our LM studies showed that the femoral plates of these species had EEs present along the plate ridges (visible with PhC as dark dots in rows), we were not able to determine if the EEs were mostly confined to the plate ridges (as in *e.g. Bry. aaseae*), or if well-developed EEs covered the entire plate (as in *Bry. wallacearthuri* sp. nov.) because only EEs that occur along ridges are clearly visible in LM. There were no available SEM images for *Bry. iohannis* or *Bry. decoratus* and the available SEM images for *Bry. nigripunctatus* were not suitable for studying this character. We could not determine the condition of the femoral plates in *Bry. parvuspolaris* as these were not well visible in the published micrographs (only PhC available).

The femoral plates of legs IV, besides bearing a dentate collar in *Bry. amphoterus*, *Bry. instabilis*, *Bry. iohannis*, *Bry. maculatus*, *Bry. nigripunctatus, Bry. olszanowskii*, *Bry. parvuspolaris*, *Bry. pucapetricolus* sp. nov., *Bry. wallacearthuri* sp. nov., and *Bry. weglarskae*, could in the '*weglarskae* group' also be seen to have a slightly different appearance to the femoral plates of legs III. Some species that did not have pores present on the femoral plates of legs I–III had clearly visible pores on the femoral plates of legs IV (*e.g. Bry. australasiaticus*, *Bry maculatus*). The femoral plates IV sometimes appeared to have EEs developed to a lesser degree and arranged more loosely than on femoral plates I–III (*e.g. Bry. iohannis*, *Bry. maculatus*). In all cases, the morphology of the EEs of the coxal and femoral plates resembled those of the dorsal and ventral plates of that species.

The examined paratype of *Bry. arenosus* was not in a suitable orientation for observing the leg structures. The coxal area of the Burren *Bry*. cf. *parvulus* specimens appeared smooth, with intracuticular pillars weakly visible in LM. The femoral region of all *Bry*. cf. *parvulus* legs was clearly thickened and covered with densely arranged, well visible intracuticular pillars, sometimes also with pores visible in LM (Fig. 5C). While these leg areas appeared thickened, the development of distinct plates with well-defined borders was not discernable with LM alone. The published SEM micrograph of the Italian '*Bry. parvulus*' (Figure 91 in Maucci, 1986) did not have sufficient focus on the legs for any further observations.

Morphometry relating to the gonopore

Prior to initiating an examination focused on morphometric characteristics relating to the gonopore, we evaluated morphological characters in the studied taxa for evidence of allometry. This was done to ensure the suitability of the use of ratios (*psc* and *pbl*) to reduce the effects of body size in our species comparisons below. Slopes of the regression lines of log-log transformed measurement data were compared to a slope of 1 following checks for outliers and independence of observations (Durbin Watson test) whenever $n \geq 8$. Following the methods and criteria of Bartels et al. (2011) none of the evaluated characters showed evidence of allometry (*i.e.* the slope of the regression line was not significantly different from a slope of 1 shown by t-tests ($p = 0.05$)) (Supplementary File 4). Thus, it was determined that the use of ratios was suitable for further comparisons of the measured traits between taxa.

We measured the diameter of the female and male gonopore (in μm and calculated as a *psc* value) and the distance between the gonopore and anus aperture (in μm and calculated as *psc* and *pbl* values) for suitably oriented individuals of *Bry. pucapetricolus* sp. nov., *Bry. wallacearthuri* sp. nov., and other '*weglarskae* group' comparative specimens. We also measured these traits in all suitable specimens of *Par.* cf. *chitonides* and *Pseudechiniscus* sp. collected from the Burren. We observed differences in the means and ranges for these characters between sexes and between species (Tables 1–3, Supplementary Files 5, 6).

Table 1: Measurements (µm) relating to the anus and gonopore in observed type material or reference specimens. n= number of individuals measured for that character, x̄= mean, s= standard deviation, f= females, m= males.

Species	Sex	Gonopore diameter						Gonopore to anus distance					
		n	µm		*psc*		n	µm		*psc*		*pbl*	
			x̄	s	x̄	s		x̄	s	x̄	s	x̄	s
'*Brc. intermedius laevis*' (Greenland)	f	2	8.5	1.3	42.1	6.2	2	21.4	1.5	105.6	7.5	12.7%	1.1
	m	1	2.2	-	12.9	-	1	14.3	-	84.1	-	10.8%	-
Bry. aaseae Kristensen et al., 2010	f	10	7.0	0.7	41.4	5.5	10	13.7	1.6	81.2	12.3	12.2%	0.9
	m	10	2.0	0.3	12.1	2.4	10	9.0	2.1	55.4	13.7	10.3%	1.0
Bry. australasiaticus Gąsiorek et al., 2020	f	2	5.8	0.8	39.5	10.5	2	13.0	0.0	88.7	11.5	13.6%	0.4
Bry. decoratus Gąsiorek et al., 2020	f	3	5.6	1.0	35.7	4.6	3	14.3	1.6	90.9	6.0	12.7%	0.6
Bry. iohannis Bertolani et al., 1996	f	10	7.0	0.9	33.9	4.8	12	18.9	1.4	91.8	12.2	12.9%	1.3
Bry. instabilis Gąsiorek and Degma, 2018	f	2	9.6	0.1	48.8	3.7	2	14.6	0.1	74.7	5.4	13.1%	1.8
Bry. maculatus Gąsiorek et al., 2017	f	2	10.3	0.1	50.6	0.0	2	16.0	0.3	78.5	0.6	11.9%	1.0
Bry. mareki Kayastha et al., 2017	f	2	7.3	1.7	36.9	8.3	2	19.3	5.4	97.15	26.8	12.4%	0.5
Bry. nigripunctatus Gąsiorek et al., 2020	f	4	7.9	0.5	44.8	4.9	4	17.9	3.5	100.5	11.7	13.3%	1.8
	m	3	3.7	0.3	22.3	2.0	3	10.0	2.7	59.7	15.9	7.4%	1.4
Bry. olszanowskii Kaczmarek et al., 2018	f	4	8.0	0.4	42.0	1.1	4	14.8	0.6	78.1	3.5	12.1%	0.7
Bry. cf. *parvulus* (Ireland)	f	1	7.4	-	44.4	-	1	18.4	-	109.7	-	13.1%	-
Bry. pucapetricolus sp. nov.	f	10	6.1	0.7	36.8	6.2	10	13.8	1.6	83.5	10.4	11.2%	0.9
	m	10	2.3	0.5	14.3	3.2	10	9.6	1.3	60.9	7.9	8.3%	1.0
Bry. wallacearthuri sp. nov.	f	11	7.2	0.7	41.9	2.9	10	17.1	2.8	99.9	12.6	13.5%	1.2
	m	3	2.3	0.5	14.9	4.2	3	8.5	2.5	54.9	12.1	7.4%	1.7
Bry. weglarskae (Pilato, 1972)	f	2	5.1	0.8	27.0	3.0	1	14.1	-	77.5	-	10.9%	-
Par. cf. *chitonides* Cuénot, 1926 (Ireland)	f	7	9.4	0.6	-	-	8	18.6	2.3	-	-	11.5%	0.1
	m	6	2.7	0.5	-	-	6	15.4	1.4	-	-	10.0%	1.3
Pseudechiniscus sp. (Ireland)	f	6	8.3	0.9	37.3	6.5	7	17.7	1.6	77.8	9.5	10.3%	0.7
	m	11	3.7	1.4	18.6	4.8	11	11.4	2.6	58.7	10.8	7.8%	1.1

Among the examined material, four *Bryodelphax* species had available specimens of both sexes where the gonopore diameter and gonopore to anus distance were suitable for measurement. These species were *Bry. aaseae* (the original species description specified that only females were found (Kristensen et al., 2010)) (Fig. 7D), *Bry. nigripunctatus*, *Bry. pucapetricolus* sp. nov., and *Bry. wallacearthuri* sp. nov. In all of these species the female gonopore diameter was larger than the male gonopore diameter. Moreover, the female and male ranges were discriminatory as both µm and *psc* values. The distance between the female gonopore and anus was longer than the male gonopore and anus distance for all four species (in terms of µm, *psc*, and *pbl*). In *Bry. nigripunctatus* and *Bry. wallacearthuri* sp. nov. the ranges for all values of gonopore to anus distance were discriminatory by sex, whereas in *Bry. aaseae* and *Bry. pucapetricolus* sp. nov. there were slight overlaps in the male maxima and female minima.

Bry. aaseae and *Bry. pucapetricolus* sp. nov. were the only species for which there were n≥ 10 measurable individuals of both sexes. For these two species, we used t-tests or Mann-Whitney U tests to look for statistically significant intraspecific difference between the sexes in the gonopore diameter and gonopore to anus distance *psc* and the gonopore to anus distance *pbl* values. Mann-Whitney U tests showed the female gonopore diameter *psc* was significantly larger than the male gonopore diameter *psc* in both *Bry. aaseae* ($U= 100.0$, $p< 0.001$) and *Bry. pucapetricolus* sp. nov. ($U= 100.0$, $p< 0.001$). Independent t-tests found that the female gonopore to anus distance *psc* and *pbl* were also

significantly greater than the male gonopore to anus distance *psc* and *pbl* in both *Bry. aaseae* (t= 4.4, $p<$ 0.001 for *psc* and t= 4.5, p< 0.001 for *pbl*) and *Bry. pucapetricolus* sp. nov (t= 5.5, $p<$ 0.001 for *psc* and t= 7.4, p< 0.001 for *pbl*).

For interspecific statistical comparisons of the gonopore diameter *psc*, gonopore to anus *psc*, and gonopore to anus *pbl* values we performed one-way ANOVAs following nonsignificant Levene's and Shapiro-Wilk tests for all *Bryodelphax* for which we were able to obtain measurement data for n≥ 10. These were *Bry. aaseae* females and males, *Bry. iohannis* females, *Bry. pucapetricolus* sp. nov. females and males, and *Bry. wallacearthuri* sp. nov. females. Independent one-way ANOVA of the female gonopore diameter *psc* of the four species showed significant difference across all groups (F= 6.0, $p<$ 0.002, ω^2= 0.3). Post hoc testing with Tukey's correction showed the significant difference occurred between *Bry. aaseae* and *Bry. iohannis* (p= 0.011) and *Bry. iohannis* and *Bry. wallacearthuri* sp. nov. ($p<$ 0.004). Independent one-way ANOVA of the female gonopore to anus distance *psc* of the four species showed significant difference across all groups (F= 5.1, $p<$ 0.004, ω^2= 0.2). Post hoc testing with Tukey's correction showed the significant difference occurred between *Bry. aaseae* and *Bry. wallacearthuri* sp. nov. ($p<$ 0.006) and *Bry. pucapetricolus* sp. nov. and *Bry. wallacearthuri* sp. nov. Independent one-way ANOVA of the female gonopore to anus distance *pbl* of the four species showed significant difference across all groups (F= 8.0, $p<$ 0.001, ω^2= 0.3). Post hoc testing with Tukey's correction showed the significant difference occurred between *Bry. iohannis* and *Bry. pucapetricolus* sp. nov. and *Bry. pucapetricolus* sp. nov. and *Bry wallacearthuri* sp. nov.

The male gonopore diameter and male gonopore to anus distance *psc* and *pbl* was compared between *Bry. aaseae* and *Bry. pucapetricolus* sp. nov. (both n= 10). Significant difference between these two species was not found by a Mann-Whitney U test for the male gonopore diameter *psc* values (U= 24.5, p= 0.06) or an independent t-test for the male gonopore to anus *psc* values (t= -1.2, p= 0.30). However, when the µm measurement of the male gonopore to anus distance is expressed as a *pbl* value the difference between the two species is highly significant for that character (U= 94.5, $p<$ 0.001) as shown by a Mann-Whitney U test.

Anus morphology

Our microscopy studies of the representative specimens of the Burren heterotardigrade genera *Bryodelphax*, *Parechiniscus*, and *Pseudechiniscus* showed variation of the anus morphology at the genus and possibly species level. The details of the variation were mostly visible only using SEM (Fig. 9) but some general differences were visible with LM (Fig. 8).

Our SEM analyses suggest that the anal system of *Bry. pucapetricolus* sp. nov. consists of two small, rigid lateral lobes and an apparently lamellar central terminal structure, which may appear longitudinally folded. The anal aperture is positioned at the junction of the lateral lobes and the terminal lamellar structure. The cuticle of all components appears to be smooth (Figs. 8A, 9A). In *Bry. wallacearthuri* sp. nov. the anal system appeared similarly composed to that of *Bry. pucapetricolus* sp. nov. (Fig. 8B). However, in the specimen of *Bry. wallacearthuri* sp. nov. that was in a suitable position for viewing the anus in SEM, the anus was in an opened position so that additional lateral folds were visible on either side of the lamellar central terminal structure (Fig. 9B), which could not be observed in the *Bry. pucapetricolus* sp. nov. specimens with SEM (Fig. 9A). The additional lateral folds are smaller than the main lateral lobes. In addition, the lateral lobes of the *Bry. wallacearthuri* sp. nov. anal system appeared larger and more flexible than in *Bry. pucapetricolus* sp. nov. In LM the structure of the anal systems of *Bry. pucapetricolus* sp. nov. and *Bry. wallacearthuri* sp. nov. gave a four-lobed appearance, probably caused by the presence of the central terminal laminar structure. The anal areas of both species were observed to be free from visible fine pillars that are present on the surrounding ventral cuticles. We reviewed all published SEM images of other *Bryodelphax* species to facilitate other intrageneric comparisons but did not find any micrographs that clearly showed the anal system.

The anal system of the *Par.* cf. *chitonides* specimens was observed (Figs. 8C, 9C). Its system is composed of two similar lateral lobes, well-defined, nearly rectangular in shape and a terminal lobe. The lateral lobes are of a similar size to the terminal lobe but the terminal lobe has a fusiform rather than rectangular appearance. The anal aperture occurs at the junction of the three components. The cuticle of the three components does not have a smooth texture. In LM, the lateral and terminal lobes appear well defined and differentiated from each other. The anal system is positioned within a zone in which intracuticular pillars, strongly visible on most of the ventral surface, are absent (Fig. 8C).

We observed using SEM that the *Pseudechiniscus* sp. anal system is composed of two similar rounded, (partially fused) lateral lobes, which are heavily textured with multiple folds and small, globular swellings and a large, unsmooth, papillose terminal lobe (Fig. 9D). The anal aperture occurs at the junction of the three components. In LM the three main components are apparent, particularly the terminal lobe. The anal system is with visible intracuticular pillars (Fig. 8D), but the precise texture of the lateral lobes is visible only in SEM.

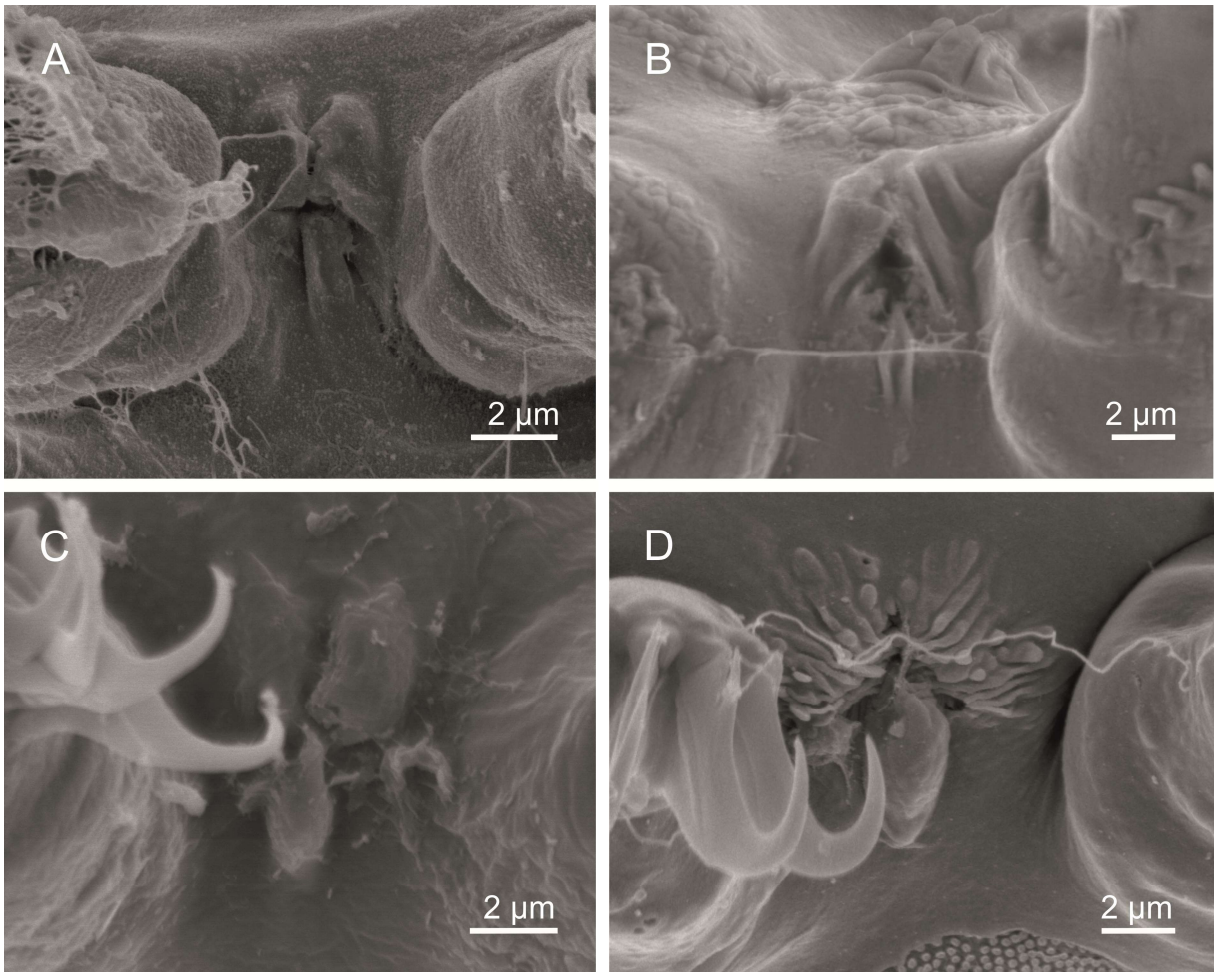

Figure 9: Morphology of the anal system in various limnoterrestrial heterotardigrade taxa (SEM). **A** *Bry. pucapetricolus* sp. nov.; **B** *Bry. wallacearthuri* sp. nov.; **C** *Par.* cf. *chitonides* (Ireland); **D** *Pseudechiniscus* sp. (Ireland).

Description of the new species

Tardigrada Doyère, 1840
Heterotardigrada Marcus, 1927
Echiniscoidea Richters, 1926
Echiniscidae Thulin, 1928
Bryodelphax Thulin, 1928

***Bryodelphax pucapetricolus* sp. nov.** (Figs. 2A-C, 3H, 4B, 8A, 9A, 10–16, 27A)

ZooBank: urn:lsid:zoobank.org:act:0AC14EEB-BC67-4AB5-B23D-835940B0C79E

Type material: 44 specimens on slides (holotype: adult female (Fig. 10A, B) and paratypes: 13 adult females, 17 adult males, 7 adults of undeterminable sex, 3 four-clawed juveniles, 3 two-clawed larvae) and 13 specimens on a SEM stub

Additional material from the type population: 10 specimens reserved for genetic analyses (6 sequenced individuals preserved on voucher slides SPbU299(1–6))

Type locality: Burren National Park, County Clare, Republic of Ireland, 53° 0' 57" N, 8° 58' 58" W, 29 m asl, pleurocarpous moss on limestone pavement, *leg.* E. DeMilio, 17/08/2013

Type repository: The holotype (slide NHMD 922681) and 16 slide mounted paratypes (slides NHMD 922682–922697) and 13 paratypes on a SEM stub (NHMD 922698) are deposited in the Natural History Museum of Denmark, Copenhagen, Denmark. Twenty-one paratypes (slides CE.ER2.1.01–CE.ER2.1.03, CE.ER2.1.05, CE.ER2.1.07, CE.ER2.1.10–CE.ER2.1.12, CE.ER2.1.15, CE.ER2.1.17, CE.ER2.1.18, CE.ER2.1.20–CE.ER2.1.23, CE.ER2.1.26, CE.ER2.1.29, CE.ER2.1.32, CE.ER2.1.38, CE.ER2.1.47, CE.ER2.1.48) are kept in the collection of ED. Three paratypes (slides CE.ER2.1.06, CE.ER2.1.33, CE.ER2.1.44) are deposited in the Bertolani Collection, Department of Life Sciences, University of Modena and Reggio Emilia, Italy. One paratype (slide CE.ER2.1.04) is in the collection of DVT. One paratype (slide CE.ER2.1.35) is deposited at the Department of Animal Taxonomy and Ecology, Institute of Environmental Biology, Adam Mickiewicz University, Poznań, Poland. One paratype (slide UNICT 6010) is deposited in the Binda and Pilato Collection, University of Catania, Italy.

Other population: vicinity of Bellharbour, County Clare, Republic of Ireland, moss on stone wall, *leg.* V. Panov, 24/09/2004 (61 specimens on slides (32 adult females, 15 adult males, 14 four-clawed juveniles, slides SPbU223(18–25, 28–32, 36, 38, 39, 62) and 23 specimens on a SEM stub (SPbU-9) in the collection of DVT).

Etymology: Specific name meaning 'rock dwelling púca', derived from 'púca' the mischievous, shape-shifting spirit of Irish folklore (Irish *púca*= ghost/spirit (anglicized '*pooka*' or '*puck*')) and '*petricolus*' (Latin) referring to the association of the species with limestone pavement.

Species description

Body length (adult) 100.8–134.7 μm, other morphometric data given in Table 2. Cuticle color pale greenish-yellow prior to slide mounting. Red eyes present (observed on one individual in temporary water mount) or absent or not visible after mounting in PVA. Paired cephalic cirri and clavae present. Internal cirrus with expanded basal part (LM) formed by a poorly differentiated, weak cirrophore (SEM). External cirrus with small cirrophore. Cirrus A with evident cirrophore. All cephalic cirri without terminal bifurcation. Other dorsal and lateral cirri absent. Primary clava cylindrical with bluntly tapered apex (Figs. 11A, B, 16B). Secondary clava roughly spatulate, attached to head by a narrower basal portion that expands to a free-hanging slightly asymmetric, broader distal portion following a minor constriction (Figs. 11A-C, 16B). Ten buccal papulae present (Fig. 16B). Buccal-pharyngeal apparatus with long stylet sheaths (6.5–9.7 μm, 40.1–62.0 *psc*) and long stylet supports (4.6–7.1 μm a 28.0–53.4 *psc*). Buccal tube rigid.

Dorsal plates clearly demarcated and without thickened lateral edges (Figs. 13, 14A). Dorsal cuticular plate sculpture consists of three main types of element: round intracuticular pillars, pores, and epicuticular elements (EEs) in form of variably sized, individually well-differentiated, rounded elevations (Figs. 3H, 4B, 10A, C, 11A, B, E, 12A, 13, 14A, 15). Knobby dorsal cuticle relief appears moderately developed in PhC with visible dark, circular areas clearly present but not in particularly high contrast (standard) and with limited distribution (Fig. 4B).

Cephalic plate (cep) with rounded anterior margin, m-shaped posterior margin, and keyhole-shaped dorsomedial depression (Fig. 11A, B). All three sculpture element types present on cep. Intracuticular pillars cover entire cep surface including within keyhole-shaped depression. Pores scattered randomly on cep, more plentiful toward posterior margin. EEs visible on entire cep surface.

Pair of lateral cephalic plates (lcp) present (Figs. 11A-C, 13B, 16B). Lcps evident in LM, but without strongly sclerotized appearance. Lcps sculptured with intracuticular pillars, scarce pores, and weak EEs. Lcp not in contact with cep. In LM, weak fine pillars present diffusely on areas surrounding lcp and along entire lateral sides of body between dorsal plate lateral margins and leg coxae (Figs. 11A, B, 13B). Neck plate (np) weakly sculptured with all three element types. Cep and np separated by notable distance (4.2–6.4 μm, 25.8–40.9 *psc*) (Fig. 11E).

Scapular plate (scp) with single median longitudinal ridge, two lateral longitudinal ridges, anterior latitudinal ridge, two central latitudinal ridges, and posterior latitudinal ridge (Figs. 3H, 10A, C, 11E, 15A, B). Central latitudinal ridges narrower than anterior and posterior latitudinal ridges (Figs. 11E, 15B). Scp lateral margins without strongly thickened appearance. Scp with all three sculpture element types present. Intracuticular pillars visible on entire scp, with those of largest diameter on middle–posterior parts of longitudinal ridges. Pores arranged in distinct transverse band along scp posterior latitudinal ridge margin and in less distinct transverse bands elsewhere on scp, but absent from longitudinal ridges (Fig. 11E). EEs well developed on scp and positioned in at least two rows on anterior latitudinal ridge, in single rows on each central latitudinal ridge, and in band of approximately 3–4 rows of EEs along posterior latitudinal ridge. Few EEs present between anterior and central latitudinal ridges. EEs most developed and distributed most densely on median longitudinal ridge (Fig. 15B).

Median plates 1 and 2 (m1 and m2) each with transversal crest forming a primary division into an anterior part (a) and posterior part (p). M1a, m1p, m2a, and m2p all secondarily divided into anterior and posterior portions by median transverse furrows (Figs. 13A, 15A). M1a and m2a each with median longitudinal ridge, less well developed on m2a (Fig. 15). M1a roughly trapezoidal in form. M1p roughly pentagonal in form. Intracuticular pillars small, visible on entire m1a and m1p parts, slightly larger on both posterior portions. Pores mostly small, randomly distributed on both the anterior and posterior portions of m1and m1p. Pores absent within median transverse furrows (Fig. 15A). EEs present on m1, best developed and most clearly visible on m1a posterior portion margin, where varyingly sized EEs occur in 1–2 rows (Figs. 3H, 11E, 15B), but also present on m1p (Fig. 13A).

M2a pentagonal with triangular anterior margin. M2p pentagonal with roughly triangular posterior margin. M2p clearly narrower than m2a (Figs. 10A, C, 13A, 15A). Intracuticular pillars of uniform size visible on entire m2a but only sparsely present within median transverse furrow and less evident on m2p. Pores present on m2a in two bands (one on either side of median transverse furrow) and sparsely on both anterior and posterior portions of m2p (Fig. 15A). EEs present on both portions of m2a but most conspicuously in a line along m2a posterior portion margin (Fig. 4B). EEs present but poorly developed on m2p (Fig. 13A).

Table 2: Measurements (µm) of *Bryodelphax pucapetricolus* sp. nov. adults with associated *psc* or *pbl* values. cep= cephalic plate, scp= scapular plate, np= neck plate, l= length, w= width, h= height, ⌀= diameter, n= number of individuals measured for that character, $\bar{x}$= mean, s= standard deviation.

Character	Holotype		Paratypes						Series			
	Female		Females			Males			n	$\bar{x}$		s	
	µm	*psc*	µm	*psc*	n	µm	*psc*	n		µm	*psc*	µm	*psc*
body length	128.6	843.7	9	109.4–134.7	572.5–843.7	10	100.8–125.3	634.0–806.8	20	119.4	736.3	8.3	68.4
scp	15.2	-	9	15.2–19.1	-	10	14.7–17.2	-	20	16.3	-	1.3	-
internal cirrus	8.2	53.5	9	6.4–8.4	36.1–55.6	10	6.3–9.1	38.1–53.4	20	7.1	43.7	0.8	5.5
external cirrus	12.8	83.7	8	9.2–12.8	55.3–76.5	10	9.9–15.5	63.6–91.2	19	11.8	73.1	1.4	9.1
cirrus A	33.5	219.6	9	24.9–30.0	137.2–176.7	10	23.1–32.1	145.4–203.2	20	27.7	171.0	2.7	21.3
cirrus A *pbl*	26.0%		9	19.4–24.0%		10	21.8%–27.4%		20	23.2%		1.9	
primary clava	4.8	31.5	9	3.2–4.1	19.3–26.8	10	3.3–5.5	20.5–35.8	20	4.1	25.6	0.6	4.4
secondary clava l	3.3	21.5	9	2.7–5.2	14.3–30.4	10	3.2–7.1	20.8–41.3	20	4.3	26.3	1.0	6.0
secondary clava w	2.7	17.7	9	1.8–3.3	11.6–17.8	10	2.2–3.9	14.0–19.1	20	2.6	15.6	0.5	2.6
buccal tube l	19.5	127.8	8	15.7–21.1	82.0–137.7	9	15.7–20.7	96.0–136.0	18	18.0	111.9	1.9	16.0
stylet sheath l	7.3	48.2	9	6.7–9.0	43.1–58.4	9	6.5–9.7	40.1–62.0	19	8.0	49.6	0.8	5.8
stylet support l	5.2	34.0	8	5.1–7.1	28.0–53.4	7	4.6–6.6	28.4–44.8	16	6.0	37.5	0.9	7.2
cep to np	4.3	27.9	8	3.0–6.0	19.6–32.8	8	2.9–6.4	18.7–40.9	17	4.5	27.7	1.2	6.3
np w	1.5	9.6	8	1.3–2.7	8.4–14.6	9	1.6–3.7	9.4–16.0	18	2.0	12.3	0.6	3.2
external claw I l	-	-	8	7.1–8.4	40.6–52.7	10	6.7–8.7	43.7–53.4	18	7.7	47.9	0.5	3.3
external claw I h	5.5	35.8	8	4.7–5.8	30.4–36.4	10	4.9–6.3	31.6–39.0	19	5.4	33.9	0.4	2.7
internal claw I l	-	-	8	7.5–8.8	44.9–57.8	8	7.6–9.1	51.4–57.5	16	8.4	51.8	0.5	4.2
internal claw I h	5.8	37.8	8	5.1–6.2	31.7–40.9	8	5.4–6.5	33.9–43.1	17	5.9	36.7	0.4	3.4
spur I l	-	-	7	0.9–1.4	5.1–8.8	8	1.0–1.5	6.1–8.7	15	1.1	6.9	0.2	1.1
spur I insertion point	-	-	7	1.2–1.7	6.6–10.7	8	1.1–1.7	6.8–10.2	15	1.4	8.9	0.2	1.4
external claw II l	-	-	9	6.2–7.8	35.8–51.3	9	6.8–8.1	44.4–50.7	18	7.1	45.0	0.5	4.3
external claw II h	5.5	36.1	9	4.5–5.6	25.6–36.1	9	4.8–5.8	30.8–36.6	19	5.2	32.1	0.4	3.2
internal claw II l	-	-	8	6.9–8.2	39.3–49.2	7	7.3–8.8	48.6–57.3	15	7.9	47.8	0.5	4.4
internal claw II h	6.3	41.5	8	4.7–6.0	28.2–34.7	8	5.2–6.4	33.7–42.5	17	5.6	34.5	0.5	3.9
Spur II l	-	-	8	0.9–1.3	4.5–8.3	7	0.9–1.3	5.6–8.5	15	1.0	6.4	0.1	1.0
Spur II insertion point	-	-	8	1.2–1.6	6.3–9.0	7	1.3–1.5	8.6–9.7	15	1.4	8.5	0.1	1.0
external claw III l	-	-	7	6.1–8.1	39.5–45.0	9	6.8–8.3	42.2–52.1	16	7.2	44.5	0.6	3.1
external claw III h	6.0	39.6	7	4.3–5.8	26.8–32.6	10	4.5–5.9	29.3–38.0	18	5.2	32.5	0.5	3.3
internal claw III l	-	-	6	7.2–8.9	44.5–53.2	9	7.2–8.4	45.1–50.8	15	7.8	48.4	0.5	2.3
internal claw III h	6.7	44.2	6	4.9–6.1	30.6–35.3	9	5.0–6.2	32.9–37.4	16	5.6	34.9	0.5	3.0
Spur III length	-	-	6	1.0–1.2	6.0–6.7	9	0.8–1.2	5.3–7.5	15	1.0	6.4	0.1	0.5
Spur III insertion point	-	-	6	1.3–1.7	8.0–9.7	9	1.1–1.5	7.0–9.5	15	1.4	8.7	0.1	0.7
external claw IV l	7.9	51.9	4	7.4–8.1	43.0–47.5	6	7.2–8.3	46.7–52.2	11	7.9	47.9	0.4	3.0
external claw IV h	6.1	40.0	4	5.5–6.3	31.3–35.8	6	5.3–6.0	31.0–35.9	11	5.8	35.0	0.3	2.7
internal claw IV l	-	-	3	7.4–9.0	45.9–49.0	6	7.4–9.1	50.0–56.3	9	8.4	50.7	0.6	3.4
internal claw IV h	6.4	42.2	3	6.0–6.6	32.7–38.5	6	5.7–6.3	36.0–40.2	10	6.2	37.7	0.3	2.7
spur IV l	-	-	3	1.1–1.3	6.0–7.5	6	1.0–1.2	6.6–7.0	9	1.1	6.7	0.1	0.4
spur IV insertion point	-	-	3	1.5–1.8	8.3–11.5	6	1.3–2.0	7.6–12.0	9	1.6	9.6	0.2	1.7
sense organ I	1.2	7.9	8	1.0–1.4	6.1–8.6	6	1.0–1.4	7.6–12.0	15	1.2	8.2	0.1	1.8
sense organ III	-	-	3	1.0–1.4	5.2–8.9	2	0.7–1.0	4.5–5.7	5	1.0	6.1	0.3	1.7
sense organ IV	1.8	11.9	9	1.0–1.9	5.2–11.7	10	1.0–2.0	5.8–12.8	20	1.6	9.8	0.3	2.2
gonopore ⌀	6.3	41.6	9	5.2–7.3	28.3–47.6	10	1.5–2.9	9.5–19.4	20	4.2	25.6	2.0	12.5
gonopore to anus	14.9	97.9	9	11.6–17.0	61.0–91.5	10	8.4–11.9	49.8–74.6	20	11.7	72.2	2.6	14.7
gonopore to anus *pbl*	11.6%		9	9.9%–12.6%		10	6.9–10.1%		20	9.8%		1.8	

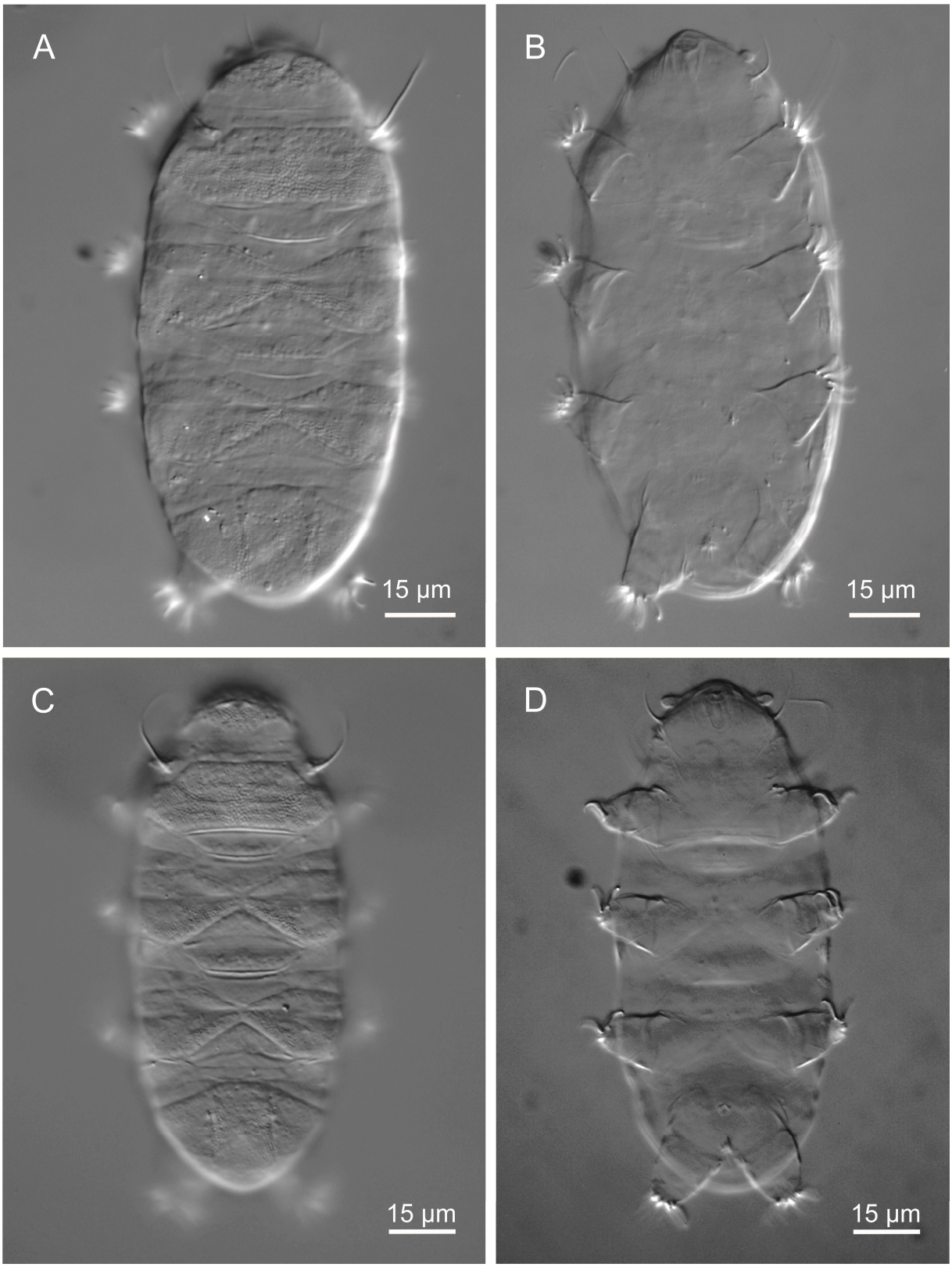

Figure 10: *Bry. pucapetricolus* sp. nov. *habitus* (DIC). **A** dorsal female holotype; **B** ventral female holotype; **C** dorsal male paratype; **D** ventral male paratype.

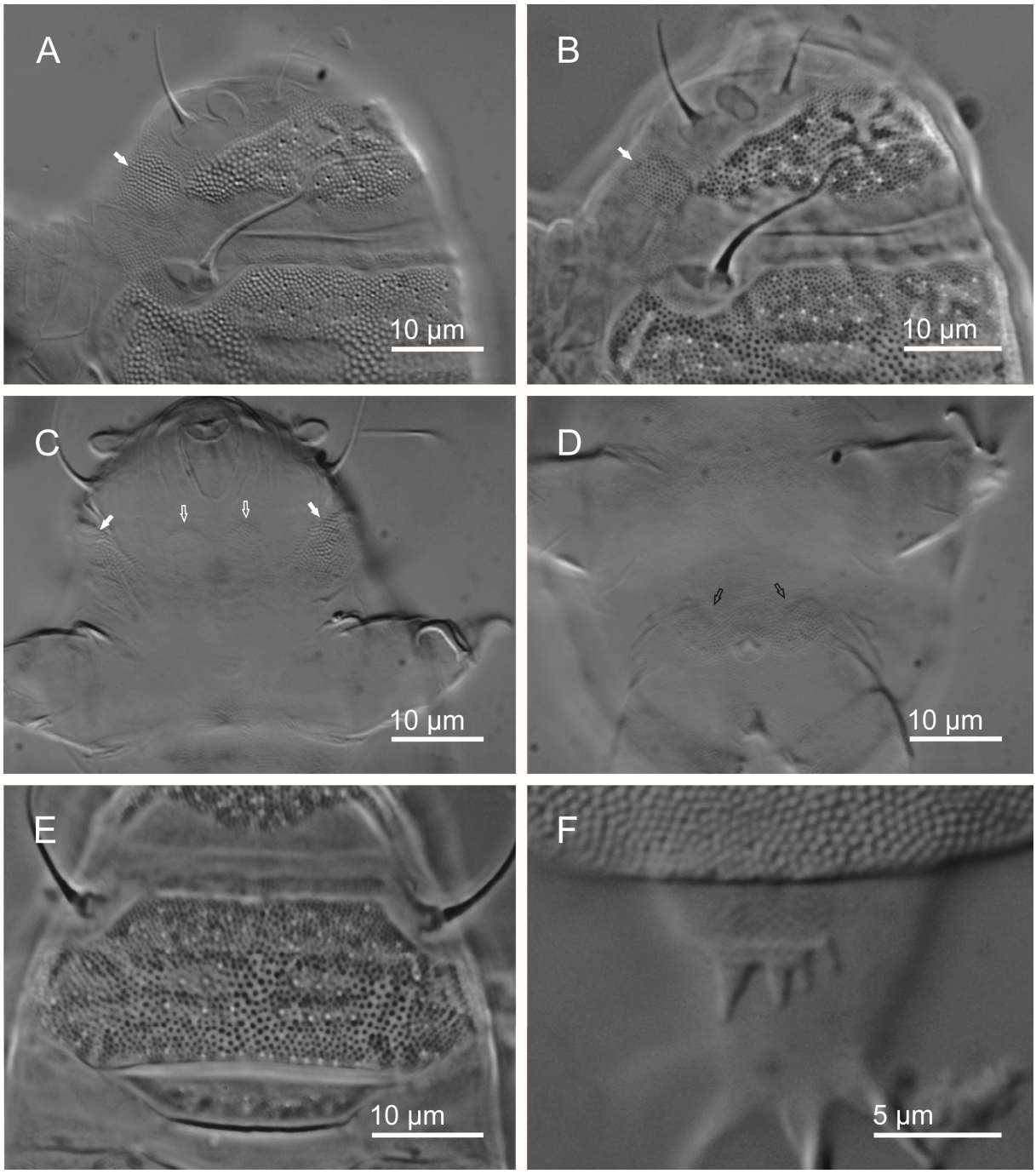

Figure 11: *Bry. pucapetricolus* sp. nov. structures. **A** dorsolateral cephalic region (DIC); **B** dorsolateral cephalic region (PhC); **C** ventral cephalic region (DIC); **D** ventral caudal region (DIC), male; **E** scapular plate structure and sculpture element distribution (PhC); **F** dentate collar, leg IV (DIC). White filled arrow= lateral cephalic plate, white hollow arrows= subcephalic ventral plates, black hollow arrows= lateral gonoplates.

Median plate 3 (m3) composition can appear different in LM and SEM. In LM, m3 composition appears to include a transversal crest forming a primary transverse division between a false anterior part (a) and posterior part (p) (similar to m1 and m2). False m3a appears roughly triangular and to have a median transverse furrow forming a secondary division (Figs. 12B, C, 13A). In LM false m3p appears roughly trapezoidal, narrow, without a secondary division. Portion of false m3a anterior to false secondary median transverse furrow with all three main types of sculpture visible, portion posterior to median transverse furrow sculptureless. False m3p with small intracuticular pillars visible on its entirety, only few scattered pores present, and EES not visible (Figs. 10A, C, 12B, 13A).

In SEM, m3 composition without primary division formed by a transversal crest between an anterior and

posterior part but with a median transverse furrow present (Fig. 15A, C). M3 with poorly developed median longitudinal ridge. Distribution of m3 sculpture elements creates the illusion of both a primary and secondary division in LM due to a tertiary division that exists between sculptured and smooth portions of m3 anterior to the transverse median furrow (Fig. 15C). Evident EEs and pores present on m3 anterior portion, with EEs at frontal margin best developed, followed caudally by a sculptureless band immediately anterior to median transverse furrow, with remainder of plate posterior to median transverse furrow sculptured very weakly by minute EEs only (barely visible in SEM). Point of transition between sculptured and unsculptured areas of m3 anterior portion (tertiary division) corresponds to the false secondary division in SEM.

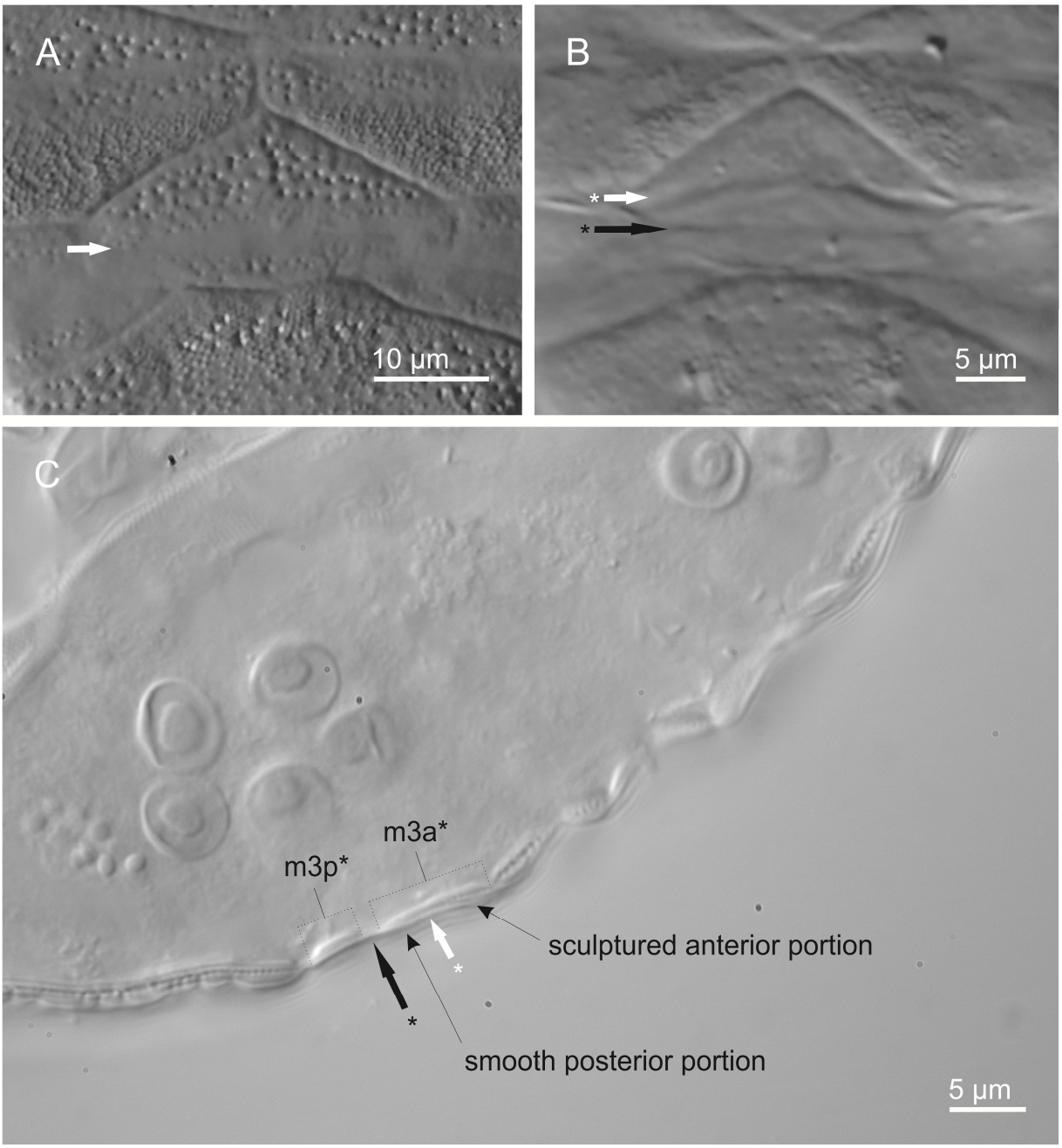

Figure 12: Structure of median plate 3 (DIC). **A** typical *Bryodelphax* m3 structure (*Bry*. cf. *parvulus* (Ireland)); **B** aberrant appearance of *Bry. pucapetricolus* sp. nov. m3 form; **C** sagittal view of *Bry. pucapetricolus* sp. nov. m3. Asterisk (*) indicates structure condition as perceived in LM only, white solid arrow= median transverse furrow, white asterisk arrow= false median transverse furrow, black asterisk arrow= false transversal crest.

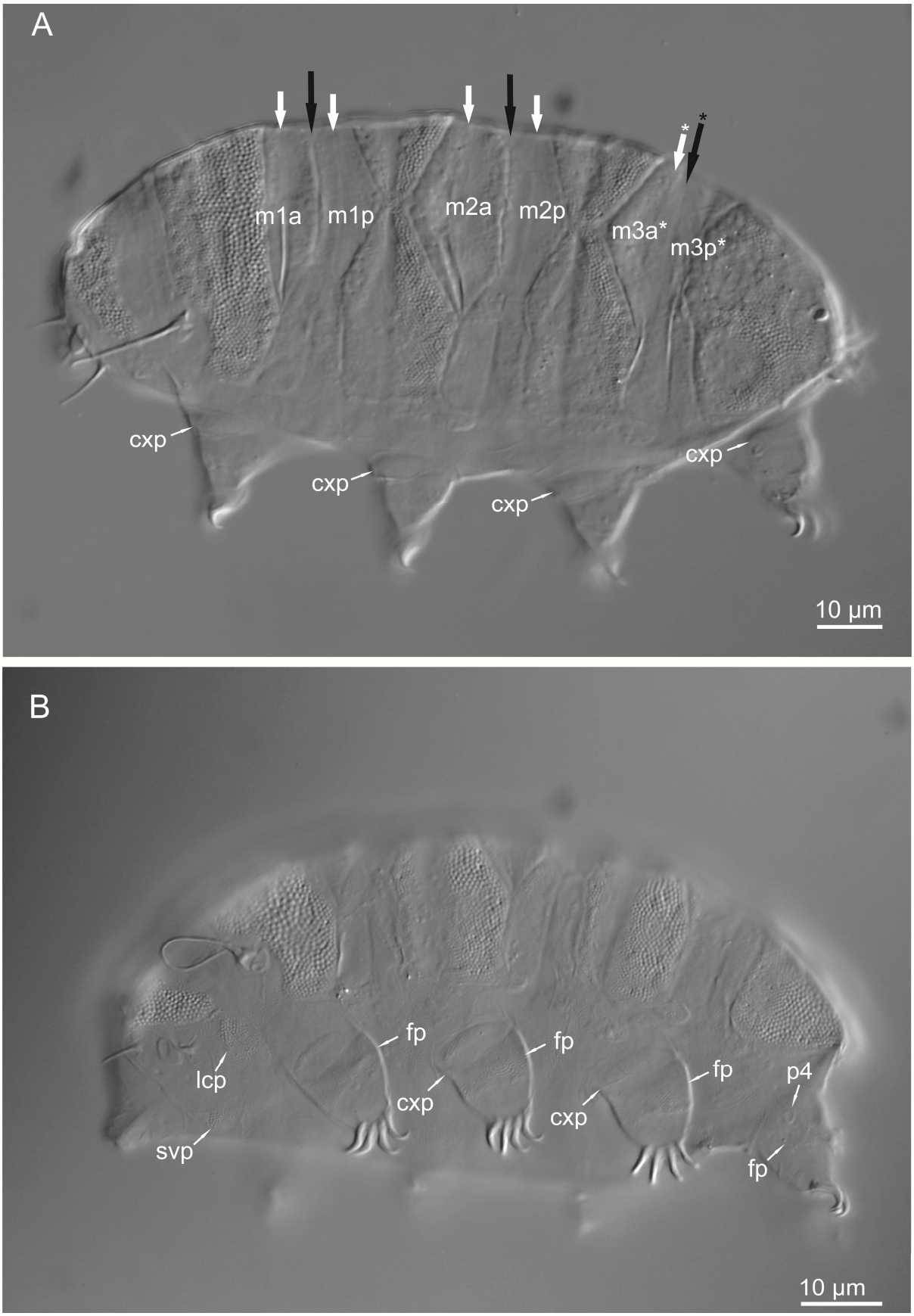

Figure 13: *Bry. pucapetricolus* sp. nov. lateral view (DIC). **A** divisions of the dorsal median plates; **B** leg plates. Asterisk (*) indicates structure condition as perceived in LM only, black solid arrow= transversal crest, white solid arrow= median transverse furrow, black asterisk arrow= false transversal crest, white asterisk arrow= false median transverse furrow, cxp= coxal plate, fp= femoral plate, p4= sense organ of leg IV, lcp= lateral cephalic plate, svp= subcephalic ventral plate.

Paired plate 1 (pp1) and paired plate 2 (pp2) similar in appearance, both with a medially interrupted transverse groove separating an anterior part and broader posterior part. Transverse groove sculptureless under LM (Figs. 4B, 10A, C, 12A). Transverse groove interrupted at body midline by a longitudinal ridge covered by visible intracuticular pillars (Figs. 12A, 15A). Intracuticular pillars clearly visible on pp1 and pp2 anterior and posterior parts, but noticeably larger in diameter on posterior portions than on anterior portions (Fig. 13). Pores distributed randomly on pp1 and pp2 anterior and posterior parts. EEs most pronounced along pp1 and pp2 anterior and posterior margins (Figs. 13, 15A).

Caudal plate (cap) with typical dual longitudinal ridges and two difficult to see central latitudinal ridges (Figs. 4B, 10A, C, 15A). All ridges bearing EEs (Fig. 15A, C). Cap anterior margin with trapezoidal arched median section. Intracuticular pillars visible on entire cap with pillars of largest diameters at plate central interior region, including midsections of longitudinal ridges (Figs. 4B, 13A, 14A). Pores well distributed across cap surface, but slightly fewer present at mid-interior region and absent from longitudinal ridges (Figs. 14A, 15A, C). EEs present on entire cap (Fig. 15A, C).

Lateral intersegmental plate (lip) present in pairs at both lateral sides of each median plate (6 pairs total) (Figs. 10A, C, 13, 15A). Anterior lip of each pair slightly larger and extends further onto lateral sides of body than posterior lip. Difference in lengths between anterior and posterior lip in a pair approximately the same for each pair (*i.e.* no decrease in the relative lengths of lips in a pair in a rostral–caudal direction) (Fig. 13). At m1, division between anterior and posterior lip aligned with secondary division between m1p anterior and posterior parts (Figs. 10C, 13). At m2, division between anterior and posterior lip aligned with posterior corner of m2p anterior portion (Figs. 10C, 13). At m3, division between anterior and posterior lip aligned with division between m3 and caudal plate (Fig. 12A). All lips sculptured with visible (sometimes only weakly) intracuticular pillars, usually more distinct at lip lateral edge (Fig. 13). Pores occasionally visible on some lips. EEs absent on lips (Fig. 15A).

Each leg with well-defined coxal plate and lesser developed femoral plate (Figs. 13, 14). Fine pillars weakly visible on all leg surfaces, stronger on leg plates. Coxal plates without other sculpture (Figs. 13, 14B). Femoral plates with one pair of distal epicuticular ridges, not well developed and sometimes poorly evident in LM (Fig. 13). Presence of proximal pair of weakly developed epicuticular femoral ridges indicated (Fig. 14B) but to be confirmed with further SEM on additional specimens. Femoral plates sculptured with visible intracuticular pillars and barely visible EEs upon distal epicuticular ridges in LM but clearly present in SEM, pores absent (Figs. 14B-D). Dentate collar present, appearance variable between individuals and between legs of a single individual, with 3–7 teeth. Teeth of variable length, triangular, separated at their bases (Figs. 11F, 14D).

Leg sense organs present on legs I, III, and IV (*i.e.* p1, p3 and p4 present) (Fig. 14). P1, a small and rounded papilla, located upon distal margin of femoral plate (Fig. 14B). P3, a minute button-like papilla present on external surface of coxa (Fig. 14C), can be difficult to see, especially if animal is oriented dorsoventrally. P4, slightly larger than p1 and p3, a rounded papilla, positioned coxally (Fig. 14D). Claws of typical arrangement and form. Basal spurs absent on external claws, present on internal claws. Spurs nearly straight and oriented towards claw base.

Fine pillars visible on entire ventral surface (Figs. 6E, 10 B, D, 11C, D). Ventral plates present (Figs. 10B, D, 11C, D, 27A), weakly sclerotized, sometimes difficult to observe in LM, positioned in 2 rows: Row 1, a pair of round, weakly demarcated svps (Figs. 11C, 13B, 16B); and Row 2, a pair of lateral gonoplates (Figs. 6E, 11D, 16C). Plate configuration and morphology constant within population and between sexes. In LM, svps observed with visible intracuticular pillars only, or pillars with few EEs around plate circumference (Fig. 11C); lateral gonoplates appear as mounds sculptured with intracuticular pillars (more distinct upon plates than surrounding ventral cuticle) and EEs but sometimes EEs indistinct (Figs. 6E, 11D). In SEM, svps appear as mounds located within individual depressions in cuticle, weakly sculptured (Fig. 16B); gonoplates appear as mounds sculptured with weakly developed EEs (Fig. 16C).

Female gonopore somewhat small in diameter (Table 1), surrounded by typical rosette of 6 cells (Fig. 10B). Male gonopore circular with hood formed by thickening at the circumference anterior visible in LM (Figs. 6E, 10D) and SEM (Fig. 16C). Female gonopore of larger diameter and positioned more rostrally from anus than male gonopore (Tables 1, 2). Anal system composed of two small, rigid lateral lobes and lamellar central terminal structure with central longitudinal fold (Figs. 8A, 9A). Anal aperture at junction of lateral lobes and terminal laminar structure. Cuticle of anal system smooth (Fig. 8A).

Ontogeny. Number of instars that occur within each developmental stage unknown. Eggs and shed exuvia not found. Three two-clawed larvae observed, body length 65.7–80.3 μm. Dorsal plate margins distinct but not all characters fully developed, *e.g.* scapular plate longitudinal and latitudinal ridges not apparent as in adults, median plates appear less developed than adults with internal divisions and distribution of sculpture elements not well defined, and lips present but with indistinct sculpturing. Gonopore and anus absent.

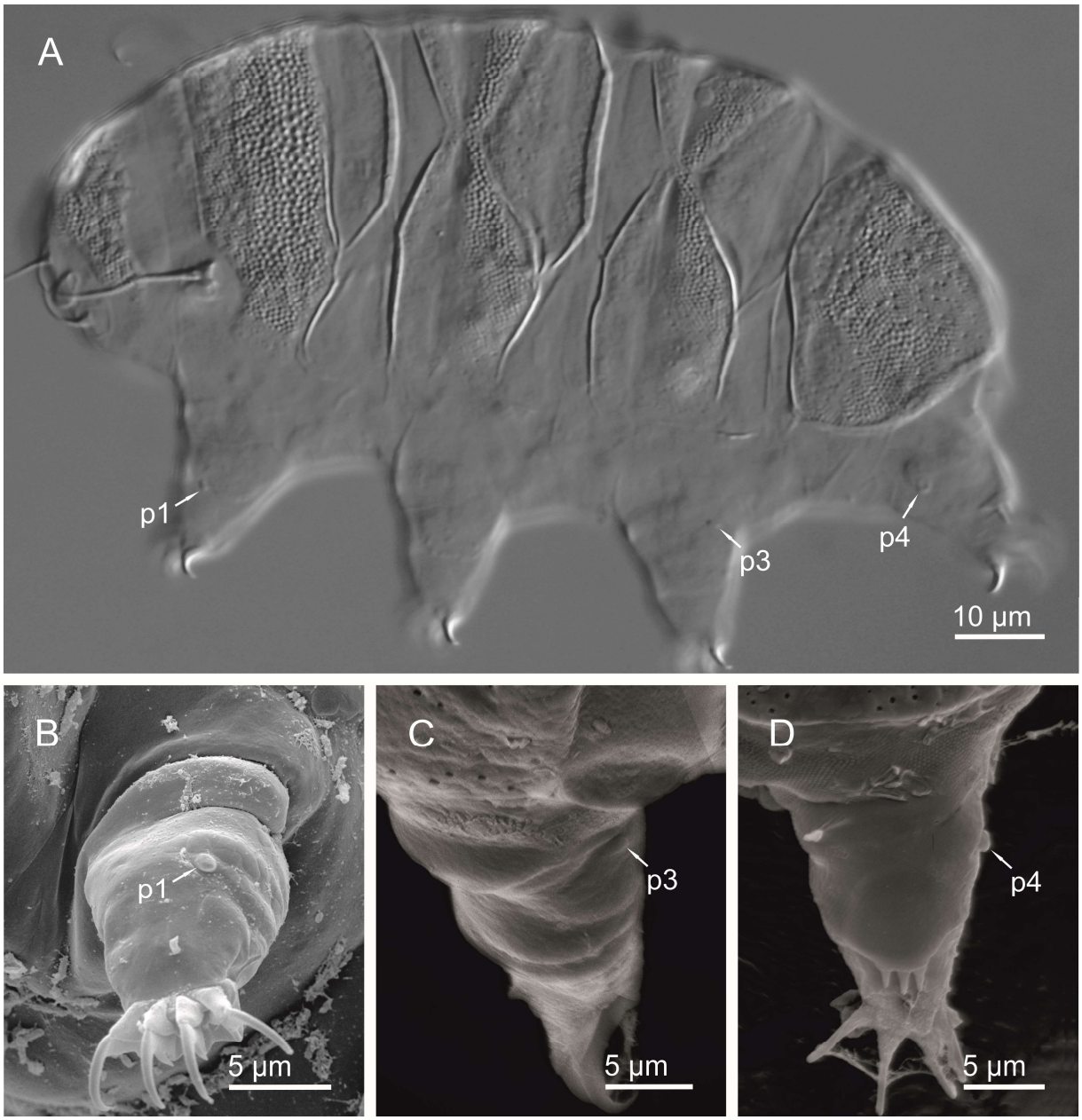

Figure 14: *Bry. pucapetricolus* sp. nov. leg structures. **A** leg sense organs (DIC); **B** leg I (SEM); **C** leg III (SEM); **D** leg IV with dentate collar (SEM). p1= sense organ of leg I, p3= sense organ of leg III, p4= sense organ of leg IV.

Two four-clawed juveniles observed. Body lengths 96.7 and 98.9 µm. The following characters were observed to be developed as in adults: division of m3; dorsal cuticular sculpture; ventral sculpture of fine pillars; leg plates; leg sense organs; dentate collar; and anal system. Ventral plates not fully developed as in adults. At subcephalic position, intracuticular pillars visible on weak mounds where plates will develop. At position where lateral gonoplates will develop, intracuticular pillars visible in patches together with weak indications of EEs, but mounds not fully formed.

Genotyping and phylogenetic analysis

Sequences were obtained for the four targeted molecular markers stated above from seven individuals. All obtained sequences were deposited in GenBank (https://www.ncbi.nlm.nih.gov/genbank/) under the following accession numbers: OM910770–OM910776 (18S rRNA, 842–1119 bp); OM910763–OM910769 (28S rRNA, 691–762 bp); OM902677–OM902683 (ITS-1, 619-663 bp); OM901123–OM901129 (COI; 612–695 bp). All nuclear markers are identical for all specimens, while three haplotypes were revealed in the mitochondrial marker. Two haplotypes are identical when viewed as proteins and the third differs from them in one amino acid only. The phylogenetic analysis (18S + 28S, Fig. 17) showed full support of the genus *Bryodelphax*, which consisted of a fully supported cluster embracing the Indomalayan-Australasian species and a poorly resolved paraphyletic complex

of Palaearctic species. *Bry. pucapetricolus* sp. nov. belongs to the latter, being most similar to *Bry. instabilis* from Poland.

Morphological differential diagnosis

Bry. pucapetricolus sp. nov. is different from *Bryodelphax* species belonging to the '*parvulus* group' due to the presence of ventral plates in *Bry. pucapetricolus* sp. nov. Within the '*weglarskae* group', *Bry. pucapetricolus* sp. nov. is most similar to the species that have been described with two or three rows of ventral plates (*Bry. amphoterus*, *Bry. maculatus*, *Bry. mareki*, and *Bry. nigripunctatus*) but differs to them in the following characters:

Bry. amphoterus. *Bry. pucapetricolus* sp. nov. lacks slightly star-shaped sculpture elements described for *Bry. amphoterus*. Ventral plates strongly sclerotized and evident on *Bry. amphoterus* (according to Gąsiorek et al., 2020a) compared to weakly sclerotized ventral plates on *Bry. pucapetricolus* sp. nov. *Bry. amphoterus* described as lacking leg sense organs while p1, p3, and p4 are present on *Bry. pucapetricolus* sp. nov. Spurs are present on all claws of *Bry. amphoterus*, but only on the internal claws of *Bry. pucapetricolus* sp. nov.

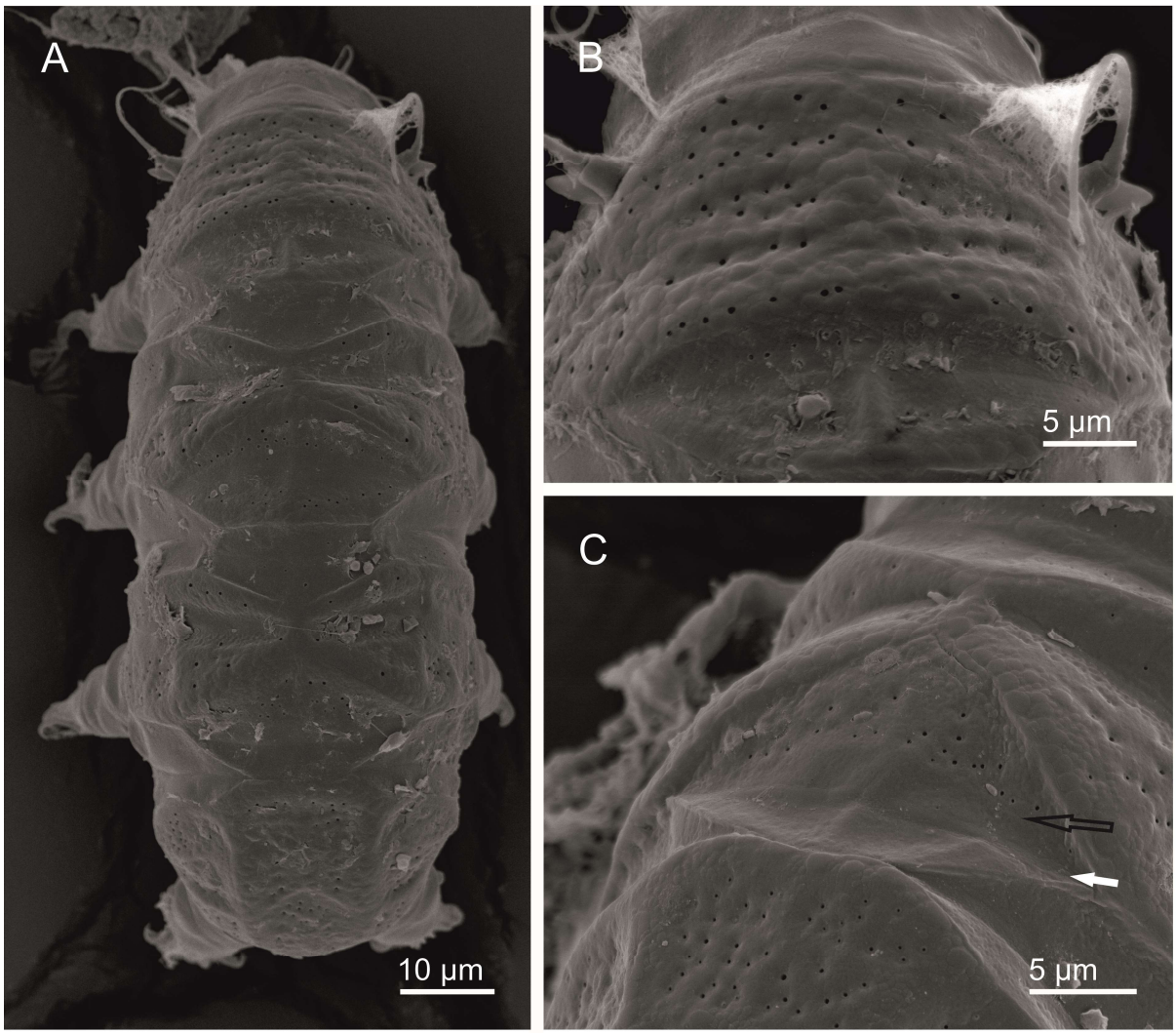

Figure 15: Dorsal structures of *Bry. pucapetricolus* sp. nov. (SEM) **A** *habitus*; **B** scapular plate with sculpture elements; **C** actual structure of median plate 3. White solid arrow= median transverse furrow, black hollow arrow= tertiary division between sculptured and smooth areas.

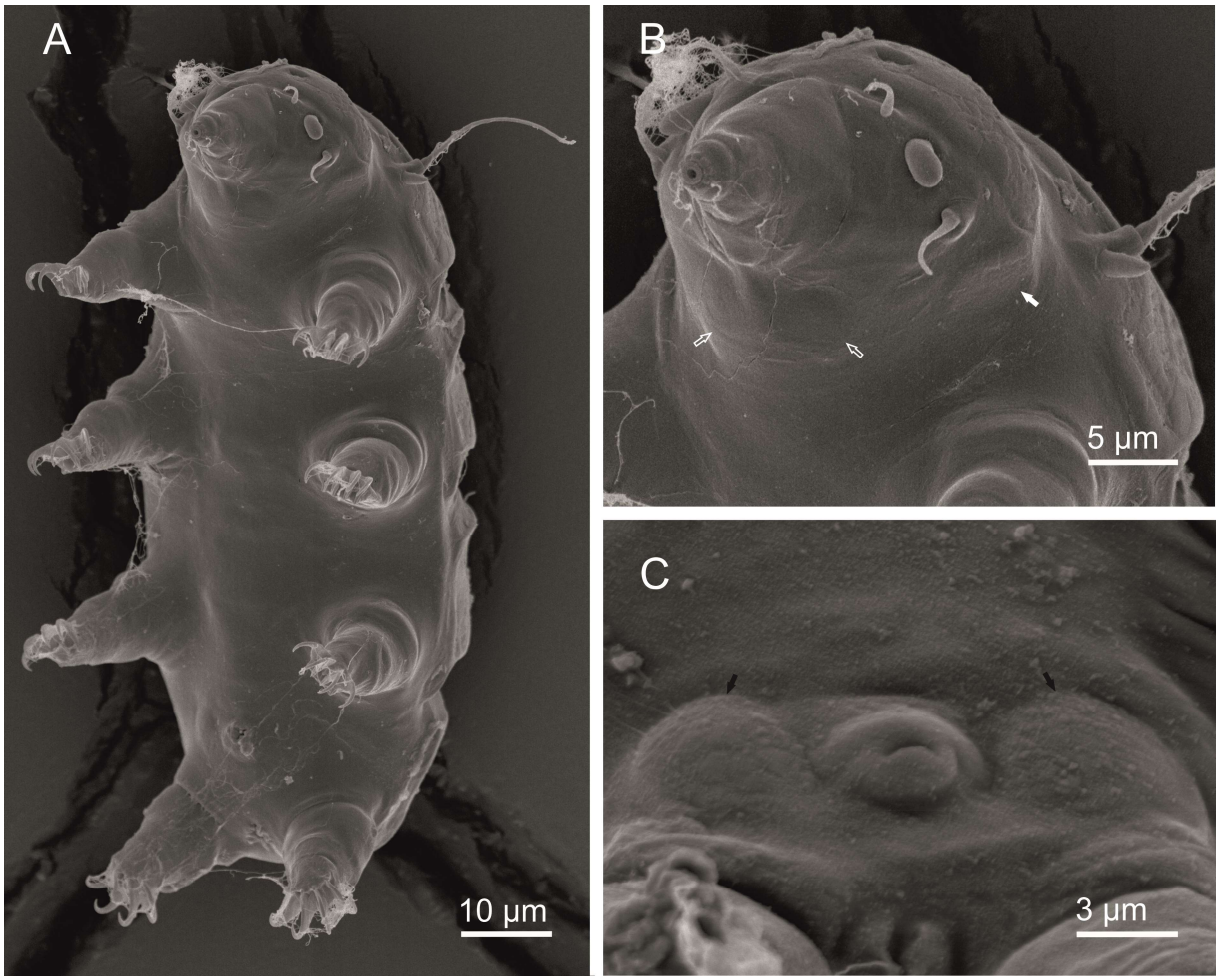

Figure 16: Ventrolateral and ventral structures *Bry. pucapetricolus* sp. nov. (SEM). **A** *habitus*; **B** cephalic region; **C** lateral gonoplates, male gonopore. White filled arrow= lateral cephalic plate, white hollow arrows= subcephalic ventral plates, black filled arrows= lateral gonoplates

Bry. maculatus. Bifurcated cirri A occasionally observed on *Bry. maculatus* but not on *Bry. pucapetricolus* sp. nov. EEs of *Bry. maculatus* cuticular sculpture of uniform size and distributed differently than various sized EEs of *Bry. pucapetricolus* sp. nov. (Fig. 3D, H). Dorsal plate relief of *Bry. maculatus* is high contrast with many dark circular areas visible in PhC, while dorsal plate relief of *Bry. pucaperticolus* sp. nov. does not show high contrast in PhC and less abundant dark areas occur. Lcps of *Bry. maculatus* weakly developed and difficult to observe, while lcps are evident and well-developed on *Bry. pucapetricolus* sp. nov. In LM m3 of *Bry. maculatus* does not appear divided because the portion of the plate anterior to its median transverse furrow is entirely sculptured, while m3 of *Bry. pucapetricolus* sp. nov. appears divided in LM. *Bry. maculatus* has three rows of evident ventral plates (a pair of svps, a pair of lateral gonoplates, and a single posterior gonoplate (*i.e.* plate posterior to the gonopore)), while *Bry. pucapetricolus* sp. nov. has only two rows of weakly developed plates. Sculpture of leg plates different (see 'Leg plates' section above). Leg sense organs of *Bry. maculatus* (p1 and p4) visible only in SEM, while these and p3 are visible on *Bry. pucapetricolus* sp. nov. in LM and SEM. *Bry. maculatus* female gonopore diameter *psc* greater than that of *Bry. pucapetricolus* sp. nov.

Bry. mareki. The original description of *Bry. mareki* includes only three rows of ventral plates but both paratypes that we examined had at least seven rows of ventral plates (Fig. 7C). EEs of *Bry. mareki* cuticular sculpture are smaller, of more uniform size, and more numerous than those of *Bry. pucapetricolus* sp. nov. (Fig. 3E, H). The development of the cucticular relief of *Bry. mareki* is poor, showing only low contrast and few dark areas in PhC, compared to the more developed cuticular relief of *Bry. pucapetricolus* sp. nov. Lcps of *Bry. mareki* weakly developed, but strongly developed in *Bry. pucapetricolus* sp. nov. Femoral plates sculptured differently (see 'Leg plates' section above). P3 absent from *Bry. mareki* but present on *Bry. pucapetricolus* sp. nov. Dentate collar absent from *Bry. mareki* but present on *Bry. pucapetricolus* sp. nov.

Bry. nigripunctatus. Dorsal sculpture of *Bry. nigripunctatus* with strongly developed irregular,

polygonal EEs, while EEs of *Bry. pucapetricolus* sp. nov. less well-developed and rounded (Fig. 3F, H). Dorsal plate relief of *Bry. nigripunctatus* in PhC high contrast with many visible black areas, while relief of *Bry. pucapetricolus* sp. nov with less contrast and with less abundant dark areas in PhC. In LM m3 of *Bry*. *nigripunctatus* does not appear divided because the portion of the plate anterior to its median transverse furrow is entirely sculptured, while m3 of *Bry. pucapetricolus* appears divided in LM. Ventral plates of *Bry. nigripunctatus* are well-defined and strongly sculptured with the sexes having a different number of plates rows, while ventral plates of *Bry. pucapetricolus* sp. nov. are weakly defined and in the same configuration for both sexes. Ventral plates at corresponding positions of different shapes in the two species (Fig. 6E, F). Leg plates sculptured differently (see 'Leg plates' section above). Sense organs were described as absent from legs I–III in *Bry. nigripunctatus* while p1 and p3 are present (along with p4) on *Bry. pucapetricolus* sp. nov. Female and male gonopore diameter *psc* are greater in *Bry. nigripunctatus* than in *Bry. pucapetricolus* sp. nov. (Table 1). Female gonopore to anus distance *psc* and *pbl* greater in *Bry. nigripunctatus* than in *Bry. pucapetricolus* sp. nov. (Table 1).

We briefly compare *Bry. pucapetricolus* sp. nov. to all congeners belonging to the '*parvulus* group' because the ventral plates of *Bry. pucapetricolus* sp. nov. are only weakly developed. Such plates may have not been reported in the original descriptions of the '*parvulus* group species', particularly older taxa. *Bry. pucapetricolus* sp. nov. differs from them in the following characters:

Bry. alzirae (du Bois-Reymond Marcus, 1944). The dentate collar of *Bry. alzirae* was described as having 12 thin teeth, which is outside the range of observed variability (3–7 teeth) of *Bry. pucapetricolus* sp. nov. Spurs absent from internal claws of *Bry. alzirae,* but present on *Bry. pucapetricolus* sp. nov. internal claws.

Bry. arenosus. Distribution of sculpture elements on dorsal plates differs between the two species *e.g*. anterior portion of m3 of *Bry. arenosus* is entirely sculptured, while this portion has an unsculptured section in *Bry. pucapetricolus* sp. nov. The description of *Bry. arenosus* specifically states that ventral pillars and plates, leg sense organs, and dentate collar are absent, while these structures are all present on *Bry. pucapetricolus* sp. nov.

Bry. asiaticus. Distribution of sculpture elements on dorsal plates differs between the two species *e.g*. anterior portion of m3 of *Bry. asiaticus* is entirely sculptured while this portion has an unsculptured section in *Bry. pucapetricolus* sp. nov. Leg sense organs and dentate collar described as absent on *Bry. asiaticus*, while these are present on *Bry. pucapetricolus* sp. nov. Ventral plates are specifically mentioned as absent in original description of *Bry. asiaticus*, while ventral plates are present on *Bry. pucapetricolus* sp. nov.

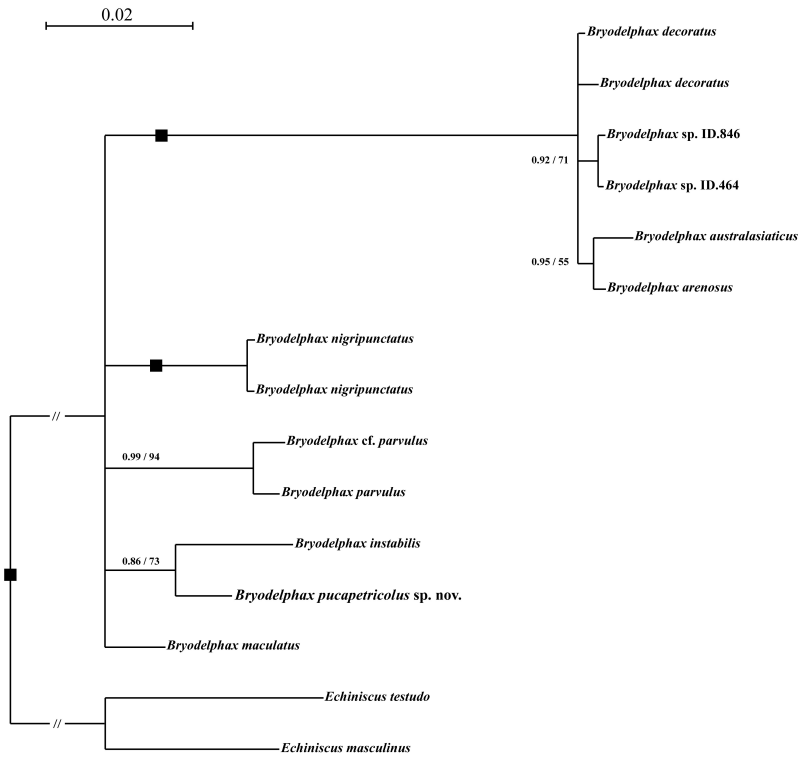

Figure 17: Phylogeny of *Bryodelphax* based on concatenated 18S + 28S rRNA sequences. Numbers at nodes indicate Bayesian posterior probability values (BI, first values) and bootstrap values (ML, second values). Black dots indicate the nodes supported by values of 1.0/100% with both methods. Branches with support below 0.85 in BI (70% in ML) were collapsed. Scale bar and branch lengths refer to the Bayesian analysis.

Bry. brevidentatus. Ventral plates are specifically mentioned as absent in original description of *Bry. brevidentatus*, while ventral plates are present on *Bry. pucapetricolus* sp. nov. The particular form of the dentate collar (with five short triangular teeth) of *Bry. brevidentatus* is dissimilar to that of *Bry. pucapetricolus* sp. nov.

Bry. crossotus. Grigarick, Schuster and Nelson, 1983. Sense organs are absent on legs I and III of *Bry. crossotus* but present on *Bry. pucapetricolus* sp. nov. The dentate collar of *Bry. crossotus* has scalloped edges, compared to actual teeth in *Bry. pucapetricolus* sp. nov.

Bry. dominicanus. (Schuster and Toftner, 1982). Leg sense organs and the dentate collar are absent on *Bry. dominicanus* but present on *Bry. pucapetricolus* sp. nov.

Bry. lijiangensis. Lateral body cirri and projections on the paired plates are present on of *Bry. lijiangensis* but are absent from *Bry. pucapetricolus* sp. nov. and all other congeners. We are in agreement with several previous authors (*e.g.* Kristensen et al., 2010) that *Bry. lijiangensis* belongs to another genus due to the presence of these appendages and other characters.

Bry. mateusi. Distribution of pores on the dorsal cuticle is different in the two species (*e.g.* pores are absent on the paired plate posterior portions of *Bry. mateusi* but present on those of *Bry. pucapetricolus* sp. nov.). Ventral plates were specifically stated as absent in the re-examination of *Bry. mateusi* by Pilato et al. (2010) but are present on *Bry. pucapetricolus* sp. nov.

Bry. meronensis. The position of the largest intracuticular pillars on the dorsal cuticle is different in the two species (intracuticular pillars clearly larger on the caudal plate than on the scapular plate and other plates of *Bry. meronensis,* whereas the largest intracuticular pillars appear to occur on the scapular plate of *Bry. pucapetricolus* sp. nov.). The distribution of pores on the dorsal cuticle is different between the two species (*e.g. Bry. meronensis* is described with pores on the center of the scapular plate, while pores are absent from that area of the scapular plate of *Bry. pucapetricolus* sp. nov.). Leg sense organs are absent on *Bry. meronensis* but present on *Bry. pucapetricolus* sp. nov. Ventral plates are specifically stated as absent in original description of *Bry. meronensis*, while ventral plates are present on *Bry. pucapetricolus* sp. nov.

Bry. ortholineatus (Bartoš, 1963). The transverse furrow of the paired plates of *B. ortholineatus* is poorly defined compared to the evident furrow of *Bry. pucapetricolus* sp. nov. paired plates. Spurs are absent on all claws of *B. ortholineatus* but present on *Bry. pucapetricolus* sp. nov. internal claws.

Bry. parvulus. Comparisons with this species are difficult because of historical taxonomic issues surrounding it (*e.g.* see Pilato et al., 2010) but it differs evidently from *Bry. pucapetricolus* sp. nov. by the absence of the dentate collar on *Bry. parvulus.*

Bry. tatrensis. Distribution of pores on the dorsal cuticle different in the two species. (*e.g.* pores are very rare or absent on the central portion of the caudal plate and absent on the paired plate posterior portions of *Bry. tatrensis* but present on those areas of *Bry. pucapetricolus* sp. nov.). Ventral plates specifically stated as absent in re-examinations of *Bry. tatrensis* (Pilato, 1972; Kaczmarek et al., 2005) but are present on *Bry. pucapetricolus* sp. nov.

Finally, we briefly compare *Bry. pucapetricolus* sp. nov. to the known *Bryochoerus* species because when observed in LM the m3 of *Bry. pucapetricolus* sp. nov. appears divided, thus matching Marcus' (1936) principal criterion for *Bryochoerus. Bry. pucapetricolus* sp. nov. differs from the described *Bryochoerus* taxa:

Brc. intermedius intermedius (Murray, 1910). Dentate collar absent from *Brc. intermedius intermedius* but present on *Bry. pucapetricolus* sp. nov. Claw spurs absent from *Brc. intermedius intermedius* but present on *Bry. pucapetricolus* sp. nov. internal claws. A comparison of the condition of the m3 *Brc. intermedius intermedius* to that of *Bry. pucapetricolus* sp. nov. was not possible in our examination of an Australian *Brc. intermedius intermedius* specimen because the median plates of the latter are partially subducted beneath adjacent plates due to contraction (Fig. 5F).

Brc. intermedius hawaiicus (Thulin, 1928). Body length of *Brc. intermedius hawaiicus* (190–220 µm (probably excluding the head and legs IV)) longer than the maximum observed for *Bry. pucapetricolus* sp. nov. (134.7 µm including the head). Median plates of *Brc. intermedius hawaiicus* divided into nearly equal parts, while in *Bry. pucapetricolus* sp. nov. median plate anterior parts are clearly larger than posterior parts. Dentate collar absent from *Brc. intermedius hawaiicus* (Plate XIX, Figure 36c in Murray, 1910) but present on *Bry. pucapetricolus* sp. nov.

Brc. intermedius laevis (Marcus, 1936). M1 and m2 posterior portions are unsculptured in *Brc. intermedius laevis*, while these are clearly sculptured on *Bry. pucapetricolus* sp. nov. Dentate collar of *Brc. intermedius laevis* described with five basally close teeth compared to a variable number of teeth (usually less than five) that are typically clearly separated in *Bry. pucapetricolus* sp. nov. (rarely two teeth share a common base but are still well separated from other tooth bases).

Our examination found that some specimens identified as '*Brc. intermedius laevis*' from Greenland in the NHMD collection probably represent multiple *Bryodelphax* taxa (described or undescribed). However, eight specimens (listed in Comparative Material) matched more closely to the original description of *Brc. intermedius laevis* (Marcus, 1936). These eight specimens displayed the characteristics of (almost) sculptureless m1 and m2 posterior parts (Fig. 5D) and dentate collar with five teeth. When it was observable on these Greenlandic '*Brc. intermedius laevis'* specimens, m3 appeared in LM to have a primary division formed by a transversal crest in addition to the typical transverse furrow, similarly to

Bry. pucapetricolus sp. nov. (primary division shown to be false in SEM on the latter). However, the distribution of the sculpture elements is different on the m3 of each taxon. The m3 in the '*Brc. intermedius laevis*' is covered with strongly visible intracuticular pillars on its entirety with a band of well-developed EEs at its anterior (Fig. 5E), while the m3 of *Bry. pucapetricolus* sp. nov. has a smooth, sculptureless section at the central and posterior areas (Fig. 12B, C). Median plates of all eight '*Brc. intermedius laevis'* all appeared noticeably broader than those of *Bry. pucapetricolus* sp. nov. (Fig. 5D).

Brc. liupanensis. Body length minimum and maximum higher for *Brc. liupanensis* (125–163 μm) than *Bry. pucapetricolus* (100.8–134.7 μm for the type series of sp. nov.). Stylet supports absent/not observed in *Brc. liupanensis* but present in *Bry. pucapetricolus* sp. nov. Sense organs p1 and p4 not observed on *Brc. liupanensis*, while both are evident on *Bry. pucapetricolus* sp. nov. Dentate collar absent on *Brc. liupanensis* but present on *Bry. pucapetricolus* sp. nov.

Gene sequences similarity analyses

The ranges of uncorrected genetic *p*-distances between the studied population of *Bry. pucapetricolus* sp. nov. and other *Bryodelphax* species for which homological sequences are available from GenBank (Supplementary File 7), are as follows:

18S: 0.31%–2.90% (mean 1.60%), with the most similar being *Bry. maculatus* from Poland (KY609137, Gąsiorek et al., 2017), and the least similar being *Bry. australasiaticus* from Malaysia (MT333468, Gąsiorek et al., 2020a).

28S: 3.48%–8.32% (mean 6.39%), with the most similar being *Bry. maculatus* (MT333464, Gąsiorek et al., 2017), and the least similar being *Bry. decoratus* from Indonesia (MT333462, Gąsiorek et al., 2020a).

ITS-1: 22.84%–28.78% (mean 27.45%), with the most similar being *Bry. maculatus* (MT333479, Gąsiorek et al., 2017), and the least similar being *Bry. arenosus* from Western Borneo and *Bry. decoratus* (MT346599–MT346600, Gąsiorek et al., 2017 and MT333478, Gąsiorek et al., 2020a).

COI: 20.21%–20.92% (mean 20.59%), with the most similar being *Bry. mareki* from Canada (MW655785, Kayastha et al., 2021, to haplotype 2), and the least similar being the same sequence of *Bry. mareki* (to haplotype 3).

Uncorrected genetic *p*-distances between the COI haplotypes of *Bry. pucapetricolus* sp. nov. are within 0.89%–2.66% interval.

***Bryodelphax wallacearthuri* sp. nov.** (Figs. 2D-F, 3I, 4A, 6A, C, 8B, 9B, 18–26, 27B)

ZooBank: urn:lsid:zoobank.org:act:CCE4DFAE-5D4C-481F-AFB8-A0B458BC1F4B

Type material: 16 specimens on slides (holotype: adult female (Figs. 21, 22) and paratypes: 11 adult females, 3 adult males, 1 four-clawed juvenile) and 3 specimens on a SEM stub

Type locality: vicinity of Glensleade, County Clare, Republic of Ireland, 53° 4' 12" N, 9° 9' 36" W, 104 m asl, acrocarpous moss on limestone pavement, *leg*. E. DeMilio, 17/08/2013

Type repository: The holotype (slide NHMD 922699) and 10 slide mounted paratypes (slides NHMD 922700–922709) and 3 paratypes on a SEM stub (NHMD 922710) are deposited in the Natural History Museum of Denmark, Copenhagen, Denmark. Two paratypes (slides CE.ER1.1.04 and CE.ER1.1.31) are kept in the collection of ED. One paratype (slide CE.ER1.1.99) is deposited in the Bertolani Collection, Department of Life Sciences, University of Modena and Reggio Emilia, Italy. One paratype (slide CE.ER1.1.105) is deposited at the Department of Animal Taxonomy and Ecology, Institute of Environmental Biology, Adam Mickiewicz University, Poznań, Poland. One paratype (slide UNICT 6011) is deposited in the Binda and Pilato Collection, University of Catania, Italy.

Other population: Plitvice Lakes National Park, Ličko-senjska županija, Croatia, moss on stone, *leg.* I. Nikolaeva, 27/06/2006 (8 specimens (6 adult females, 2 four-clawed juveniles (slides SPbU229 64, 72, 73, 78, 79)) in the collection of DVT).

Etymology: Specific name is in dedication to the eminent evolutionary biologist and author, Professor (emeritus) Wallace Arthur (National University of Ireland Galway).

Species description

Body length (adult) 96.0–144.5 μm, other morphometric data given in Table 3. Cuticle colorless or white to light grey prior to slide mounting. Eyes absent or not visible after mounting in PVA. Paired cephalic cirri and clavae present. Internal cirrus with well-defined, swollen base (LM) formed by a poorly differentiated, weak cirrophore (SEM). External cirrus with small cirrophore. Cirrus A with evident cirrophore (Fig. 20A, B). All cephalic cirri without terminal bifurcations. Other dorsal and lateral cirri absent. Primary clava cylindrical with bluntly tapered apex (Figs. 20 A, B, 26A). Secondary clava roughly elliptical, attached to head by a broader basal portion that continues into a slightly tapered apex without a constricted portion in central part of clava (Figs, 19A–D). Internal buccal-pharyngeal structures not discernable in type series.

Dorsal plates clearly demarcated and with greatly thickened lateral edges (Fig. 23A). Dorsal cuticular plate sculpture consists of three main types of element: round intracuticular pillars, pores, and epicuticular elements (EEs) in form of large, individually well-differentiated, irregular polygons (Figs. 2F, 3I, 20). All three element types clearly visible (Figs. 18, 19A, 20, 22A). Knobby dorsal cuticle relief appears well developed in PhC with highly contrasting and abundant black circular areas (Figs. 4A, 22A).

Cephalic plate (cep) with rounded anterior margin, m-shaped posterior margin, and keyhole-shaped dorsomedial depression (Fig. 20A, B). All three sculpture element types present on cep (Fig. 19A, B). Intracuticular pillars visible on entire cep including within keyhole-shaped depression. Pores scattered randomly on cep, abundant on its entirety. EEs highly visible on entire cep surface.

Pair of lateral cephalic plates (lcp) present. Lcps strongly sclerotized with all three types of sculpture element present (Figs. 19A-D, 26A, B). Lcp barely in contact with cep posterior margin. In LM, weak fine pillars present diffusely on areas surrounding lcp and along entire lateral sides of body between dorsal plate lateral margins and leg coxae (Fig. 19A). Neck plate well-defined and strongly sculptured with all three element types (Figs. 18C, 20A, B).

Scapular plate (scp) with single median longitudinal ridge, two lateral longitudinal ridges, anterior latitudinal ridge, two central latitudinal ridges, and posterior latitudinal ridge (Fig. 2D, F). Central latitudinal ridges of similar width to anterior and posterior latitudinal ridges (Figs. 20B, C). Scp lateral margins well-defined. In lateral view scp lateral margins appear strongly thickened (Fig. 23A). Scp with all three sculpture element types present and strongly visible (Figs. 18, 20).

Table 3: Measurements (µm) of *Bryodelphax wallacearthuri* sp. nov. adults with associated *psc* or *pbl* values. cep= cephalic plate, scp= scapular plate, l= length, w= width, h= height, ⌀= diameter, n= number of individuals measured for that character, $\bar{x}$= mean, s= standard deviation.

Character	Holotype		Paratypes						Series			
	Female		Females			Males		n	$\bar{x}$		s	
	µm	*psc*	n	µm	*psc*	n	µm	*psc*		µm	*psc*	µm	*psc*
body length	120.6	696.0	11	98.2–144.5	611.5–810.7	3	96.0–133.4	719.3–753.4	15	124.8	739.9	14.3	52.3
scp	17.3	-	11	12.5–18.8	-	3	12.7–18.5	-	15	16.9	-	2.0	-
internal cirrus	6.5	37.3	11	4.5–7.9	35.7–46.3	3	4.9–7.1	38.1–40.5	15	6.9	40.5	1.0	3.7
external cirrus	11.3	65.1	10	8.3–13.8	64.9–84.0	3	8.2–14.1	64.1–76.3	14	11.7	69.5	1.8	5.4
cirrus A	34.2	197.1	11	27.1–43.6	189.5–247.1	3	27.7–39.7	214.2–221.2	15	37.6	221.8	5.2	15.8
cirrus A *pbl*	28.3%		11	23.7%–37.3%		3	28.8%–29.8%		15	30.1%		3.1	
primary clava	3.4	19.7	11	3.0–5.1	20.9–27.5	3	2.8–4.4	22.2–24.4	15	3.9	23.3	0.6	2.4
secondary clava l	5.2	29.9	10	2.8–5.2	15.3–30.0	3	2.6–4.9	20.7–26.4	14	4.1	24.2	0.8	4.3
secondary clava w	3.0	17.1	11	2.3–5.2	12.6–28.8	3	2.0–2.8	15.3–16.0	15	3.0	17.9	0.8	3.9
external claw I l	8.3	48.1	11	7.1–10.5	41.8–59.8	2	7.0–8.2	54.6–54.9	14	8.9	53.3	1.1	4.8
external claw I h	6.2	35.9	11	4.8–7.3	35.9–43.3	2	5.3–6.6	41.8–43.8	14	6.6	39.6	0.8	2.4
internal claw I l	9.4	54.5	10	8.0–11.4	47.4–66.6	2	8.2–8.3	54.6–65.5	13	9.6	57.9	1.1	5.7
internal claw I h	6.8	39.1	10	5.6–8.3	37.3–45.1	2	5.8–6.8	45.0–45.5	13	7.1	42.5	0.8	3.0
spur I l	-	-	9	0.7–1.2	5.2–7.3	2	0.8–1.1	6.0–6.1	11	1.1	6.2	0.2	0.7
spur I insertion point	-	-	9	0.7–1.8	5.7–9.5	2	1.0–1.7	7.7–8.9	11	1.4	7.9	0.3	1.1
external claw II l	7.8	45.1	9	6.7–10.1	45.1–55.9	3	7.2–9.5	49.3–53.7	13	8.6	51.2	1.0	2.9
external claw II h	6.0	34.9	9	5.0–7.5	34.9–41.8	3	5.1–7.1	38.5–41.6	13	6.5	39.0	0.8	2.0
internal claw II l	9.1	52.4	9	7.0–11.7	52.4–62.0	3	8.0–9.9	53.1–63.5	13	9.5	56.5	1.2	4.1
internal claw II h	6.8	39.2	9	5.5–8.3	38.2–44.7	3	5.7–7.3	39.4–44.9	13	7.0	41.9	0.8	2.3
spur II length	-	-	6	0.6–1.1	4.3–6.8	1	0.8	6.3	7	0.9	5.6	0.2	0.9
spur II insertion point	-	-	7	0.9–1.6	6.2–9.5	1	1.1	8.6	8	1.3	7.6	0.2	1.1
external claw III l	8.7	50.0	7	8.4–9.6	47.5–57.5	2	7.1–9.6	51.6–55.9	10	9.0	52.1	0.8	3.6
external claw III h	6.5	37.3	9	5.5–7.6	34.7–43.8	2	5.4–7.0	37.8–42.2	12	6.7	39.3	0.7	2.4
internal claw III l	9.1	52.6	7	9.8–11.5	54.0–64.9	2	7.4–10.0	53.9–57.8	10	10.0	57.5	1.1	3.9
internal claw III h	6.7	38.7	9	5.6–8.0	36.8–44.7	2	5.8–7.5	40.3–45.8	12	7.1	41.6	0.7	3.0
spur III l	1.0	6.0	4	0.9–1.2	4.8–6.5	1	0.8	5.9	6	1.0	6.0	0.1	0.6
spur III insertion point	1.0	5.5	4	1.2–1.5	6.6–8.0	1	1.2	9.4	6	1.3	7.4	0.2	1.3
external claw IV l	9.5	54.6	9	8.3–10.8	46.2–65.8	2	9.0–9.9	53.2–59.5	12	9.7	56.7	0.8	5.6
external claw IV h	7.2	41.4	10	5.5–8.1	36.2–47.6	3	6.4–7.4	39.9–50.0	14	7.3	43.0	0.8	3.4
internal claw IV l	10.3	59.5	9	7.2–11.6	51.2–70.3	2	9.7–10.7	57.6–64.2	12	10.3	60.0	1.2	5.5
internal claw IV h	7.7	44.4	10	6.2–8.8	41.0–50.1	3	6.4–7.8	42.3–50.2	14	7.8	46.0	0.8	3.2
spur IV l	0.9	5.4	7	0.9–1.5	4.9–9.2	2	0.7–1.1.	4.9–5.9	10	1.2	6.5	0.3	1.3
spur IV insertion point	1.4	8.1	6	1.4–1.8	7.3–10.8	2	1.0–1.4	6.7–7.4	9	1.4	8.1	0.2	1.2
sense organ I	-	-	-	-	-	-	-	-	-	-	-	-	-
sense organ IV	1.5	8.8	10	1.5–2.5	8.1–14.8	3	1.6–2.0	9.8–13.2	14	1.8	11.0	0.3	2.0
gonopore ⌀	7.1	40.9	10	5.4–8.0	36.3–46.1	3	1.7–2.7	10.9–14.4	14	6.1	36.1	2.2	11.9
gonopore to anus	15.7	90.6	9	11.5–21.0	84.1–124.1	3	6.2–11.2	41.0–63.2	13	15.1	89.5	4.6	23.1
gonopore to anus *pbl*	13.0%		9	11.8%–15.5%		3	5.5%–8.4%		13	12.1%		2.9	

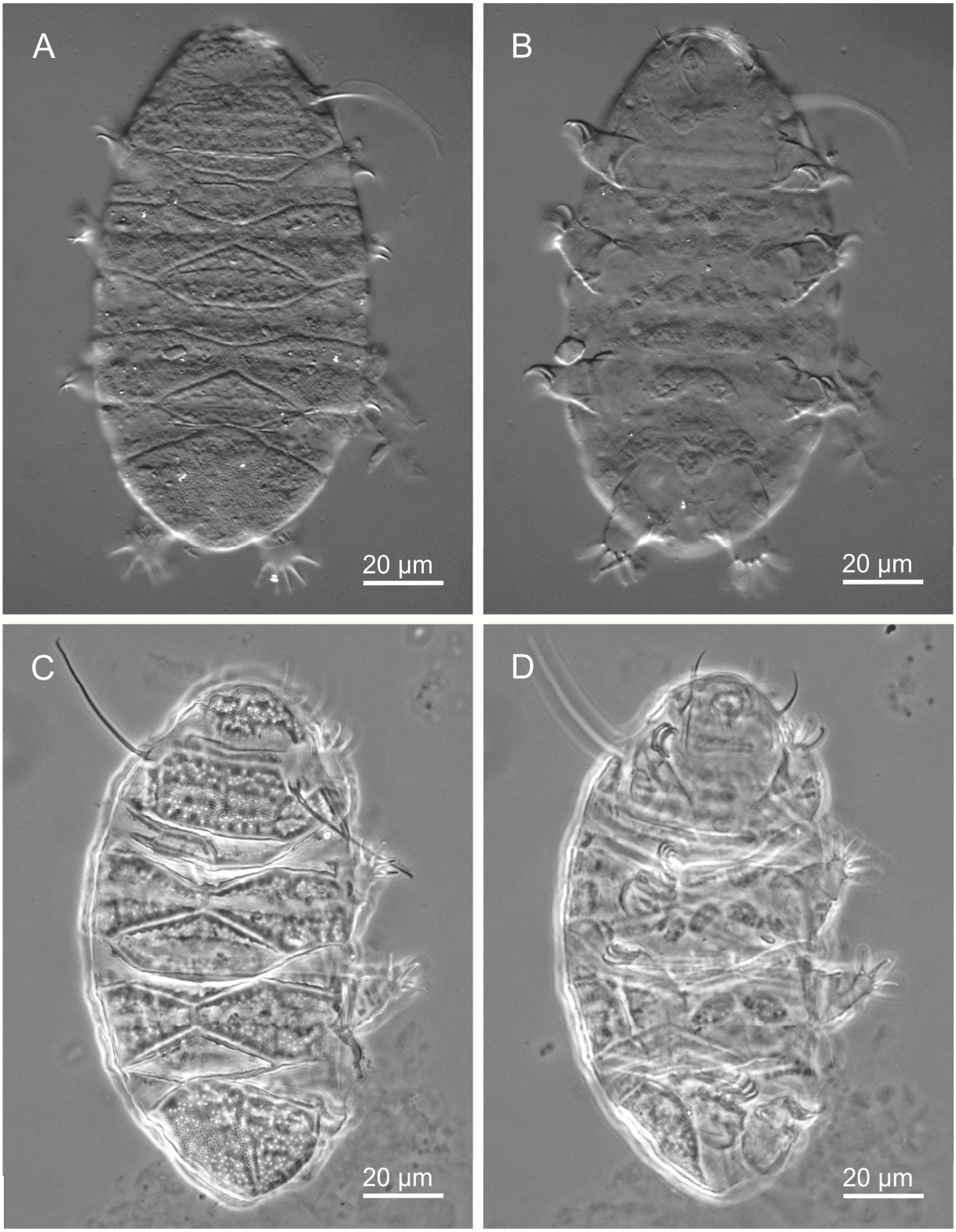

Figure 18: *Bry. wallacearthuri* sp. nov. *habitus*. **A** dorsal female paratype (DIC); **B** ventral female paratype (DIC); **C** dorsal male paratype (PhC); **D** ventral male paratype (PhC).

Intracuticular pillars visible on entire scp, with those of largest diameter on middle–posterior parts of longitudinal ridges (Figs. 2F, 20B). Pores arranged in vague transverse bands mostly placed between latitudinal ridges, but absent upon longitudinal ridges (Fig. 20A, B). EEs strongly visible and well-developed on scp entirety. Single rows of large individual EEs occur on each latitudinal ridge, with largest EEs occurring on posterior latitudinal ridges. EEs occur between anterior and central latitudinal ridges, and more sparsely between central and posterior latitudinal

ridges. EEs most densely distributed on median longitudinal ridge (Figs. 3I, 20).

Median plates 1 and 2 (m1 and m2) each with a transversal crest forming a primary division into an anterior part (a) and posterior part (p). M1a, m1p, m2a, and m2p all secondarily divided into anterior and posterior portions by median transverse furrows (Figs. 4A, 18A, 21A, 22A). Presence of median longitudinal ridges undetermined for all median plates. M1a roughly trapezoidal in form. M1p roughly pentagonal in form. Intracuticular pillars visible on entire m1a and m1p parts with only few pillars visible within median transverse furrows. Intracuticular pillars appear largest on m1a posterior portion. Pores scattered on m1a anterior and posterior portions and less evidently (in PhC) on m1p anterior and posterior portions (Figs. 4A, 22A). EEs strongly developed, clearly visible on entire m1, most strongly along m1a and m1p posterior margins where large EEs occur in single rows (Fig. 3I).

M2a pentagonal with triangular anterior margin. M2p pentagonal with roughly triangular posterior margin. M2p narrower than m2a. Intracuticular pillars small, visible on entire m2 but fewer and more difficult to see within median transverse furrows. Pores scattered abundantly on all parts of m2, but rare within median transverse furrows (Fig. 22A). EEs strongly developed on m2a and m2p, especially visible in lines along all m2a margins and m2p posterior margin, EEs absent within median transverse furrows (Figs. 4A, 22A).

Median plate 3 undivided (*i.e.* without a median transversal crest forming a primary transverse division between an anterior part and posterior part) but with a broad, weakly sculptured central median transverse furrow (Fig. 21A). M3 roughly triangular in form with slightly curved posterior margin. Intracuticular pillars present on entirety of m3, but very weakly visible in the central median transverse furrow. Pores present on entirety of m3, more abundant and more strongly visible on the area anterior to the median transverse furrow, fewer on area posterior to median furrow, rare within median furrow. EEs on m3 strongly developed, clearly visible in lines along all m3 margins, absent within median transverse furrow. Tertiary division absent.

Paired plate 1 (pp1) and paired plate 2 (pp2) similar in appearance, both with a medially interrupted transverse groove separating an anterior part and broader posterior part (Figs. 4A, 18A, C, 21A, 22A). Transverse groove with small, hardly visible intracuticular pillars present within. Transverse groove interrupted at body midline by a longitudinal ridge with visible intracuticular pillars. Intracuticular pillars clearly visible on pp1 and pp2 anterior and posterior parts, without noticeable difference in pillar diameter between parts. Pores abundant and distributed randomly on pp1 and pp2 anterior and posterior parts (Fig. 18C). EEs strongly developed, highly visible on both parts of pp1 and pp2, most evident in lines along anterior and posterior margins (Figs. 4A, 18C, 22A).

Caudal plate (cap) with typical dual longitudinal ridges and two well-developed central latitudinal ridges. All ridges bear large EEs. Cap anterior margin with rounded arched median section (Fig. 18A). Intracuticular pillars clearly visible on entire cap with pillars of largest diameters at plate central interior region, including the midsections of longitudinal ridges. Pores abundant, distributed on entire cap, but slightly fewer present at mid-interior region. EEs strongly developed, visible on entire cap, most apparent in a line along anterior cap margin (Figs. 18C, 22A).

Lateral intersegmental plate (lip) present in pairs at both lateral sides of each median plate (6 pairs total) (Fig. 18A). Anterior lip of each pair slightly larger and extends further onto lateral sides of body than posterior lip. Difference in lengths between anterior and posterior lip in a pair decreases in rostral caudal direction (*i.e.* relative difference between lips at m1 greatest, at m3 least) (Fig. 22). At m1, division between anterior and posterior lip aligned with m1p anterior portion (Fig. 18A). At m2, division between anterior and posterior lip aligned with m2p anterior portion (Fig. 18A). At m3, division between anterior and posterior lip aligned with division between m3 and caudal plate (Fig. 21A). All lips sculptured with visible intracuticular pillars, pores, and EEs (Fig. 22A).

Each leg with thick, well-defined coxal and femoral plates (Figs. 21, 22, 23). Fine pillars weakly visible on plated and unplated leg surfaces. Pores not visible on coxal plates. In LM, coxal plates appear sculptured with a single row of EEs (Figs. 21A, 22A, 23A-C). In SEM, entire coxal plate surface evidently covered with EEs, including upon an elevated ridge (Figs. 23E, F). EEs on ridge appear in LM as a single row of EEs on coxal plate. Femoral plates with an evident pair of distal and an evident pair of proximal epicuticular ridges (Figs. 21, 22, 23A-C). Femoral plates sculptured with intracuticular pillars, and large, well-developed EEs along all femoral plate epicuticular ridges (visible in LM and SEM), as well as on the entire femoral plate surfaces (visible in SEM only, Fig. 23E-G), pores absent. Dentate collar present, with variable appearance between individuals and between legs of a single individual, with 4–10 teeth. Teeth with thin, elongate, sinuous appearance, not short or triangular in form, occasionally sharing a common base (Figs. 23G, 24C).

Leg sense organs present on legs I and IV (*i.e.* p1 and p4 present) (Figs. 21A, 22A, 23). P1 located on distal-most femoral plate epicuticular ridge, and clearly distinguishable only in SEM due to presence of large EEs at same position (Fig. 23B, E). P4, a rounded papilla located near to proximal margin of femoral plate. Claws of typical arrangement and form (Fig. 24D, G). Basal spurs absent on external claws, present on internal claws. Spurs slightly curved and oriented towards claw base (Figs. 23F, 24B).

Fine pillars weakly visible on entire ventral surface (Fig. 19C, E). Ventral plates present, strongly sclerotized, well-defined, positioned in 9 rows (Figs. 18B, D, 21B, 22B, 25A, 26A, 27B): Row 1, svps merged into a single solid ridge-like form (Figs. 19C-F); Row 2, one plate in line with legs I; Rows 3, five plates and Row 4, two plates, both Rows 3 and 4 between legs I and II; Row 5, four plates and Row 6, two plates, both Rows 5 and 6 between legs II and III; Row 7, two plates in line with legs III; Row 8, two lateral gonoplates; and Row 9, one posterior gonoplate (Figs. 24A, B, 26C). Plate configuration and morphology constant within population and between sexes. In LM, ventral plates show conspicuous intracuticular pillars, pores, and EEs (Figs. 6A, C, 18B, D). In LM and SEM, Row 2 single plate and Row 3 central plate, although well-developed and demarcated, appear more weakly sculptured than all other ventral plates (Figs. 19E, F, 25B, 26A) which show large pores (some with protruding collars in SEM (Fig. 25B, C), and strongly developed, conspicuous EEs (Figs. 21B, 22B).

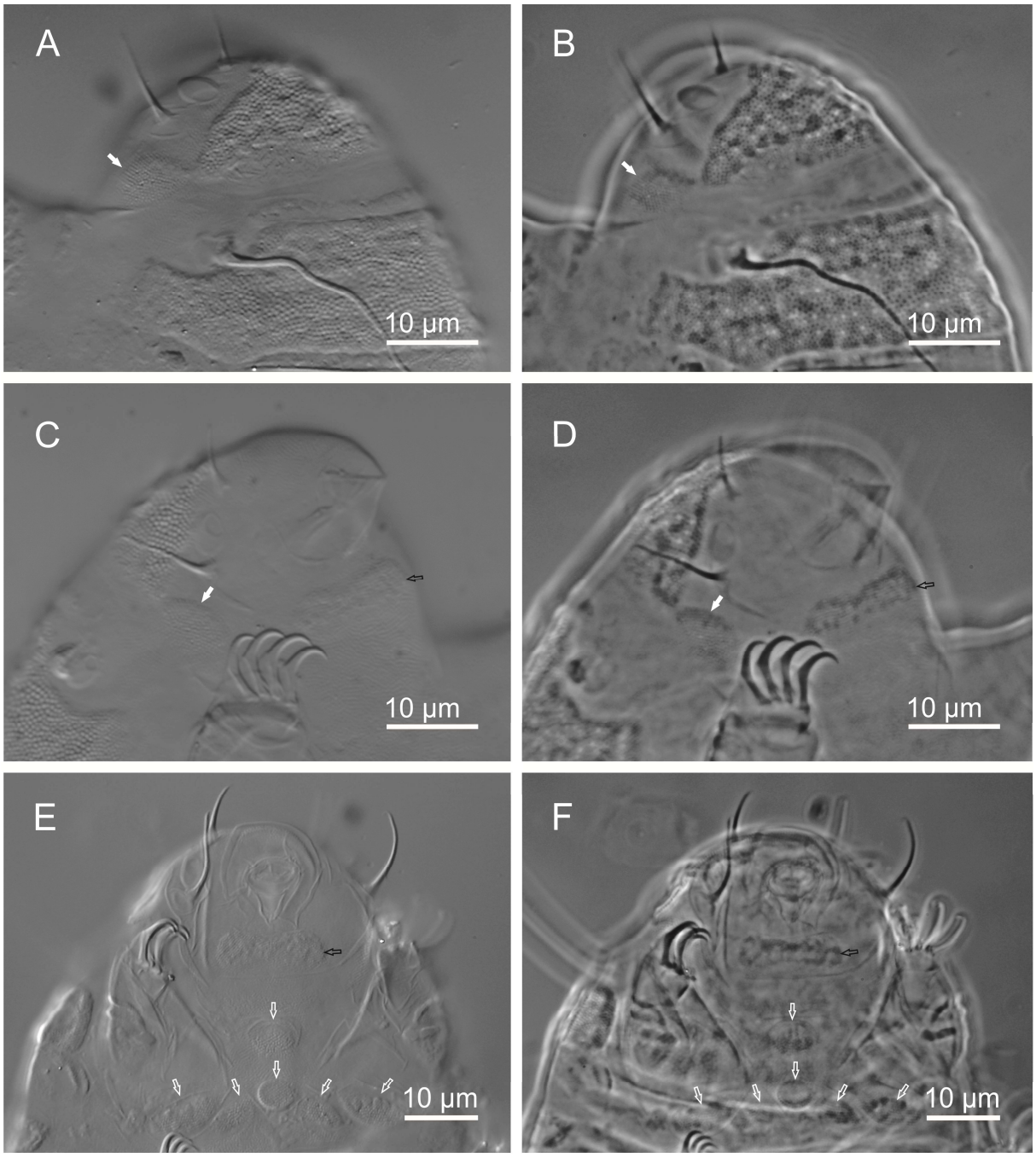

Figure 19: Anterior structures of *Bry. wallacearthuri* sp. nov. **A** dorsal cephalic region and scapular plate (DIC); **B** dorsal cephalic region and scapular plate (PhC); **C** ventrolateral cephalic region (DIC); **D** ventrolateral cephalic region (PhC); **E** ventral plates (DIC), plates in Rows two and three; **F** ventral plates (PhC), plates in Rows two and three. Filled white arrows= lateral cephalic plates, black hollow arrows= fused subcephalic ventral plates, white hollow arrows= other ventral plates.

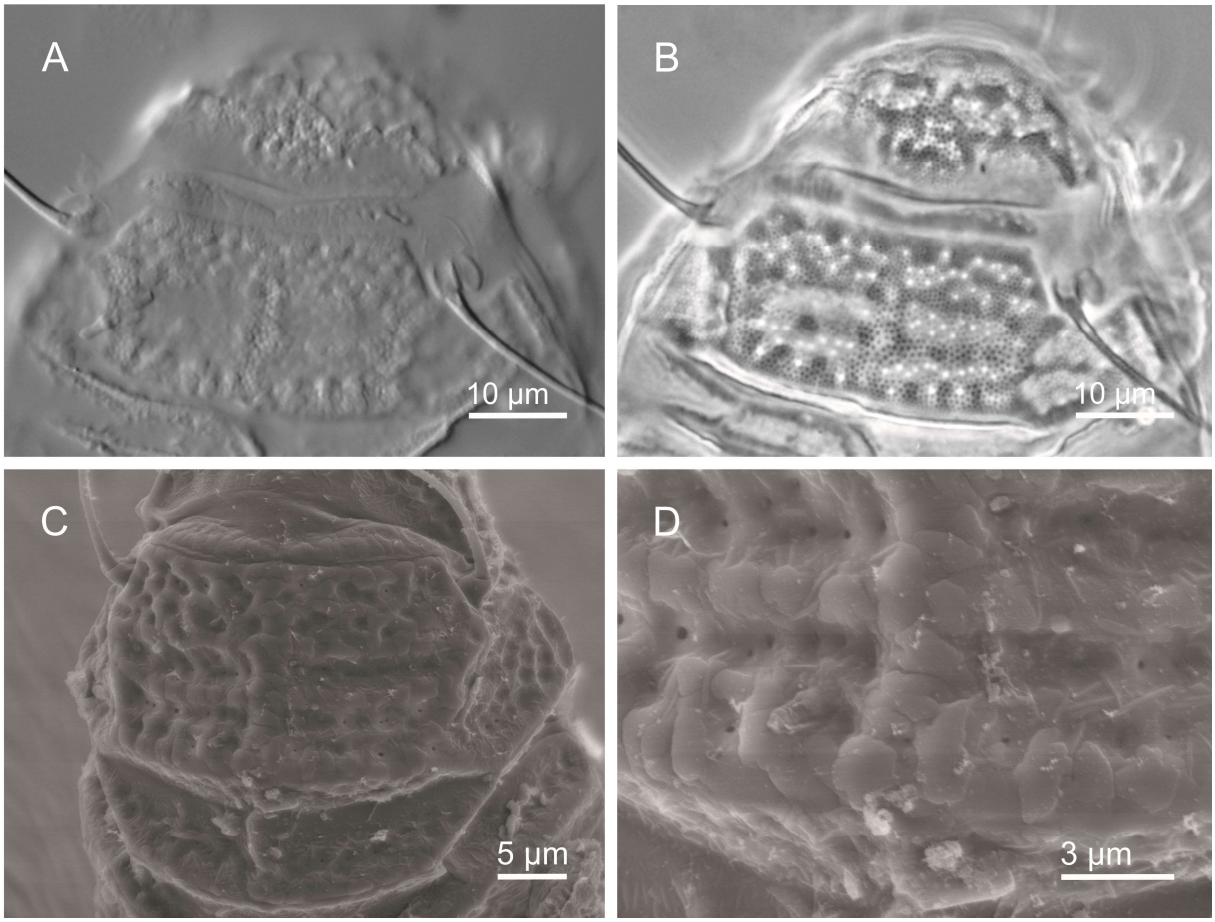

Figure 20: *Bry. wallacearthuri* sp. nov. scapular plate. **A** in DIC; **B** in PhC; **C** overview in SEM; **D** detail of sculpture elements in SEM.

Female gonopore somewhat broad in diameter (Table 3), surrounded by typical rosette of 6 cells (Figs. 18B, 24A, 26C). Male gonopore circular with evident sculpture elements around circumference (Fig. 24B). Anterior hood not observed in LM. Details of male gonopore morphology not observed in SEM. Female gonopore of larger diameter and positioned more rostrally from anus than male gonopore (Table 1). Anal system composed of flexible lateral lobes with additional lateral folds on either side of a lamellar central terminal structure (Figs. 8B, 9B).

Ontogeny. Number of instars that occur within each developmental stage unknown. Eggs and two-clawed larvae not found. One four-clawed juvenile observed, body length 92.2 µm. Most adult characters, including well-developed ventral plates observed. Gonopore absent. Development of the anal system could not be observed due to specimen orientation.

Morphological differential diagnosis

Bry. wallacearthuri sp. nov. is different from *Bryodelphax* species belonging to the '*parvulus* group' due to the presence of ventral plates in *Bry. wallacearthuri* sp. nov. Within the '*weglarskae* group', *Bry. wallacearthuri* sp. nov. is most easily separated from species that have a different number of rows of ventral plates: *Bry. aaseae* and *Bry. iohannis* (both with 10 rows); possibly *Bry. kristenseni* (10 rows (but see below on the possibility of 9 rows)); *Bry. olszanowskii* (8 rows); *Bry. australasiaticus*, *Bry. decoratus,* and *Bry. sinensis* (all with 7 rows); *B. maculatus* (3 rows); *B. nigripunctatus* (3 rows in females, 2 rows in males); and *B. amphoterus*, *Bry. mareki* and *Bry. pucapetricolus* sp. nov. (each with 2 rows, but see our observations on the number of plates in *Bry. mareki* above). *Bry. wallacearthuri* sp. nov. is most similar to those '*weglarskae* group' species that share the same number of rows of ventral plates (nine): *Bry. instabilis*, possibly *Bry. kristenseni*, *Bry. parvuspolaris* (according to our results stated below), and *Bry. weglarskae*. *Bry. wallacearthuri* sp. nov. differs to these species in the following characters:

Bry. instabilis. EEs of the dorsal cuticular sculpture of *Bry. instabilis* appear to be positioned into a close-fitting, mosaic-like network (Fig. 3C), while on *Bry. wallacearthuri* sp. nov. EEs are positioned apart as individual elements (Fig. 3I). Dorsal plate relief of *Bry. instabilis* is poorly developed and is of low contrast with very few dark circular areas visible in PhC., whereas *Bry. wallacearthuri* sp. nov. shows high contrasting and abundant black circular areas in PhC (Fig. 4A).

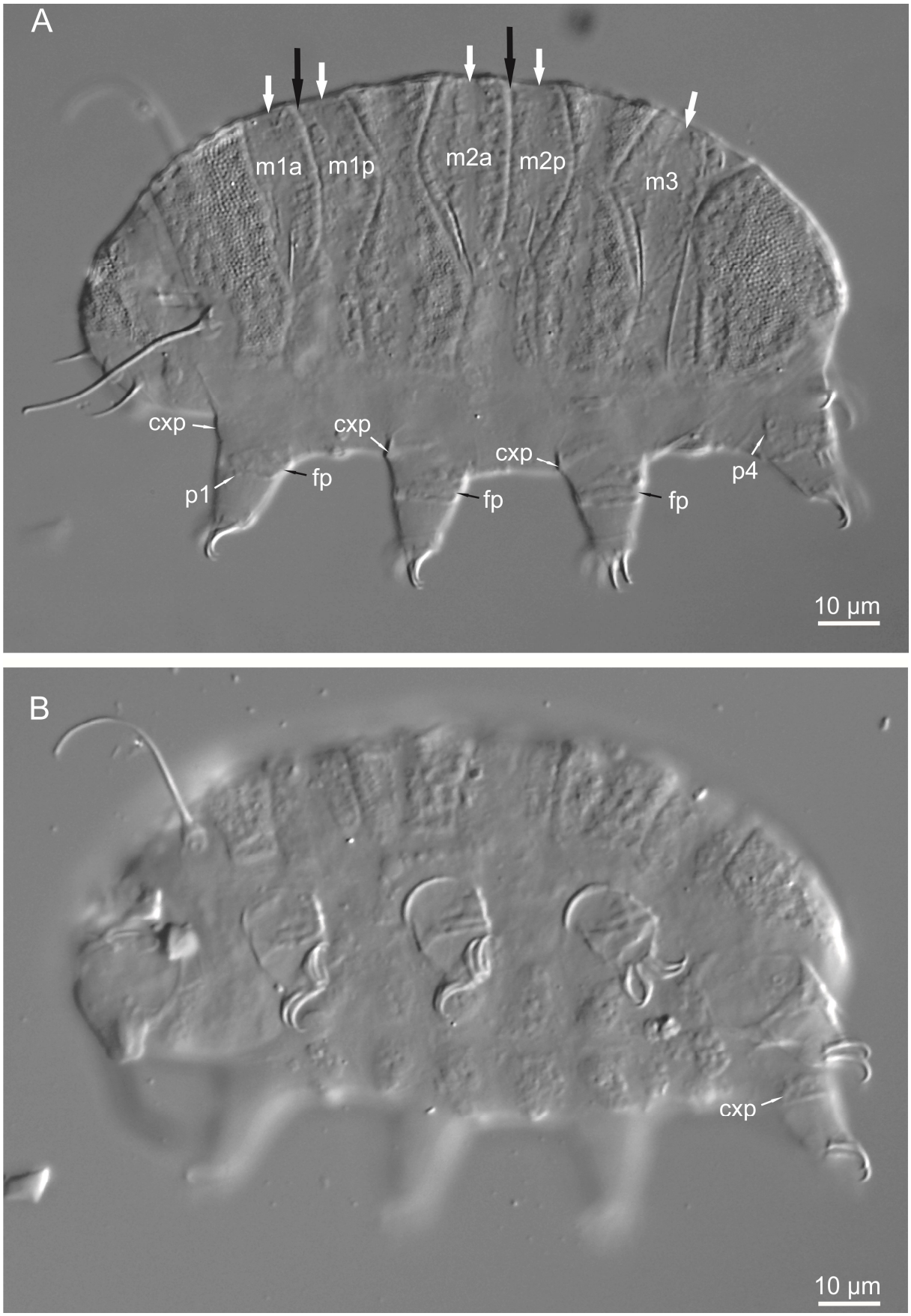

Figure 21: *Bry. wallacearthuri* sp. nov. holotype (DIC). **A** divisions of the dorsal median plates and leg structures; **B** ventrolateral view including ventral plates. Black solid arrow= transversal crest, white solid arrow= median transverse furrow, cxp= coxal plate, fp= femoral plate, p1= sense organ of leg I, p4= sense organ of leg IV.

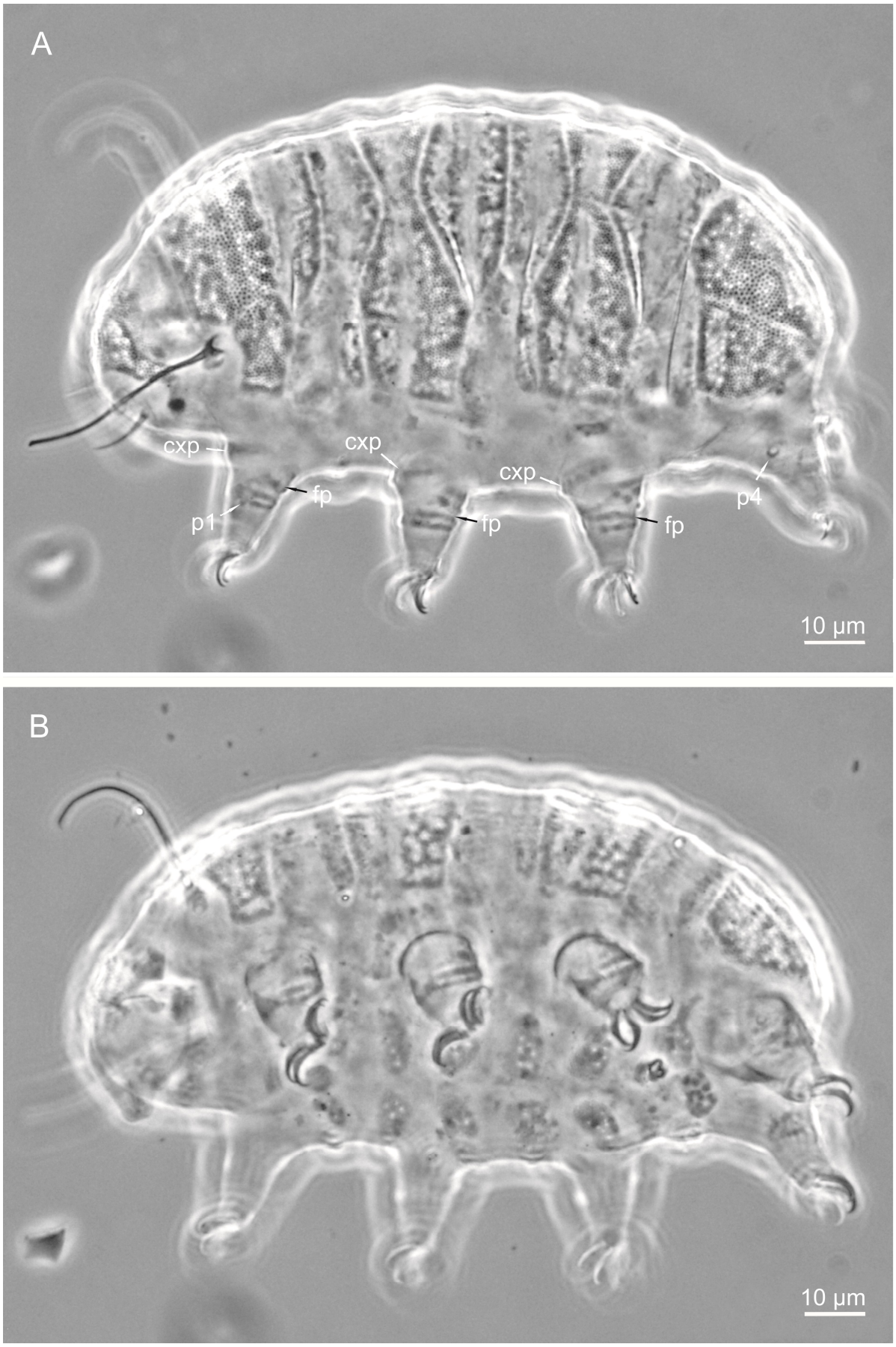

Figure 22: *Bry. wallacearthuri* sp. nov. holotype (PhC). **A** dorsal plates and leg structures; **B** ventrolateral view including ventral plates. cxp= coxal plate, fp= femoral plate, p1= sense organ of leg I, p4= sense organ of leg IV.

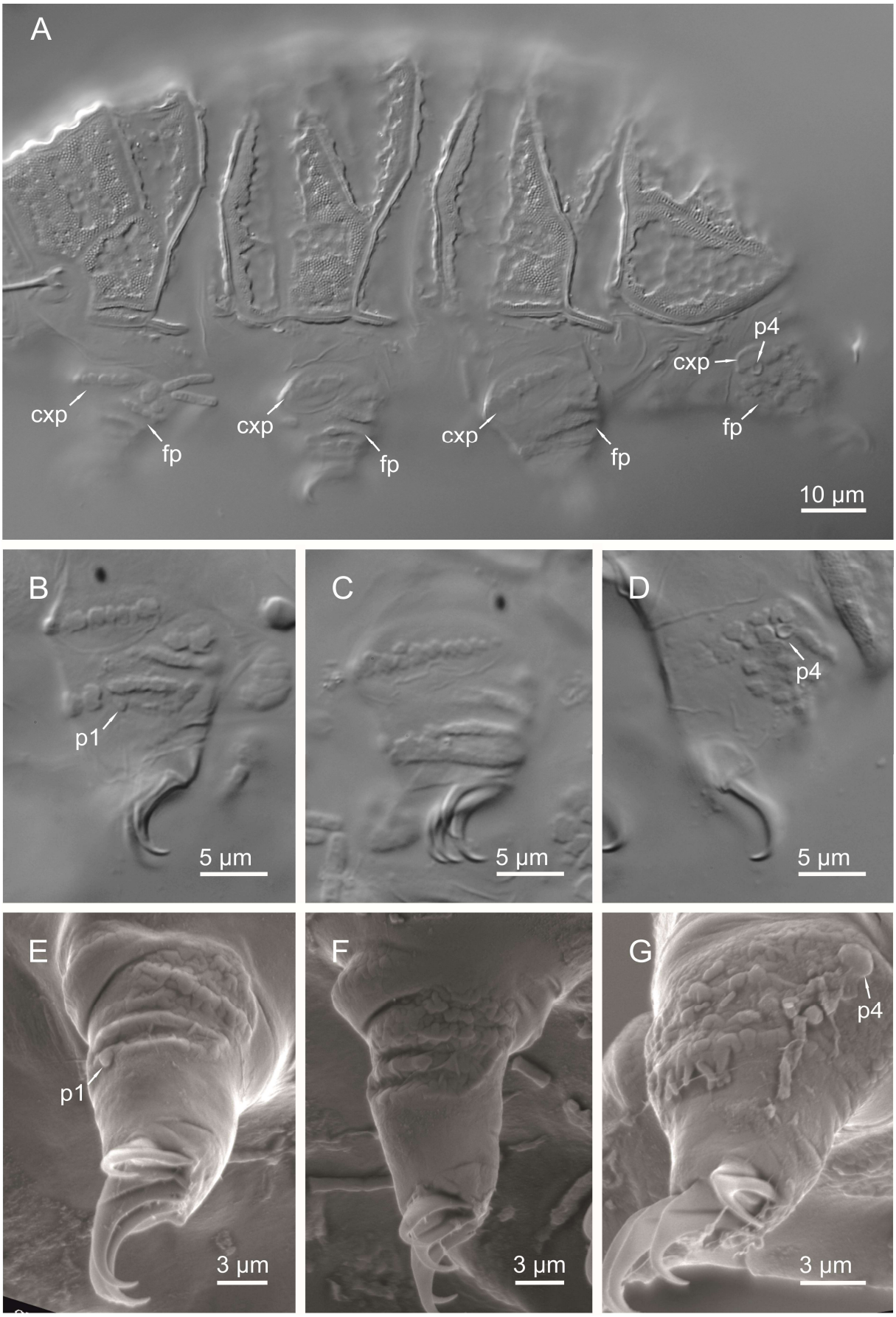

Figure 23: *Bry. wallacearthuri* sp. nov. leg structures. **A** overview of leg structures (DIC); **B** leg I (DIC); **C** leg III (DIC); **D** leg IV (DIC); **E** leg I (SEM); **F** leg III (SEM); **G** leg IV with dentate collar (SEM). p1= sense organ of leg I, p4= sense organ of leg IV.

*B. instabili*s was described as showing sexual dimorphism of the primary and secondary clavae, while the clavae of *Bry. wallacearthuri* sp. nov. are similar between the sexes. Lcps of *Bry. instabilis* are weakly developed, while lcps of *Bry. wallacearthuri* sp. nov. are strongly sclerotized and heavily sculptured. Svps of *Bry. instabilis* are rounded, very weakly demarcated areas that occur as separate entities, while the svps of *Bry. wallacearthuri* sp. nov. are very well defined, heavily sculptured, and fused into a single structure. The other ventral plates of *Bry. instabilis* are also weakly developed with the first two rows of plates described as being typically visible only in SEM. All ventral plates of *Bry. wallacearthuri* sp. nov. are strongly developed, heavily sculptured and clearly visible in LM. The two species have a different number of plates in Row 3 (either two or four plates in *Bry. instabilis* vs. always five in *Bry. wallacearthuri* sp. nov.) and in Row 5 (either two or four plates in *Bry. instabilis* vs. always four in *Bry. wallacearthuri* sp. nov.). *Bry. instabilis* was described as having ventral intracuticular pillars being either absent or present, while they are always present and conspicuous in *Bry. wallacearthuri* sp. nov. The sculpture of the coxal and femoral leg plates are different in the two species (see Leg plates section above). The female gonopore diameter *psc* is greater in *Bry. instabilis* than in *Bry. wallacearthuri* sp. nov. (Table 1). The female gonopore is positioned more closely to the gonopore (*psc* value) in *Bry. instabilis* than in *Bry. wallacearthuri* sp. nov. (Table 1).

Bry. kristenseni. The ventral plate configuration is different between *Bry. kristenseni* and *Bry. wallacearthuri* sp. nov. The number of rows of ventral plates was not precisely described for *Bry. kristenseni* because the authors (Lisi et al., 2017) were not able to positively confirm the presence/absence of a median unpaired ventral plate at a position in line with legs I. If this plate is absent in *Bry. kristenseni* then that species would also have 9 rows of ventral plates as does *Bry. wallacearthuri* sp. nov., however the rows of ventral plates differ in the position on the body and the number of plates per row between the two species. Additionally, the ventral plates of *Bry. kristenseni* were described as faint or almost invisible, which is very different to the strongly sclerotized, evident ventral plates of *Bry. wallacearthuri* sp. nov. *Bry. kristenseni* does not have a sense organ on legs IV (not visible in LM) or a dentate collar, both of which are easily observable on *Bry. wallacearthuri* sp. nov. with LM.

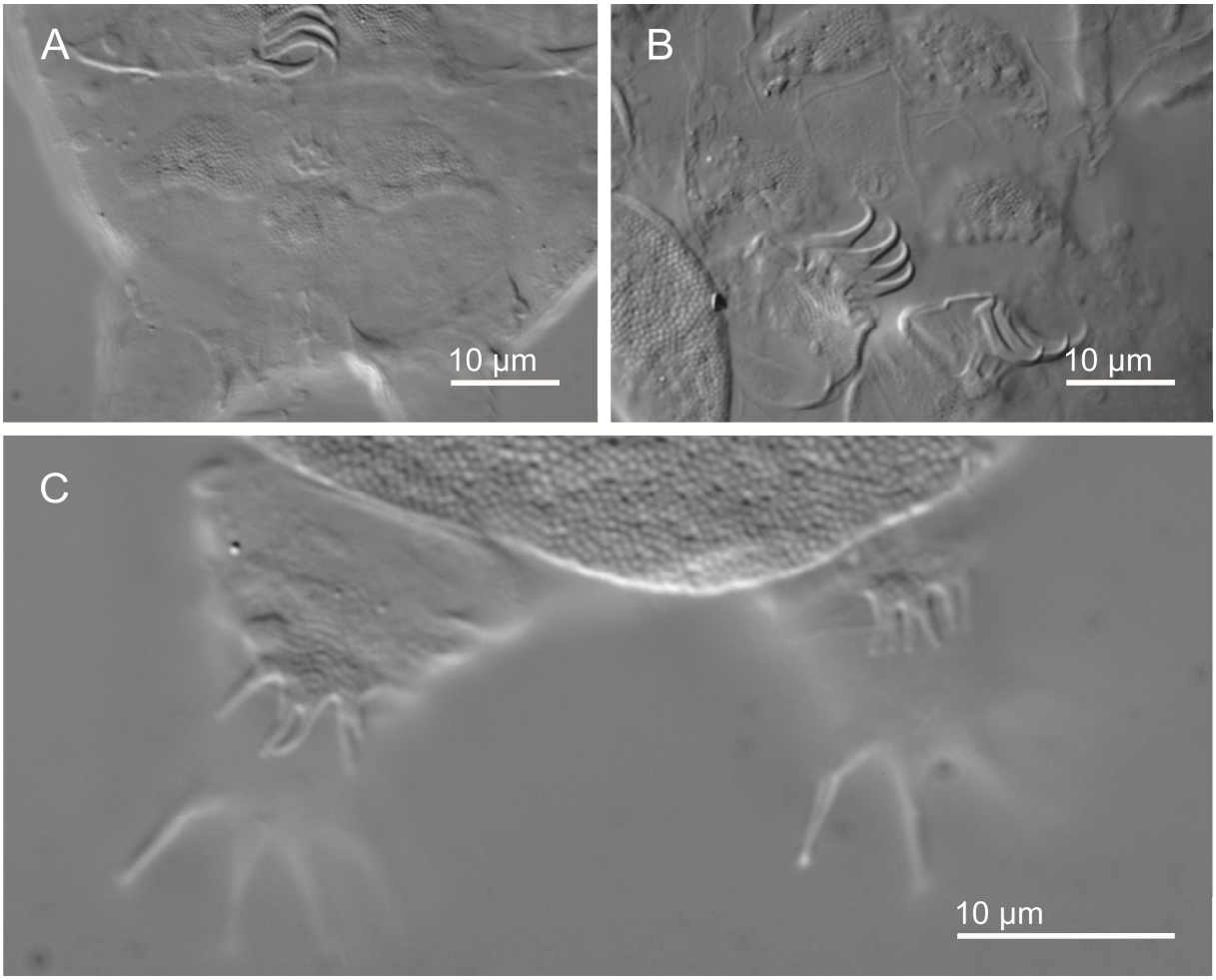

Figure 24: *Bry. wallacearthuri* sp. nov caudal region (DIC). **A** lateral and posterior gonoplates, female; **B** lateral and posterior gonoplates, male; **C** legs IV with dentate collar.

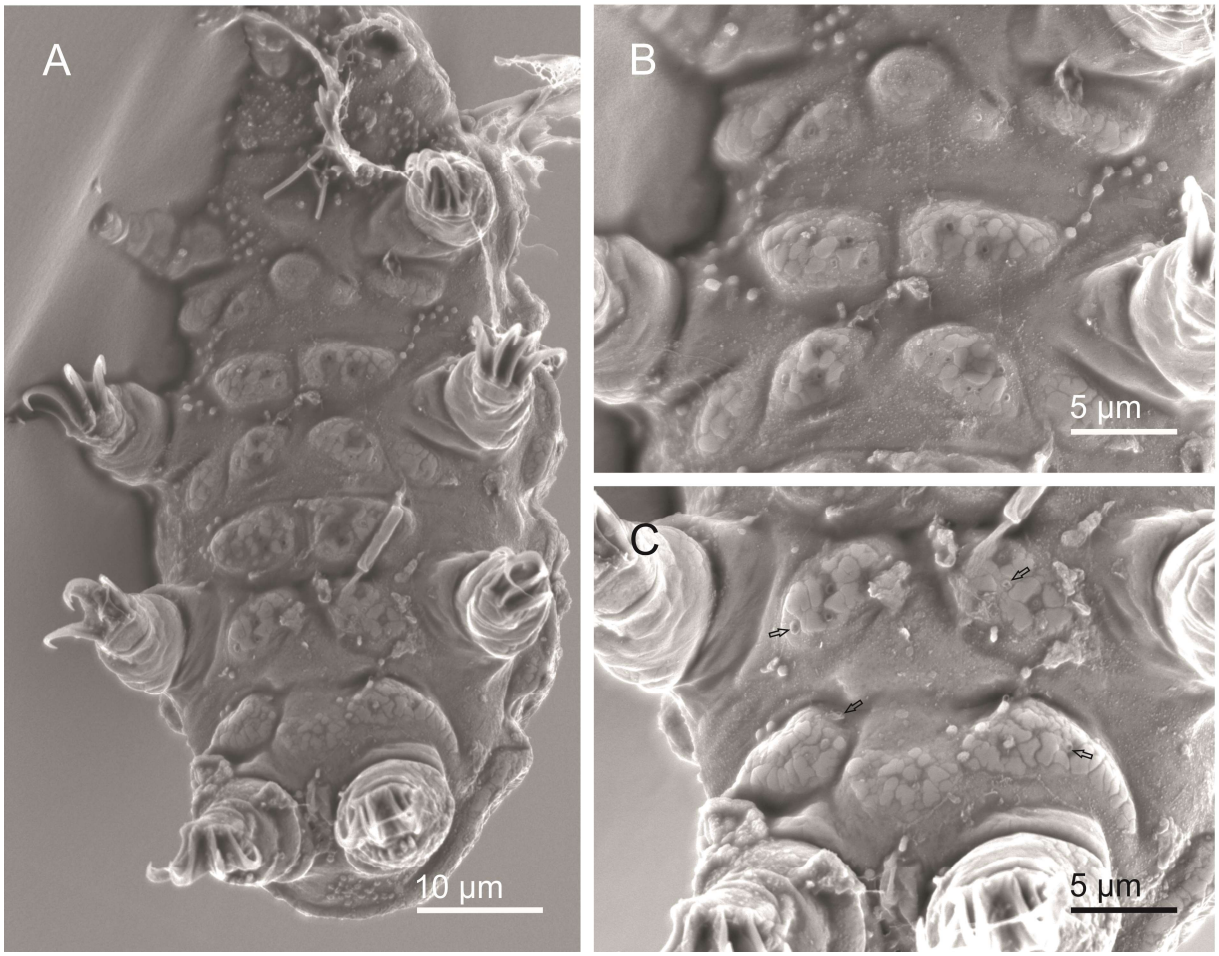

Figure 25: Ventral plate morphology in *Bry. wallacearthuri* sp. nov (SEM). **A** ventral overview; **B** ventral plate Rows three, four, and five; **C** ventral plate Row seven, lateral and posterior gonoplates (Rows eight and nine). Black hollow arrows= collared pores on ventral plates.

Bry. parvuspolaris. Dorsal cuticular sculpture of *Bry. parvuspolaris* appears to have weakly developed EEs showing low relief with low contrast and few black circular areas in PhC, while EEs of *Bry. wallacearthuri* sp. nov. are strongly developed showing high relief with high contrast and abundant black circular areas in PhC (Fig. 4A). Lcps of *Bry. parvuspolaris* are weakly developed, whereas lcps of *Bry. wallacearthuri* sp. nov. are strongly developed and heavily sculptured. Svps of *Bry. parvuspolaris* occur as two rounded, weakly demarcated areas, while svps of *Bry. wallacearthuri* sp. nov. are strongly sclerotized, heavily sculptured, and fused into a single plate. The ventral plates are sculptured differently between the two species with a different plate configuration in the nine plate rows. In Row 3 *Bry. parvuspolaris* is described as having a single plate, while *Bry. wallacearthuri* sp. nov. has five plates in Row 3. In Row 5 *Bry. parvuspolaris* has two plates, while *Bry. wallacearthuri* sp. nov. has four. *Bry. parvuspolaris* was described as having pillars absent from within the transverse grooves of the paired plates, while pillars are visible on these areas of *Bry. wallacearthuri* sp. nov. *Bry. parvuspolaris* lacks p4 or it was not visible in LM, while p4 is evident on *Bry. wallacearthuri* sp. nov. in LM. Dentate collar form is different between the two species with teeth only poorly developed in *Bry. parvuspolaris* compared to normally developed teeth on the *Bry. wallacearthuri* sp. nov. dentate collar.

Bry. weglarskae. Cephalic cirri are bifurcated in *Bry. weglarskae* but all cirri of *Bry. wallacearthuri* sp. nov. have typical single terminations. Dorsal plate relief of *Bry. weglarskae* is not strongly developed showing low contrast and only few dark circular areas visible in PhC, whereas Br*y. wallacearthuri* sp. nov. has strongly developed dorsal plates relief showing high contrast and abundant black circular areas in PhC (Fig. 4A). Lcps of *Bry. weglarskae* are weakly developed and difficult to observe, whereas lcps of *Bry. wallacearthuri* sp. nov. are strongly sculptured and apparent. Transverse grooves of paired plates of *Bry. weglarskae* are unsculptured, while visible intracuticular pillars are present in transverse grooves of *Bry. wallacearthuri* sp. nov. paired plates. Svps are two separate, rounded areas in *Bry. weglarskae*, whereas svps of *Bry. wallacearthuri* sp. nov. are consistently fused into a single bar-like structure. Ventral plate sculpture and shapes and

sizes of some corresponding ventral plates differ between the two species (Figs. 6A vs 6B and 6C vs. 6D). Femoral plates sculptured differently. The female gonopore diameter *psc* and the distance between the female gonopore and anus (*psc* and *pbl*) are greater in *Bry. wallacearthuri* sp. nov. than *Bry. weglarskae* (Table 1).

We also compare *Bry. wallacearthuri* sp. nov. to *Bry. iohannis* because the plate configuration within rows is similar between the two species, although *Bry. iohannis* has an additional single plate positioned immediately caudal to the svp row that is not present in *Bry. wallacearthuri* sp. nov. Furthermore, *Bry. wallacearthuri* sp. nov. differs from *Bry. iohannis* by the dorsal plate relief, which is low in *Bry. iohannis* showing low contrast with few very dark circular areas visble in PhC (Fig. 4C), compared to the well-developed relief of *Bry. wallacearthuri* sp. nov. showing highly contrasting abundant dark circular areas on the cuticle in PhC (Fig. 4A). Transverse grooves of paired plates of *Bry. iohannis* are unsculptured, while visible intracuticular pillars are present in transverse grooves of *Bry. wallacearthuri* sp. nov. paired plates. Svps of *Bry. iohannis* are distinctly separate, rounded areas while these plates are fused in *Bry. wallacearthuri* sp. nov. Teeth of the *Bry. iohannis* dentate collar are in the form of shorter triangular teeth, compared to the irregular sinuous teeth of the *Bry. wallacearthuri* sp. nov. dentate collar. The female gonopore diameter *psc* is significantly larger in *Bry. wallacearthuri* sp. nov. than in *Bry. iohannis* (Table 1). Other morphometric differences include shorter mean lengths of all cirri (*psc*, *pbl*) in *Bry. iohannis* and shorter mean lengths and heights of all claws (*psc*) in *Bry. iohannis* (Table 3, Supplementary File 6).

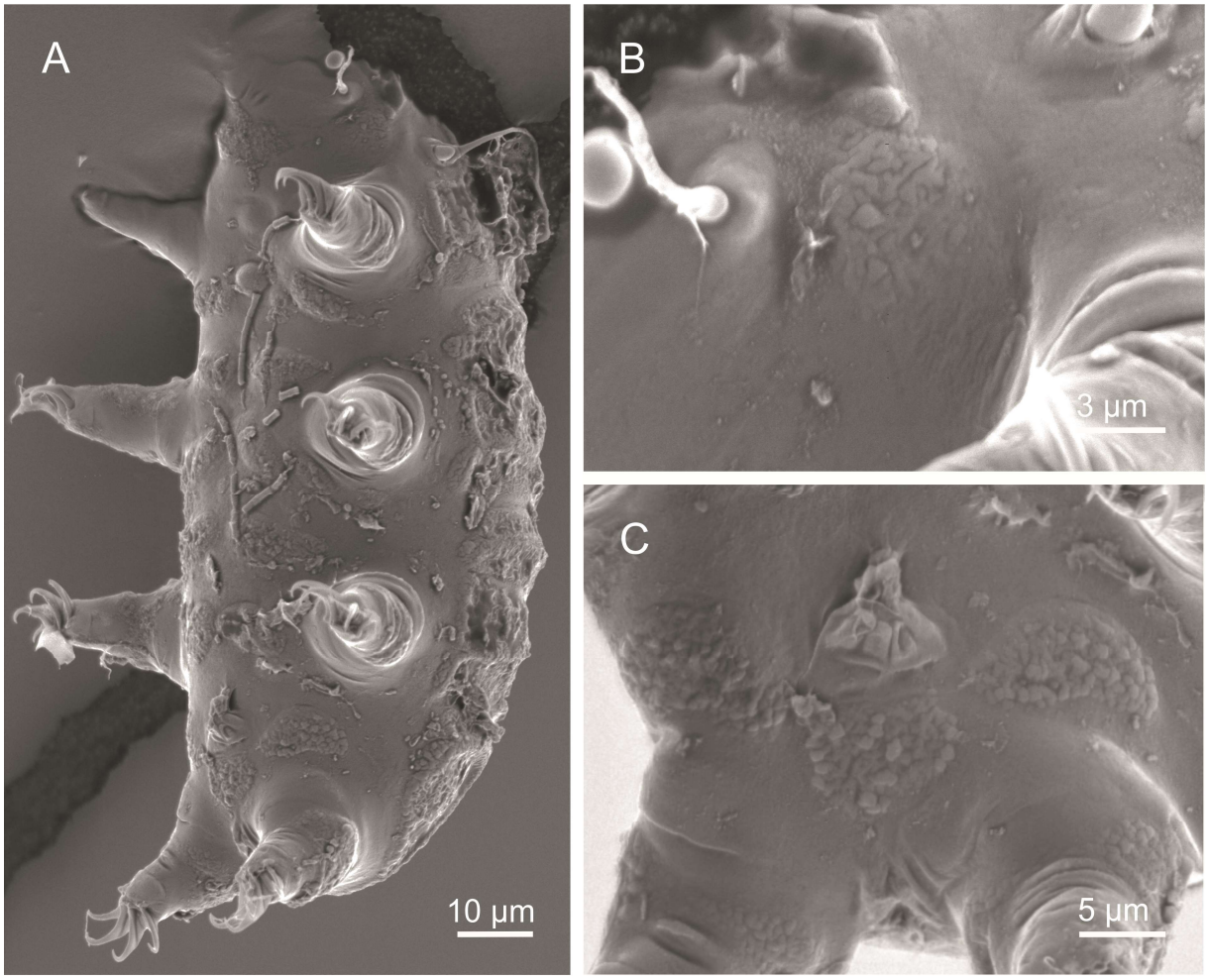

Figure 26: Ventrolateral and ventral structures of *Bry. wallacearthuri* sp. nov. (SEM). **A** ventrolateral overview; **B** lateral cephalic plates with sculpture elements; **C** lateral and posterior gonoplates, female.

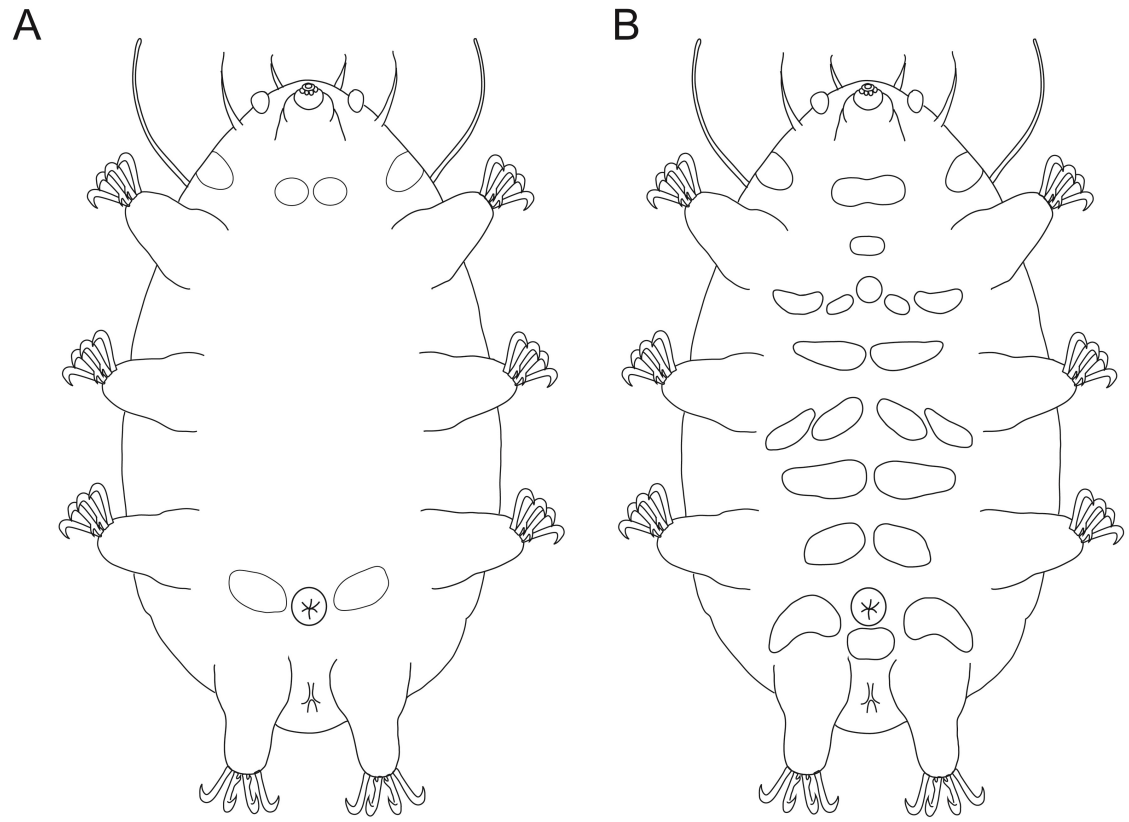

Figure 27: Schematic representation of the sexually monomorphic ventral plate configurations in the new species. **A** *Bryodelphax pucapetricolus* sp. nov.; **B** *Bryodelphax wallacearthuri* sp. nov.

Discussion

Habitat associations

The Burren region is recognized as biodiverse and host to a complex habitat mosaic of international conservation interest (Murphy and Fernandez, 2009). Our collection of two new *Bryodelphax* species and *Par.* cf. *chitonides*, a species not previously known from Ireland, from only two samples of moss may preliminarily suggest that the habitats of the Burren could be important for assessing biodiversity at the level of the microscopic component of the region's biota. The Burren's expanse of limestone pavement habitat may prove to be of particular importance regarding *Bryodelphax* species as more AITS samples from the area are investigated. Rock was stated as the substrate for the type populations of five *Bryodelphax* species (*Bry. aaseae*, *Bry. asiaticus, Bry. australasiaticus*, *Bry brevidentatus*, and *Bry. mareki*) and the secondary locations of populations of the two new species. The type location substrate of an additional two previously described species (*Bry. amphoterus* and *Bry instabilis*), as well as the two new species described herein, is further specified as carbonate rock. Dastych (1980, 1988) found *Bryodelphax* species associated with calciferous rock substrata in Poland, but otherwise rare. While the habitat preference of a species should not be assumed on the basis of only a few samples, the addition of two further new species associated with limestone does support a potential lithophylic habitat preference for *Bryodelphax*.

Phylogenetic analysis

The overall topology of the consensus tree obtained in our analyses (Fig. 17) is similar to that of Gąsiorek et al. (2020a), although some differences occur. Both studies demonstrate that, with the chosen markers, a geographic partitioning of species with a monophyletic clade comprising Indomalayan-Australasian *Bryodelphax* species occurs in both trees. However, the clustering pattern within this clade is different. *Bry. australasiaticus* and *Bry. decoratus* clustered together in Gąsiorek et al. (2020a), while *Bry. australasiaticus* is clustered with *Bry. arenosus* in our results. Also dissimilar is the suggested paraphyly of the complex of species of Palaearctic origin in our results compared to the monophyletic clade formed by this group in Gąsiorek et al. (2020a). The newly obtained sequences show *Bry. pucapetricolus* sp. nov. positioned within *Bryodelphax* and clustered with *Bry. instabilis* with moderate support. This result demonstrates that a species that could potentially be interpreted as *Bryochoerus* if only LM observations are considered (such as *Bry. pucapetricolus* sp. nov.) is not delimited

from *Bryodelphax* on the basis of these markers. As more molecular data are added, including for the variable ITS1 and COI regions, for *Bryodelphax* species and other specimens that show a characteristic *Bryochoerus* m3 the relationships between *Bryodelphax* species, the distribution of traits among them, and the validity of the genus *Bryochoerus* can be investigated to greater resolution.

Morphological analyses

SEM analyses of specimens collected from the Burren were critical for exploring the taxonomic value in limnoterrestrial heterotardigrades of the morphological variation of structures including those discussed below.

Cuticular sculpture and relief

While the primary literature on *Bryodelphax* species has mostly been in a consensus on the nature and appearances of intracuticular pillars and pores (*e.g.* Pilato, 1972; Bertolani et al., 1996; Fontoura et al., 2008; Kristensen et al., 2010; Gąsiorek et al., 2017; Lisi et al., 2017; Kaczmarek et al., 2018), the third type of sculpture element that we treated in our analyses, epicuticular elements, is less well characterized. Previous authors have described their observations of these structures in various ways. Schuster and Toftner (1982) described "fossae" in the cuticle of *Bry. dominicanus*, which likely corresponded to the undulating appearance of the plate surface formed by the epicuticular elements and pore depressions. Kristensen (1987) refers to "dark granulation" or "elevations in the cuticle". Gąsiorek et al. (2017) described "large but not strongly contrasting granules" located on "plate margins and folds" that they considered to be apparent only in SEM and "large granules" elsewhere on the dorsal cuticle, ventral plates and unplated ventral areas of *Bry. maculatus*. Kaczmarek et al. (2018) observed "large, dark granules" on the ventral plates of *Bry. olszanowskii* and regarded them to be "probably of epicuticular elevations". Gąsiorek et al. (2020a) evaluated "dark, contrasting epicuticular granules" on dorsal plates as a present/absent character within the genus *Bryodelphax*. Kayastha et al. (2021) use the absence of "epicuticular granules" as a distinguishing character of *Bry. mareki*.

At the outset of our descriptions of *Bry. pucapetricolus* sp. nov. and *Bry. wallacearthuri* sp. nov. and our associated analyses of comparative material, it was not precisely clear how each of the aforementioned authors defined "dark (epicuticular) granules". We interpreted this as the visible dark/black areas of the cuticular plates visible when specimens are viewed with PhC. When our results showed that these dark areas are present to some degree in all species that we examined, and that these results differed to those of Gąsiorek et al. (2020a) and Kayastha et al. (2021) who determined that "dark granules" are absent from the dorsal plates of some '*weglarskae* group' species, we needed to investigate this character further in order to understand these discrepancies.

Our analyses of all published *Bryodelphax* SEM images supported our LM findings in that all species examined exhibited epicuticular elevations of various morphologies and degrees of development, even in species that were originally described as having "dark granules absent" (*e.g. Bry. australasiaticus* and *Bry. mareki*). Our own results suggested the likely ubiquity of these epicuticular structures in the '*weglarskae* group' and the need for an inclusive term for descriptions of their morphological diversity, hence, "epicuticular element". This term was chosen to avoid ambiguity with the term "granules", which has been used to refer to intracuticular pillars visible as dark dots with PhC in both the traditional usage in English in various echiniscid genera (*e.g.* Murray, 1905, 1906, 1910; Petersen, 1951; Dastych, 1979) as well as more recently within *Bryodelphax* (*e.g*. Lisi et al., 2017).

We did not include enough '*parvulus* group' species to consider the extrapolation of our findings of the presence of the types of EEs we observed in the '*weglarskae*' group onto the other congeners. Gąsiorek et al. (2020a) determined that "dark granules" were absent in seven out of eight *'parvulus* group' species included in their study, suggesting that this character is very rare within that group. Our informal review of the published micrographs was not intended as a definitive evaluation of the occurrence and variation of EEs within the '*parvulus* group' taxa. More detailed studies of the plated areas of '*parvulus* group', preferably with the inclusion of SEM, are certainly needed to elucidate the features of the cuticular sculpture and relief across the entire genus. However, our preliminary results thus far can suggest the possibility that epicuticular elements are present to some degree, if only weakly developed, in all species of both the '*parvulu*s' and '*weglarskae'* groups.

Structure of median plates

Lisi et al. (2017) made an important contribution to the effort to resolve the problematic situation regarding the divisions of m3 in *Bryodelphax* and *Bryochoerus*. Those authors considered all *Bryodelphax* to show a divided m3 and recommended that the genus diagnosis be emended to include that character. This has resulted in an overlap of the diagnoses of these two genera (Degma and Guidetti, 2018). While we strongly agree with Lisi et al. (2017) on the need for clarification of the condition of m3 in *Bryodelphax* as well as *Bryochoerus*, and that there is a characteristic m3 morphology among *Bryodelphax* that should be included in the genus diagnosis, we interpret the structure of m3 differently. Lisi et al. (2017) presented micrographs of four *Bryodelphax* species (Figure 3A-D in Lisi et al., 2017) to demonstrate

what they consider as a division of m3 and stated that they observed the same on all of their examined *Bryodelphax* material. However, in our interpretation the m3s shown by Lisi et al. (2017) do not present an m3 divided into two parts by a transversal crest, rather each m3 shown is a single plate with a median transverse furrow. This can be seen in the similarity of structure when comparing the entire m3 with only the anterior part of m2 (m2a), which also exhibits a similar median transverse furrow. The *Bryodelphax* m2 (and m1) has a primary division formed by a transversal crest that occurs between m2a and m2p (and m1a and m1p) that is lacking from m3.

In our examinations of *Bry. pucapetricolus* sp. nov., the use of SEM enabled us to determine that the appearance of a *Bryochoerus* type m3 in LM can be an illusion created by a tertiary division at the border of two types of very different sculpture element conditions on the m3 anterior part. The divided appearance of m3 of the Greenlandic '*Brc. intermedius laevis'* in LM could also have a similar cause, but this will only be confirmed for that taxon with further studies of the plate structure involving SEM and new material from the German type location. Such studies will also help to clarify what Marcus' (1936) understood as a division of m3 in his definition of *Bryochoerus*. However, even if it could be shown that Marcus' own *Bryochoerus* material lacks a primary division of m3 formed by a transversal crest, and so be considered synonymous with *Bryodelphax*, the possibility of a separate genus for Murray's Pacific taxa (on the descriptions of which Marcus also based *Bryochoerus*) together with *Brc. liupanensis* would still remain.

"Divided" median plates have been described in other genera. Murray (1910) considered the divided condition of the median plates of '*Echiniscus intermedius'* to be similar only to the taxon now known as *Hypechiniscus exarmatus* (Murray, 1907) (see also Thulin 1911). Gąsiorek et al. (2020b) determined that "pseudodivisions" resulting from sutures or incisions can occur on the median plates in that genus. Tumanov (2020a) distinguished between types of divisions of the median plates created by transverse crests, folds and thickenings of the cuticle in *Pseudechiniscus*. Kristensen (1987) specified m1 in *Antechiniscus* as "undivided, but folded". Other genera where at least some of the median plates exhibit a form of division include *Cornechiniscus*, *Novechiniscus*, and *Testechiniscus* (Kristensen, 1987).

As there are various types of structures associated with the dorsal median plates that might be potentially interpreted as forming a 'division' (*e.g.* crest, furrow, fold), we recommend that as far as possible, taxonomic descriptions specify which structure type is present and is considered to produce the division in that plate. *Bryodelphax* and *Bryochoerus* could, at least until more data are added, be differentiated from each other in this manner. We propose that for a median plate to be considered as "divided" a transversal crest that divides the plate into two parts (a and p) should be present. Plates that only show a median transverse furrow should not be considered "divided". Therefore, in *Bryodelphax* the median plates are characterized as follows: Median plates 1 and 2 each divided by a transversal crest (primary division) into two parts (m1a, m1p and m2a, m2p). Each part may be further separated into an anterior and posterior portion by a median transverse furrow (secondary division). The third median plate is undivided (lacks a transversal crest forming the primary division) but a median transverse furrow (secondary division) is present that separates m3 into an anterior and posterior portion. Additional partitioning features may be present including a hard border between zones of different sculpture elements (tertiary division).

Correspondingly, we suggest that an emendation of the *Bryochoerus* diagnosis be made based upon Marcus' (1936) original criteria. The median plates of *Bryochoerus* are then characterized as follows: Median plates 1, 2, and 3 each divided by a transversal crest (primary division) into two parts (m1a, m1p and m2a, m2p and m3a, m3p). Each part may be further separated into an anterior and posterior portion by a median transverse furrow (secondary division). This similarity of the division of m3 in *Bryochoerus* to that of m1 and m2 was indicated by Marcus (1936, Figure 47) in that all three median plates have both "dorsalintersegmentplatten" and "transversalintersegmentplatten" components, which in our interpretation, correspond to m1a/m2a/m3a and m1p/m2p/m3p respectively. This plate structure is distinguishable from that of Marcus' (and Thulin's (1928)) representation of the *Bryodelphax* m3, which has a "dorsalintersegmentplatten" component only (*i.e.* m3a only) (Figure 51 in Marcus, 1936). Further analyses involving SEM and new material for the previously described *Bryochoerus* species are necessary in order to determine if this condition of the *Bryochoerus* m3 actually exists or if it is an artefact that occurs in LM observation, as no SEM observations are known to have been carried out on these taxa.

Lateral cephalic plates

Kristensen et al. (2010) clearly depicted lcps in their figures of *Bry. aaseae*, though these structures were not described in that text. Kaczmarek et al. (2018) were the first to include lcps in the description of a *Bryodelphax* species when they mentioned "an oval plate present on the ventro-lateral side, close to the head plate" of *Bry. olszanowskii.* Subsequent species descriptions have been inconsistent in the inclusion of lcps, even where lcps are strongly developed and evident (*e.g. Bry. nigripunctatus*). When included in the species description, lcps have been considered to be part of the ventral plate configuration and

included in the given ventral plate formulae (*Bry. australasiaticus*, *Bry. decoratus* in Gąsiorek et al., 2020a) or treated as a different type of structure independent from the ventral plates (*Bry. olszanowskii* in Kaczmarek et al., 2018). In agreement with Kaczmarek et al. (2018), we consider lcps to be laterally positioned structures not part of the ventral plate configuration, but nonetheless taxonomically important because of the (sometimes subtle) variation we observed in the morphology of lcps in our analyses.

Subcephalic ventral plates

Prior to our analyses, only 2/14 previously described '*weglarskae* group' species, *Bry. parvuspolaris* and *Bry. sinensis*, did not include svps in their known ventral plate configurations. Since we observed that svps occurred to various degrees of development depending on the species, it suggested the possibility that svps could actually have been present in a weakly developed state in *Bry. parvuspolaris* and *Bry. sinensis*. While we did not directly view the type material for either of these species, the presence of weakly developed svps (and lcps) were confirmed in *Bry. parvuspolaris* by one of the original describing authors (Ł. Kaczmarek, pers. comm.) who also provided us with micrographs showing these structures (Fig. 5A). This new information (with the agreement of Ł. Kaczmarek (pers. comm.)) warrants the emendation of the species diagnosis of *Bry. parvuspolaris* to include the presence of nine rows (instead of eight) of ventral plates and weakly developed lcps.

If svps, even weakly developed ones, are found to be present in *Bry. sinensis* and other '*parvulus* group' members other than our *Bry*. cf. *parvulus* (Ireland) it would indicate that ventral plates alone may not be a suitable character for defining these two groups if used on a strictly present/absent basis. A more appropriate working definition of the '*weglarskae* group' might in that case be, for example, *Bryodelphax* species that have a minimum of both svps and gonoplates (as all described '*weglarskae* group' members including the two new species presented herein, are known to have at least lateral gonoplates).

Ventral plate shape and size

Both *Bry. pucapetricolus* sp. nov. and *Bry. wallacearthuri* sp. nov. overlapped with previously known species in the configuration of the ventral plates. Yet, our investigations of the comparative type material showed that the ventral plate morphologies could differ between species that share with the same configuration in several characters, *e.g.* in the sculpturing and shape of ventral plates. As additional new species in the '*weglarskae* group' are described, there will be an increase in the likelihood of an overlap with a known species in the number of rows of ventral plates and in the configuration of those plates. In such cases it will be important to identify and scrutinize additional characteristics of the ventral plates and to check for intraspecific consistency in those traits across a number of specimens in order to optimally characterize that species. Ventral plate shape should not be used alone to separate new species to ensure that perceived differences are not a result of an artefact of preparation, specimen position, or focal plane.

The degree of development of the ventral plates may be a character requiring particular attention in the '*parvulus* group'. Although this group is defined by the absence of ventral plates, Kristensen (1987) observed some specimens identified as "*Bry. parvulus*" with weak ventral plates and suggested that thin ventral plates, if present in other known *Bryodelphax* species, could have been overlooked due to consequences of specimen preparation. Several authors that described '*parvulus* group' species specifically stated the absence of ventral plates (Kaczmarek and Michalczyk, 2004; Kaczmarek et al., 2005; Fontoura et al., 2008; Pilato et al., 2010; Gąsiorek, 2018). However, our observations of the dense concentration of fine pillars (perhaps forming a weak plate) on the Irish *Bry*. cf. *parvulus* specimens at the location and in the form corresponding to the subcephalic ventral plates also raise questions about the distribution of these structures across the genus.

Leg plates

Our analyses showed that both the coxal and femoral plates of '*weglarskae* group' species have importance in species delineation. We did not include *Bry. amphoterus*, *Bry. kristenseni* and *Bry. sinensis* in our analyses, but we expect that these species also have leg plates with morphologies of similar taxonomic value. The value of SEM analyses was evident with regard to the leg plate analyses as we found some instance where the leg plate morphology appeared very similar between species in LM but significantly different with SEM (*e.g. Bry. maculatus* vs. *Bry. wallacearthuri* sp. nov.). We did not find any published SEM images of '*parvulus* group' species that clearly showed the legs and did not recover enough *Bry*. cf. *parvulus* specimens in our samples to include our own SEM studies for that taxon. The question of whether leg plates are taxonomically important within the '*parvulus* group' as we have found in the '*weglarskae* group' remains open.

Morphology and morphometry of the reproductive and anal structures

It is generally observed in heterotardigrades that the overall form of the gonopore is different between females and males of the same species and that the female gonopore is located further from the anus than the male gonopore (Guidetti et al., 2014; Altiero et al., 2018). While the gonopore to anus distance has been recognized as important in marine tardigrade

taxonomy (*e.g.* Grimaldi de Zio et al., 1988; Hansen et al., 2016; Møbjerg et al., 2016; Møbjerg et al., 2019; Bartels et al., 2021), measurements relating to the gonopore are not in regular use for terrestrial heterotardigrade taxa. Our morphometric analyses involving the gonopore diameter and gonopore to anus distance were limited to small sample sizes and to a small number of taxa. Yet, we showed that the observed differences in the values for gonopore diameter were discriminatory in all species compared and were statistically significant between sexes in the species tested. In all cases the female gonopore was of larger diameter than the male gonopore of the same species. When comparing the female gonopore diameter *scp* between four '*weglarskae* group' species significant difference was found between some comparison pairs indicating potential usefulness as a taxonomic trait in terrestrial heterotardigrades. Significant difference was not found in the male gonopore diameter *psc* between the only two species for which n≥ 10, *Bry. aaseae* and *Bry. pucapetricolus* sp. nov., but these two species were among those pairs that did not show significant difference in the female gonopore diameter either. It is possible that statistical comparisons of the male gonopore diameters of other species pairs would show significant difference, or that intraspecific variation in the male gonopore diameter is more restricted than the female.

The distance between the gonopore and anus was confirmed to be greater in females than in males of the same species as our morphometric data in each measurement type used (µm, *psc*, *pbl*) was either completely discriminatory between sexes and/or tested for statistical significance. This preliminary data indicates that the measurement between the gonopore and anus could be useful in helping to confirm sex if an individual's gonopore morphology is not perfectly discernable, especially when considered together with gonopore diameter and treated with due caution.

When comparing the female gonopore to anus distance between species significant difference between species was found for data expressed as both *psc* and *pbl*, however the significance was detected in different pairs depending on the index used. The index type also produced a different outcome for detected significance in the statistical tests of the male gonopore between *Bry. aaseae* and *Bry. pucapetricolus*, with only data expressed as *pbl* being significantly different between the two species. Overall, our results suggest that the character may be important in species diagnostics, at least in some cases, but that the index for measurement data used can influence where significant difference lies. Following these results, we consider both the gonopore diameter and the gonopore to anus distance as potentially important features for separating *Bryodelphax* species. These measurements could also be useful for other limnoterrestrial heterotardigrade genera. We suggest that these data are gathered for other populations/species so that any taxonomic utility for terrestrial taxa can be further investigated.

Similarly to morphometrics related to the gonopore, the anus morphology has been better utilized in the taxonomy of marine heterotardigrades (*e.g.* Hallas and Kristensen, 1982; Kristensen and Higgins, 1984; Kristensen and Higgins, 1989; Hansen et al., 2012) than in terrestrial taxa. Among Echiniscoidea Richters, 1926 anus morphology was particularly relevant in the separation of *Isoechiniscoides* Møbjerg, Kristensen and Jørgensen, 2016 and *Neoechiniscoides* Møbjerg, Jørgensen and Kristensen, 2019 (Møbjerg et al., 2016; Møbjerg et al., 2019) from *Echiniscoides* Plate, 1888. Furthermore, in recognition of the importance of anus morphology at multiple taxonomic levels Møbjerg et al. (2019) included description of the anus in their new or amended family, subfamily, genera and species diagnoses.

Details of the anus morphology have not been included in modern diagnoses or emendations of terrestrial heterotardigrade taxa (see Degma and Guidetti, 2018 and *e.g.* Gąsiorek et al., 2019a; Gąsiorek and Michalczyk, 2020; Gąsiorek et al., 2020b; Degma et al., 2021b; Gąsiorek et al., 2021a; Gąsiorek et al., 2021b). Schuster (1975) and some recent authors have mentioned the anus in species descriptions in general terms *e.g.* "large tripartite anus" (Gąsiorek et al., 2019b) or "trilobed anus" for diverse taxa (Gąsiorek et al., 2020b; Vončina et al., 2020; Kiosya et al., 2021; Gąsiorek et al., 2021c). Guidetti et al. (2014) included an anus focused SEM micrograph of *Mopsechiniscus franciscae* Guidetti, Rebecchi, Cesari and McInnes, 2014 but analysis of the anal structures was not included in the description. Rocha et al. (2020) noted visible perianal structures in their species description of *Pse. saltensis* Rocha, Doma, Gonzalez Reyes and Lisi, 2020, but were not able to investigate further without SEM. Our present results demonstrate that the complexity of the anus morphology and its variation among limnoterrestrial heterotardigrades is beyond the number of lobes present and that usage of the same general description across multiple taxa is likely to insufficiently account for its diversity in form.

We regard our observations of the anus morphology of the collected limnoterrestrial heterotardigrade taxa as only prelusive to the required deeper exploration of this character, but our SEM comparisons confirm that the details of the anus morphology do have taxonomic significance, at least at genus level in limnoterrestrial heterotardigrade taxa. Species specific variations of the gonopore morphology of limnoterrestrial tardigrades has been occasionally reported (Altiero et al., 2018 and references therein). Few published SEM micrographs focus on the anal system of limnoterrestrial species making it difficult

to predict the fine scale species specific variability of the anal system in known species. A SEM figure that shows the anal systems of two *Cornechiniscus* Maucci and Ramazzotti, 1981 species (Gąsiorek and Michalczyk, 2020) does not show obvious morphological differences in the anus form. While further analyses might conclude that congeners can share a generally similar anus morphology, *e.g.* in the number of lobes, the possibility exists of species specific variations in finer details such as the shape and size of the lateral lobes (as observed in the two examined *Bryodelphax* species) or the presence and distribution of cuticular sculpture elements of the anal system. We support the inclusion of the details of the anus morphology in descriptions of new limnoterrestrial heterotardigrade taxa. At all taxonomic levels, the anus morphology should be formally determined with SEM analyses, as our LM studies alone did not reveal the morphological variability of the anal system in fine detail.

Summary of recommendations

On the basis of our results we suggest that:

- the traits that we examined (cuticular sculpture and relief, structure of median plates, lateral cephalic plates, subcephalic ventral plates, leg plates, ventral plate shape and size, measurements related to the gonopore and anus, and anal morphology) be considered in the description of new *Bryodelphax* species whenever possible in order to further document the intrageneric variation of these characters.

- the diagnosis of the genus *Bryodelphax* be further emended to include that the third median plate lacks a primary division formed by a transversal crest and consists of one plate part only. The third median plate has a transverse furrow (secondary division) and may also have an additional line at the junction of two areas of different sculpture morphologies (tertiary division).

- the diagnosis of the genus *Bryochoerus* is distinguished from that of *Bryodelphax* to include that the median plate three in *Bryochoerus* has a primary division formed by a transversal crest so that two plate parts are differentiated (m3a and m3p) *sensu* Marcus, 1936. The existence of such a condition and the validity of *Bryochoerus* requires further study.

- the species diagnosis of *Bry. parvuspolaris* be emended to include the presence of lateral cephalic plates and nine rows of ventral plates including a pair of weakly sclerotized, rounded subcephalic ventral plates.

- the species diagnosis of *Bry. aaseae* be emended to include the presence of both females and males.

- *Bry. mareki* is a valid species, evidently showing a unique EEs morphology, but the taxon requires a revision of the important character of ventral plate configuration, which in our examination was not in agreement with the original species description (Kayastha et al., 2021).

- *Bry. decoratus* should be revised in order to be better morphologically differentiated from *Bry. australasiaticus* if it is confirmed that both share the same ventral plate configuration.

- SEM is used to confirm the condition of median plate 3 in any specimens that appear in LM to meet the definition of *Bryochoerus* while the status of that genus awaits further investigation.

- details of the morphology of the anal system be included whenever possible in the diagnoses of new taxa limnoterrestrial heterotardigrade taxa, similarly to marine taxa (as *e.g.* Møbjerg et al., 2019).

Funding

This work was supported by the Irish Research Council Postgraduate Award scholarship to ED and individual funding to DVT.

Acknowledgments

We are very grateful to Profs. Roberto Bertolani, Giovanni Pilato, and Roberto Guidetti for their assistance to us in accessing type material and Prof. Louise Allcock for analytical guidance. Prof. Oscar P. V. Lisi kindly assisted with paratype deposition at the University of Catania, Italy. Prof. Łukasz Kaczmarek provided helpful communication on and contributed micrographs of *Bry. parvuspolaris*. Prof. Paul Bartels kindly corresponded on the topic of allometry. We are thankful to Prof. Martin Vinther Sørensen and Charlotte Hansen for SEM support, Dr. Laura Pavesi for collections support, Prof. Ib Friis for good nomenclature advice, and Thomas Pape and the Natural History Museum of Denmark, Zoological Museum staff that facilitated our work there. Kelvin Gillmor is gratefully acknowledged for his assistance in postage and transport of equipment. We would like to thank Irina Nikolaeva and Vadim Panov for collecting material studied herein. Finally, we would like to gratefully acknowledge the reviewers who dedicated their time to improving our manuscript with their valued suggestions and comments.

Conflict of interest

The authors declare that there are no conflicting issues related to this research article.

Supplementary files

Supplementary files associated with this article are available for download at https://jad.lu.ac.ir/article-1-210-en.html

References

Altiero, T., Suzuki, A. C. and Rebecchi, L. (2018). Reproduction, development and life cycles, *In*: Schill, R. O. (Ed.), *Water Bears: The Biology of Tardigrades*, Springer, New York. pp. 211–247. https://doi.org/10.1007/978-3-319-95702-9_8

Bartels, P. J., Nelson, D. R. and Exline, R. P. (2011). Allometry and the removal of body size effects in the morphometric analysis of tardigrades. *Journal of Zoological Systematics and Evolutionary Research*, 49 (s1): 17–25. https://doi.org/10.1111/j.1439-0469.2010.00593.x

Bartels, P. J., Fontoura, P., Nelson, D. R., Orozco-Cubero, S., Mioduchowska, M., Gawlak, M., Kaczmarek, Ł. and Cortés, J. (2021). A transisthmus survey of marine tardigrades from Costa Rica (Central America) with descriptions of seven new species, *Marine Biology Research*, 17 (2): 120–166. https://doi.org/10.1080/17451000.2021.1901936

Bartoš, E. (1963). Die Tardigraden der Chinesischen und Javanischen Moosproben. *Acta Societatis Zoologicae Bohemoslovenicae*, 27: 108–114.

Bertolani, R., Guidetti, R., Marchioro, T., Altiero, T., Rebecchi, L. and Cesari, M. (2014). Phylogeny of Eutardigrada: New molecular data and their morphological support lead to the identification of new evolutionary lineages. *Molecular Phylogenetics and Evolution*, 76: 110–126. https://doi.org/10.1016/j.ympev.2014.03.006

Bertolani, R, Guidi, A. and Rebecchi, L. (1996). Tardigradi della Sardegna e di alcune piccole isole circum-sarde. *Biogeographia*, 18: 229–247. https://doi.org/10.21426/B618110456

Cuénot, L. (1926). Description d'un tardigrade nouveau de la faune francaise. *Comptes Rendus de l'Académie des Sciences, Paris*, 182: 744–745.

Dastych, H. (1979). Tardigrada from Afghanistan with description of *Pseudechiniscus schrammi* sp. nov. *Bulletin de la Société des Amis des Sciences et des Letteres de Poznan*. Serie D. 19: 99–108.

Dastych, H. (1980). Niesporczaki (Tardigrada) Tatrzańskiego Parku Narodowego. *Monografie Fauny Polski*, 9: 1–232.

Dastych, H. (1988). The Tardigrada of Poland. *Monografie Fauny Polski*, 16: 1–255.

Dastych, H. (1999). A new species of the genus *Mopsechiniscus* Du Bois-Reymond Marcus, 1944 (Tardigrada) from the Venezuelan Andes. *Acta Biologica Benrodis*, 10: 91–101.

Degma, P. and Guidetti, R. (2007). Notes to the current checklist of Tardigrada. *Zootaxa*, 1579 (1): 41–53. https://doi.org/10.11646/zootaxa.1579.1.2

Degma, P. and Guidetti, R. (2018). Tardigrade Taxa, *In*: Schill, R. O. (Ed.), *Water Bears: The Biology of Tardigrades*, Springer, New York. pp. 371–409. https://doi.org/10.1007/978-3-319-95702-9_15

Degma, P., Bertolani, R. and Guidetti, R. (2021a). Actual checklist of Tardigrada species (2009–2021, 40th Edition: 19-07-2021). https://iris.unimore.it/retrieve/handle/11380/1178608/358743/Actual%20checklist%20of%20Tardigrada%2040th%20Edition%2019-07-21.pdf. (Accessed 20 September 2021). http://dx.doi.org/10.25431/11380_1178608

Degma, P., Meyer, H. A. and Hinton, J. A. (2021b). *Claxtonia goni*, a new species of Tardigrada (Heterotardigrada, Echiniscidae) from the island of Maui (Hawaiian Islands, U.S.A., North Pacific Ocean), with notes to the genus *Claxtonia* Gąsiorek and Michalczyk, 2019. *Zootaxa*, 4933 (4): 527–542. https://doi.org/10.11646/zootaxa.4933.4.4

DeMilio, E., Lawton, C. and Marley, N. J. (2016). Tardigrada of Ireland: a review of records and an updated checklist of species including a new addition to the Irish fanua. *ZooKeys*, 616: 77–101. https://doi.org/10.3897/zookeys.616.8222

Doyère, M. (1840). Mèmoire sur les tardigrades. *Annales des Sciences Naturelles*: 2 (14): 269–361.

du Bois-Reymond Marcus, E. (1944). Sobre tardígrados brasileiros. *Comunicaciones Zoológicas del Museo de Historia Natural de Montevideo*, 13: 1–19.

Durante Pasa, M. V. and Maucci, W. (1975). Tardigradi muscicoli dell'Istria con descrizione di due specie nuove. *Memorie dell'Istituto Italiano di Idrobiologia*, 32 (S): 69–91.

Fontoura, P. (1982). Deux nouvelles espéces de Tardigrades muscicoles du Portugal. *Publicações do Instituto de Zoologia*, 165: 5–19.

Fontoura, P. and Morais, P. (2011). Assessment of traditional and geometric morphometrics for distinguishing cryptic species for the *Pseudechiniscus suillus* complex (Tardigrada, Echiniscidae). *Journal of Zoological Systematics and Evolutionary Research*, 49: 26–33. https://doi.org/10.1111/j.1439-0469.2010.00594.x

Fontoura, P., Pilato, G. and Lisi, O. (2008). Echiniscidae (Tardigrada, Heterotardigrada) from Faial and Pico Islands, the Azores, with the description of two new species. *Zootaxa*, 1693 (1): 49–61. http://dx.doi.org/10.11646/zootaxa.1693.1.4

Gąsiorek, P. (2018). New *Bryodelphax* species (Heterotardigrada: Echiniscidae) from Western Borneo (Sarawak), with new molecular data for the genus. *Raffles Bulletin of Zoology*, 66: 371–381.

Gąsiorek, P. and Degma, P. (2018). Three Echiniscidae species (Tardigrada: Heterotardigrada) new to the Polish fauna, with the description of a new gonochoristic *Bryodelphax* Thulin, 1928. *Zootaxa*, 4410: 77–96. https://doi.org/10.11646/zootaxa.4410.1.4

Gąsiorek, P. and Michalczyk, Ł. (2020). Revised *Cornechiniscus* (Heterotardigrada) and new phylogenetic analyses negate echiniscid subfamilies and tribes. *Royal Society Open Science*, 7 (6): 200581. https://doi.org/10.1098/rsos.200581

Gąsiorek, P., Stec, D., Morek, W., Marnissi, J. and Michalczyk, Ł. (2017). The tardigrade fauna of Tunisia, with an integrative description of *Bryodelphax maculatus* sp. nov. (Heterotardigrada: Echiniscidae). *African Zoology*, 52: 77–89. https://doi.org/10.1080/15627020.2017.1297688

Gąsiorek, P., Blagden, B. and Michalczyk, Ł. (2019b). Towards a better understanding of echiniscid intraspecific variability: A redescription of *Nebularmis reticulatus* (Murray, 1905) (Heterotardigrada: Echiniscoidea). *Zoologischer Anzeiger*, 283: 242–255. https://doi.org/10.1016/j.jcz.2019.08.003

Gąsiorek, P., Morek, W., Stec, D. and Michalczyk, Ł. (2019a). Untangling the *Echiniscus* Gordian knot: paraphyly of the "arctomys group" (Heterotardigrada: Echiniscidae). *Cladistics*, 35: 633–653. https://doi.org/10.1111/cla.12377

Gąsiorek, P., Oczkowski, A., Blagden, B., Kristensen, R. M., Bartels, P. J., Nelson, D. R., Suzuki, A. C. and Michalczyk, Ł. (2020b). New Asian and Nearctic *Hypechiniscus* species (Heterotardigrada: Echiniscidae) signalize a pseudocryptic horn of plenty. *Zoological Journal of the Linnean Society*, 192 (3): 794–852. https://doi.org/10.1093/zoolinnean/zlaa110

Gąsiorek, P., Vončina, K. and Michalczyk, Ł. (2020). An overview of the sexual dimorphism in *Echiniscus* (Heterotardigrada, Echiniscoidea), with the description of *Echiniscus masculinus* sp. nov. (the *virginicus* complex) from Borneo. *Zoosystematics and Evolution*, 96 (1): 103-113. https://doi.org/10.3897/zse.96.49989

Gąsiorek, P., Vončina, K., Degma, P. and Michalczyk, Ł. (2020a). Small is beautiful: the first phylogenetic analysis of *Bryodelphax* Thulin, 1928 (Heterotardigrada, Echiniscidae). *Zoosystematics and Evolution*, 96 (1): 217–236. http://dx.doi.org/10.3897/zse.96.50821

Gąsiorek, P., Vončina, K., Ciosek, J., Veloso, M., Fontoura, P. and Michalczyk, Ł. (2021a). New Indomalayan *Nebularmis* species (Heterotardigrada: Echiniscidae) provoke a discussion on its intrageneric diversity. *Zoological Letters*, 7 (1): 1–29. https://doi.org/10.1186/s40851-021-00172-0

Gąsiorek, P., Vončina, K., Zając, K. and Michalczyk, L. (2021b). Phylogeography and morphological evolution of *Pseudechiniscus* (Heterotardigrada: Echiniscidae). *Scientific Reports*, 11 (7606). https://doi.org/10.1038/s41598-021-84910-6

Gąsiorek, P., Vončina, K., Kristensen, R. M. and Michalczyk, Ł. (2021c). High Mountain Echiniscid (Heterotardigrada) fauna of Taiwan. *Zoological Studies*, 60: 70. https://doi.org/10.6620/ZS.2021.60-70

Gouy, M., Guindon, S. and Gascuel, O. (2010). SeaView version 4: A multiplatform graphical user interface for sequence alignment and phylogenetic tree building. *Molecular Biology and Evolution*: 27: 221–224. https://doi.org/10.1093/molbe v/msp259

Grigarick, A. A., Schuster R. O. and Nelson D. R. (1983). Heterotardigrada of Venezuela (Tardigrada). *Pan-Pacific Entomologist*, 59: 64–77.

Grimaldi de Zio, S., D'Addabbo Gallo, M. and Morone de Lucia, M. R. (1988). Two new Mediterranean species of the genus *Halechiniscus* (Tardigrada: Heterotardigrada). *Bolletino di Zoologia*, 55 (1–4): 205–211.

Guidetti, R. and Bertolani, R. (2005). Tardigrade taxonomy: an updated check list of the taxa and a list of characters for their identification. *Zootaxa*, 845: 1–46. https://doi.org/10.11646/zootaxa.845.1.1

Guidetti, R., Rebecchi, L., Cesari, M. and McInnes, S. J. (2014). *Mopsechiniscus franciscae*, a new species of a rare genus of Tardigrada from continental Antarctica. *Polar Biology*, 37 (9): 1221–1233. https://doi.org/10.1007/s00300-014-1514-x

Guil, N., Jørgensen, A. and Kristensen, R. (2019). An upgraded comprehensive multilocus phylogeny of the Tardigrada tree of life. *Zoologica Scripta*: 48: 120–137. https://doi.org/10.1111/zsc.12321

Hallas, T. E. and Kristensen, R. M. (1982). Two new species of the tidal genus *Echiniscoides* from Rhode Island, U.S.A. (Echiniscoididae, Heterotardigrada), *In*: Nelson, D. R. (Ed.), *Proceedings of the Third International Symposium on the Tardigrada,* East Tennessee State University Press, Johnson City, Tennessee, pp. 179–192.

Hansen, J. G., Kristensen, R. M. and Jørgensen, A. (2012). The armoured marine tardigrades (Arthrotardigrada, Tardigrada). *The Royal Danish Academy of Sciences and Letters. Scientia Danica, Series B, Biologica*, 2: 1–91.

Hansen, J. G., Kristensen, R. M., Jørgensen, A., Accogli, G., D'Addabbo, R. and Gallo, M. (2016). Postembryonic development, paedomorphosis, secondary sexual dimorphism and population structure of a new *Florarctus* species (Tardigrada, Heterotardigrada). *Zoological Journal of the Linnean Society*, 178 (4): 871–877. https://doi.org/10.1111/zoj.12436

Jørgensen, A., Faurby, S., Hansen, J. G., Møbjerg, N. and Kristensen, R. M. (2010). Molecular phylogeny of Arthrotardigrada (Tardigrada). *Molecular Phylogenetics and Evolution*, 54: 1006–1015. https://doi.org/10.1016/j.ympev.2009.10.006

Jørgensen, A., Møbjerg, N. and Kristensen, R. M. (2011). Phylogeny and evolution of the Echiniscidae (Echiniscoidea, Tardigrada) – an investigation of the congruence between molecules and morphology. *Journal of Zoological Systematics and Evolutionary Research*, 49: 6–16. https://doi.org/10.1111/j.1439-0469.2010.00592.x

Kaczmarek, Ł. and Michalczyk, Ł. (2004). A new species *Bryodelphax asiaticus* sp. nov. (Tardigrada: Heterotardigrada: Echiniscidae) from Mongolia (Central Asia). *Raffles Bulletin of Zoology*, 52: 599–602.

Kaczmarek, Ł., Michalczyk, Ł. and Degma, P. (2005). A new species of Tardigrada *Bryodelphax brevidentatus* sp. nov. (Heterotardigrada: Echiniscidae) from China (Asia). *Zootaxa*, 1080: 33–45. https://doi.org/10.11646/zootaxa.1080.1.3

Kaczmarek, Ł., Zawierucha, K., Smykla, J. and Michalczyk, Ł. (2012). Tardigrada of the Revdelen (Spitsbergen) with the descriptions of two new species: *Bryodelphax parvuspolaris* (Heterotardigrada) and *Isohypsibius coulsoni* (Eutardigrada). *Polar Biology*, 35: 1013–1026. https://doi.org/10.1007/s00300-011-1149-0

Kaczmarek, Ł., Parnikoza, I., Gawlak, M., Esefeld, J., Peter, H-U., Kozeretska, I. and Roszkowska, M. (2018). Tardigrades from *Larus dominicanus* Lichtenstein, 1823 nests on the Argentine Islands (maritime Antarctic). *Polar Biology*, 41: 283–301. https://doi.org/10.1007/s00300-017-2190-4

Kaczmarek, Ł., Kayastha, P., Gawlak, M., Mioduchowska, M. and Roszkowska, M. (2021). An integrative description of *Diploechiniscus oihonnae* (Richters, 1903) population from near the original type locality in Merok (Norway). *Zootaxa*, 4964 (1): 083–102. https://doi.org/10.11646/zootaxa.4964.1.4

Kalyaanamoorthy, S., Minh, B., Wong, T., von Haeseler, A. and Jermiin, L. S. (2017). ModelFinder: fast model selection for accurate phylogenetic estimates. *Nature Methods*, 14: 587–589. https://doi.org/10.1038/nmeth.4285

Katoh, K., Misawa, K., Kuma, K. and Miyata, T. (2002). MAFFT: a novel method for rapid multiple sequence alignment based on fast Fourier transform. *Nucleic Acids Research*, 30 (14): 3059–3066. https://doi.org/10.1093/nar/gkf43

Kayastha, P., Roszkowska, M., Mioduchowska, M., Gawlak, M. and Kaczmarek, Ł. (2021). Integrative descriptions of two new Tardigrade species along with the new record of *Mesobiotus skorackii* Kaczmarek et al., 2018 from Canada. *Diversity*, 13 (8): 394–421. http://dx.doi.org/10.3390/d13080394

Kiosya, Y., Vončina, K. and Gąsiorek, P. (2021). Echiniscidae in the Mascarenes: the wonders of Mauritius. *Evolutionary Systematics*, 5: 93–120. https://doi.org/10.3897/evolsyst.5.59997

Kristensen, R. M. (1987). Generic revision of the Echiniscidae (Heterotardigrada) with a discussion of the origin of the family, *In*: Bertolani, R. (Ed.), *Biology of Tardigrades*. Selected Symposia and Monographs, Unione Zoologica Italiana. pp. 261–335.

Kristensen, R. M. and Higgins, R. P. (1984). A new family of Arthrotardigrada (Tardigrada: Heterotardigrada) from the Atlantic Coast of Florida, U.S.A. *Transactions of the American Microscopical Society*, 103 (3): 295–311. http://dx.doi.org/10.2307/3226191

Kristensen, R. M. and Higgins, R. P. (1989). Marine Tardigrada from the Southeastern United States Coastal Waters I. *Paradoxipus orzeliscoides* n. gen., n. sp. (Arthrotardigrada: Halechiniscidae). *Transactions of the American Microscopical Society*, 108 (3): 262–282. http://dx.doi.org/10.2307/3226344

Kristensen, R. M., Michalczyk, Ł. and Kaczmarek, Ł. (2010). The first record of the genus *Bryodelphax* (Tardigrada: Heterotardigrada: Echiniscidae) from Easter Island, Rapa Nui (Pacific Ocean, Chile) with the description of a new species, *Bryodelphax aaseae*. *Zootaxa*, 2343 (1): 45–56. http://dx.doi.org/10.11646/zootaxa.2343.1.4

Kumar, S., Stecher, G. and Tamura, K. (2016). MEGA7: Molecular evolutionary genetics analysis version 7.0 for bigger datasets. *Molecular Biology and Evolution*, 33: 1870–1874. https://doi.org/10.1093/molbe v/msw054

Larsson, A. (2014). AliView: a fast and lightweight alignment viewer and editor for large data sets. *Bioinformatics*, 30 (22): 3276–3278. http://dx.doi.org/10.1093/bioinformatics/btu531

Lisi, O., Daza, A., Londoño, R. and Quiroga, S. (2017). Echiniscidae from the Sierra Nevada de Santa Marta, Colombia, new records and a new species of *Bryodelphax* Thulin, 1928 (Tardigrada). *ZooKeys*, 703: 1–14. http://dx.doi.org/10.3897/zookeys.703.12537

Marcus, E. (1927). Zur Anatomie und Ökologie mariner Tardigraden. *Zoologische Janhbücher*, 53: 487–588.

Marcus, E. (1936). Tardigrada. *In*: Hesse, R. (Ed.) *Das Tierreich,* 66. Lieferung. Walter de Gruyter, Berlin. pp. 1–340.

Maucci, W. (1986). *Fauna d'Italia: Tardigrada*. Edizioni Calderini, Bologna, pp. 396.

Maucci, W. and Ramazzotti, G. (1981). *Cornechiniscus* gen. nov.: nuova posizione sistematica per i cosiddetti "*Pseudechiniscus* grouppo *cornutus*" con descrizione di una nuova specie (Tardigrada, Echiniscidae). *Memorie dell'Istituto Italiano di Idrobiologia*, 39: 147–151.

Miller, M. A., Pfeiffer, W. and Schwartz, T. (2010). Creating the CIPRES Science Gateway for inference of large phylogenetic trees. 2010 Gateway Computing Environments Workshop (GCE). pp. 1–8. http://dx.doi.org/10.1109/GCE.2010.5676129

Minh, B. Q., Schmidt, H. A., Chernomor, O., Schrempf, D., Woodhams M. D., von Haeseler, A. and Lanfear, R. (2020). IQ-TREE 2: New models and efficient methods for phylogenetic inference in the genomic era. *Molecular Biology and Evolution*, 37: 1530-1534. https://doi.org/10.1093/molbev/msaa015

Møbjerg, N., Kristensen, R. M. and Jørgensen, A. (2016). Data from new taxa infer *Isoechiniscoides* gen. nov. and increase the phylogenetic and evolutionary understanding of echiniscoidid tardigrades (Echiniscoidea: Tardigrada). *Zoological Journal of the Linnean Society*, 178 (4): 804–818. https://doi.org/10.1111/zoj.12500

Møbjerg, N., Jørgensen, A. and Kristensen, R. M. (2019). Ongoing revision of Echiniscoididae (Heterotardigrada: Echiniscoidea), with the description of a new interstitial species and genus with unique anal structures. *Zoological Journal of the Linnean Society*, 188 (3): 663–680. http://dx.doi.org/10.1093/zoolinnean/zlz122

Murphy, S. and Fernandez, F. (2009). The development of methodologies to assess the conservation status of limestone pavement and associated habitats in Ireland. *Irish Wildlife Manuals, No. 43*. National Parks and Wildlife Service, Department of the Environment, Heritage and Local Government, Dublin, Ireland.

Murray, J. (1905). Tardigrada of the Scottish Lochs. *Transactions of the Royal Society of Edinburgh*, 41: 677–698. https://doi.org/10.5962/bhl.title.12517

Murray, J. (1906). Tardigrada of the Forth Valley, II. *Annals of Scottish Natural History*, 60: 214–217.

Murray, J. (1907). Scottish Tardigrada, collected by the Lake Survey. *Proceedings of the Royal Society of Edinburgh*, 45 (3): 641–688. http://dx.doi.org/10.1017/s0080456800011777

Murray, J. (1910). Part V. Tardigrada. *In*: Murray, J. (Ed.). *British Antarctic Expedition, 1907-9, under the command of Sir E.H. Shackleton, c.v.o., Reports on the Scientific Investigations*, *Biology Volume I*. pp. 82–201. https://doi.org/10.5962/bhl.title.22427

Parr, S., Moran, J. and Ó Conchúir, R. (2009). Grasslands of the Burren, Western Ireland, *In*: Veen, P., Jefferson, R., de Smidt, J. and van der Straaten, J. (Eds.), *Grasslands in Europe: Of High Natural Value*. KNNV Publishing, Zeist, Netherlands. pp. 144–151. https://doi.org/10.1163/9789004278103_017

Pérez-Pech, W. A., de Jesús-Navarrate, A., DeMilio, E., Anguas-Escalante, A. and Hansen, J. G. (2020). Marine Tardigrada from the Mexican Caribbean with the description of *Styraconyx robertoi* sp. nov. (Arthrotardigrada: Styraconyxidae). *Zootaxa*, 4731 (4): 492–508. http://dx.doi.org/10.11646/zootaxa.4731.4.3

Perry, E., Miller, W. R. and Kaczmarek, Ł. (2019). Recommended abbreviations for the names of genera of the phylum Tardigrada. *Zootaxa*, 4608 (1): 145–154. http://dx.doi.org/10.11646/zootaxa.4608.1.8

Petersen, B. (1951). The tardigrade fauna of Greenland, a faunistic study with some few ecological remarks. *Meddelser om Grønland*: 150 (5): 5–94.

Pilato, G. (1972). Prime osservazioni sui tardigradi delle Isole Egadi. *Bollettino delle Sedute dell'Accademia Gioenia di Scienze Naturali in Catania*, 4: 110–124.

Pilato, G. (1974). Tre nuove specie di tardigradi muscicoli di Cina. *Animalia*, 1: 59–68.

Pilato, G., Lisi, O. and Binda, M. G. (2010). Tardigrades of Israel with description of four new species. *Zootaxa*, 2665 (1): 1–28. http://dx.doi.org/10.11646/zootaxa.2665.1.1

Plate, L. H. (1888). Beiträge zur Naturgeschichte der Tardigraden. *Zoologische Jahrbücher*, 3: 487–550. https://doi.org/10.5962/bhl.part.1265

Ramazzotti, G. and Maucci, W. (1983). Il Phylum Tardigrada (III. edizione riveduta e aggiornata). *Memorie dell' Istituto Italiano di Idrobiologia,* 41: 1–1016.

Rambaut, A., Drummond, A. J., Xie, D., Baele, G., and Suchard, M. A. (2018). Posterior summarisation in Bayesian phylogenetics using Tracer 1.7. *Systematic Biology*, 67 (5): 901–904. https://doi.org/10.1093/sysbi o/syy032

Richters, F. (1902). Beiträge zur Kenntnis der fauna der Umgebung von Frankfurt am Main Erste Fortsetzung. *Bericht der Senckenbergischen Naturforschenden Gesellschaft in Frankfurt am Main*, 34: 3–21.

Richters, F. (1926). Tardigrada, *In:* Kükenthal, W. and Krumbach, T. (Eds.), *Handbuch der Zoologie* 3, Walter de Gruyter and Co., Berlin and Leipzig, pp. 1–68.

Rocha, A., Doma, I., Gonzalez Reyes, A. and Lisi, O. (2020). Two new tardigrade species (Echiniscidae and Doryphoribiidae) from the Salta province (Argentina). *Zootaxa*, 4878 (2): 267–286. https://doi.org/10.11646/zootaxa.4878.2.3

Ronquist, F. and Huelsenbeck, J. P. (2003). MrBayes 3: Bayesian phylogenetic inference under mixed models. *Bioinformatics*, 19: 1572–1574. https://doi.org/10.1093/bioinformatics/btg180

Schultze, C. A. S. (1840). *Echiniscus Bellermanni; animal crustaceum*. Berolini. Apud G. Reimer.

Schuster, R. O. (1975). A new species of *Parechiniscus* from Utah (Tardigrada: Echiniscidae). *Memorie dell'Istituto Italiano di Idrobiologia*, Suppl. 32: 333–336.

Schuster, R. O. and Toftner, E. C. (1982). Dominican Republic Tardigrada, *In:* Nelson, D. R. (Ed.), *Proceedings of the Third International Symposium on the Tardigrada*, East Tennessee State University Press, Johnson City, Tennessee, pp. 221–235.

Thulin, G. (1911). Beiträge zur Kenntnis der Tardigraden fauna Schwedens. *Arkiv för Zoologi*, 7: 1–60. https://doi.org/10.5962/bhl.part.1270

Thulin, G. (1928). Über die Phylogenie und das System der Tardigraden. *Hereditas*, 11: 207–266. https://doi.org/10.1111/j.1601-5223.1928.tb02488.x

Tumanov, D. V. (2005). *Isohypsibius panovi*, a new species of Tardigrada from Ireland (Eutardigrada, Hypsibiidae). *Zootaxa*, 812: 1–4. https://doi.org/10.11646/zootaxa.812.1.1

Tumanov, D. V. (2020a). Analysis of non-morphometric morphological characters used in the taxonomy of the genus *Pseudechiniscus* (Tardigrada: Echiniscidae). *Zoological Journal of the Linnean Society*, 188 (3): 735–775. https://doi.org/10.1093/zoolinnean/zlz097

Tumanov, D. V. (2020b). Integrative redescription of *Hypsibius pallidoides* Pilato et al., 2011 (Eutardigrada: Hypsibioidea) with the erection of a new genus and discussion on the phylogeny of Hypsibiidae**.** *European Journal of Taxonomy*, 681: 1–37. https://doi.org/10.5852/ejt.2020.681

Urbanowicz, C. (1925). Sur la variabilité de *Macrobiotus oberhaeuseri*. *Bulletin Biologique de la France et de la Belgique (Paris)*, 59: 124–142.

Vončina, K., Kristensen, R. M. and Gąsiorek, P. (2020). *Pseudechiniscus* in Japan: re-description of *Pseudechiniscus asper* Abe et al., 1998 and description of *Pseudechiniscus shintai* sp. nov. *Zoosystematics and Evolution*, 96 (2): 527-536. https://doi.org/10.3897/zse.96.53324

Węglarska, B. (1959). Niesporczaki (Tardigrada) Polski I. Niesporczaki województwa krakowskiego. *Acta Zoologica Cracoviensia*, 4: 699–745.

Wilson, S. and Fernández, F. (2013). *National survey of limestone pavement and associated habitats in Ireland*. *Irish Wildlife Manuals, No. 73*. National Parks and Wildlife Service, Department of Arts, Heritage and the Gaeltacht, Ireland. 215 pp.

Xue, J., Li, X., Wang, L., Xian, P. and Chen, H. (2017). *Bryochoerus liupanensis* sp. nov. and *Pseudechiniscus chengi*. sp. nov. (Tardigrada: Heterotardigrada: Echiniscidae) from China. *Zootaxa*, 4291 (2): 324–334. https://doi.org/10.11646/zootaxa.4291.2.5

Yang, T. (2002). The Tardigrades from some mosses of Lijiang County in Yunnan Province (Heterotardigrada: Echiniscidae; Eutardigrada: Parachela: Macrobiotidae, Hypsibiidae). *Acta Zootaxonomica Sinica*, 27: 53–64.